UNIVERSITA' DEGLI STUDI DI PARMA

DOTTORATO DI RICERCA IN
SCIENZE DELLA TERRA

CICLO XXX

Towards a multiparameter monitoring of Apennine landslides: system development and initial testing

Coordinatore:
Chiar.mo Prof. Fulvio Celico

Tutore:
Chiar.mo Prof. Alessandro Chelli

Co-Tutore:
Chiar.mo Prof. Roberto Francese

Dottorando: Andrea Quagliarini

Anni 2014/2017

Insanity laughs under pressure we're breaking
Can't we give ourselves one more chance
Why can't we give love that one more chance
Why can't we give love give love give love give love
give love give love give love give love give love
'Cause love's such an old fashioned word
And love dares you to care for
The people on the (People on streets) edge of the night
And loves (People on streets) dares you to change our way of
Caring about ourselves
This is our last dance
This is our last dance
This is ourselves
Under pressure
Under pressure
Pressure
Under Pressure. Davide Bowie, Queen
Hot Space. 1982

Table of contents

Abstract

In this thesis, the main results of monitoring phase of Case Pennetta landslide of the Northern Apennines, which is located in Parma (Italy) are reported.

The first aim of this work is to provide and assess the suitability of a multidisciplinary approach, based on geological, geophysical, geomorphological, geotechnical and hydrogeological techniques; furthermore, another aim is to tests a set of tools in order to prepare landslide models and forecasts. For these reasons, the characterization of Case Pennetta landslide has been accomplished through the use of an integrated methodology that involves the application of various acquisition and innovative analysis techniques. In details, a single long-term monitoring system of a landslide, taking into account different scientific knowledges, case studies, tested models and verified procedures to map landslides, is proposed.

The second aim of this work is to create a model that explains in detail the dynamics that affect the investigated landslide body and the movements occurring within it, and thus, improving and reducing cost and time of mitigating the risk. In order to obtain a greater control over the whole system and to predict landslide hazards, each single variable of the phenomenon and how it varies over time were considered and evaluated. Each variable allows the study of specific triggering factors and depending on the type and number of the landslides, and the extent and complexity of the study area.

In conclusion, this work describes both realization and management of a multi-parametric system and the evaluation of results tha have allowed us to hypothesize a model that shows how physical properties vary within the landslide body.

Chapter 1

Project Introduction and Structure

1.1 Introduction, Project Motivation and Aims

A landslide is the movement of a mass of rock, earth or debris down a slope, under the influence of gravity (Varnes, 1978; Cruden, 1991; Cruden and Varnes, 1996). The term "landslide" means that may be considered almost all varieties of slope movements, including some that involve little or no true sliding (flowing, sliding, toppling or falling movements, or a combination of two or more types of movements; Varnes, 1978).

According to Varnes (1978) the attributes that have been used as criteria for identification and classification are: type of movement, kind of material, rate of movement, geometry of the area of failure and the resulting deposit, age, causes, degree of disruption of the displaced mass, relation or lack of relation of slide geometry to geologic structure, degree of development, geographic location of type examples, and state of activity.

Different phenomena may cause landslides: intense or prolonged rainfall, earthquakes, snow melting, and human activities. (Varnes, 1978; Crozier, 1986; Hutchinson, 1988; Cruden and Varnes, 1996; Dikau et al., 1996).

The broad range of landslide phenomena, and the uncertainties in data acquisition and handling explain why is difficult to define a single methodology to study landslides, and to evaluate the associated risk. Therefore landslide mapping, and landslide hazard and risk assessment evaluation require a method different from the traditional scientific approach, based on controlled experiments. Surveys carried out by geomorphologists and geologists in many areas of the world has shown that a multidisciplinary approach, based on geological, geophysical, geomorphological, geotechnical and hydrogeological techniques have to be applied. Each method allows the study of specific triggering factors and depending on the type and number of the landslides, and the extent and complexity of the study area.

A comprehensive review of direct and indirect techniques was presented by Hunt (1984), Hutchinson (1984) and McGuffey et al. (1996), whereas Ogilvy (1974), Bogoslovsky and Ogilvy (1977), Goryainov and Martveev (1988), McCann and

Forster (1990) and Hack (2000) describe geophysical techniques that may be applied to landslides.

Direct methods (Hunt 1984) are more common but require manpower and are very expensive, and most commonly mitigate the risk only in limited areas (Sharma 1997). However, during the past 20 years, developments in instrumentation and computer processing have provided other data collection techniques.

Indirect methods, like as geophysical methods provide non-destructive, portable techniques that can be used to cover large areas at relatively low costs (McGuffey et al., 1996). However, geophysical surveys are rarely utilized (Hack 2000).

Most recently, great attention is devoted to the ERI (Electrical Resistivity Imaging) method, a geophysical technique that can be used to obtain imaging sub-surface structures from electrical resistivity measurements made at the surface (Griffiths and Barker, 1993; Loke and Barker, 1996b; Giano et al., 2000; Schmutz et al., 2000; Suzuki and Higashi, 2001; Lebourg et al., 2005; Friedel et al., 2006), and that provides high spatial resolution with a relatively fast field acquisition time while being low in cost. It can be used in geophysical exploration of many landslide areas.

The impact of landslides in Italy is increased because of the growing population and the expansion of new settlements and infrastructure occurred in dangerous or potentially hazardous areas, due to the local physiographical setting (Guzzetti et al., 1999a, 2005c). Therefore, the occurrence of landslides represents an important, still open, issue.

In the project called IFFI (Italian acronym for Landslide Inventory in Italy) are listed about 615.000 events spread all over the country, affecting an area of about 23,000km^2 that, in turn, represents the 7.5% of the entire national territory (Marana, 2017).

Despite landslides are a worldwide problem that results in life losses and important damages to settlements and infrastructures each year, in many countries, the extent and complexity of societal and economic problems, as well

as the the limited available resources impede investments in order to reduce the risk represented by landslides (Plattner, 2005; Brabb and Harrod, 1989; Brabb, 1991) or to mitigate the catastrophic effects of slope failures.

The aim of this work is to provide and assess the suitability of a multi-parameter monitoring method and a set of tools, for the preparation of landslide models, and of landslide forecasts.

Therefore, a single long-term monitoring system of a landslide, taking into account different scientific knowledges, case studies, tested models and verified procedures to map landslides and predict landslide hazards, is proposed. The technique is tested on an inland landslide system located in the Northern Apennines, in the province of Parma city. The results obtained by the geophysical monitoring campaign is interpreted in terms of geophysical (resistance), geomorphological (superficial form) and hydrogeological processes (ground level variation). The outcomes of the field investigation are then used to propose a geoelectrical monitoring of landslides and to highlight the additional information that are required for any future deployments to be successful.

1.2 Thesis Structure

This thesis consists of 7 Chapters, including this one.

The first objective is presented in Chapter 2, where a brief description of the Case Pennetta landslides is given. Electrical properties of earth materials are described, as the geophysical method utilized by this research project, i.e. the Electrical Resistivity Tomography (ERT). The Literature Review is concluded describing the use of ERT both for site study and as a landslide monitoring technique.

In Chapter 3 are presented the second objective achieved and the results of the geological, geomorphological and geotechnical survey performed on the Case Pennetta landslide. This survey enabled to realize the landslide conceptual model, obtained both as a result of direct surveys and as surveys related to

subsurface characterization with the application of the Two-Dimensional Electrical Resistivity Tomography and geotechnical investigations.

The methodology used for the construction of geophysical monitoring system is explained in Chapter 4 and provides explanation of each stages of the work. Auxiliary processing methods are also described, allowing to manipulate more accurately the geophysical data.

In Chapter 5 are analyzed the relationships between the resistivity and the variation of the water content inside the landslide body, identifying landslide property trends in time-lapse resistivity monitoring data. Geophysical data have also been treated from a statistical point of view in order to better understand the results in quantitative terms.

Finally, in Chapter 6 data related to the new geological-geomorphological model and data obtained from the multi-parametric monitoring system are analyzed and discussed.

The outcomes of the monitoring results of this investigation are interpreted in Chapter 7, in terms of strengths and weaknesses of the multiparametric model realized, considering, in particular, the modalities of realization of the geoelectric system.

Chapter 2

Literature Review

This chapter provides a basic indication on the literature and on theoretical aspects of the project guidelines. The theory behind data manipulation and processing of time-lapse ERT results are discussed in Chapter 4, the Methodology Chapter.

This is followed by a short overview of the application of geoelectrical methods for investigation of landslides. An in-depth explanation of how electrical resistivity tomography (ERT) works and how is used to investigate landslide systems is reported. Finally, ERT monitoring together with several examples of its application to better understand landslide processes, are shown.

This Chapter leads to a better understanding of the groundwater movement and the physical properties variation inside the landslide body. Section 2.2 is aimed at informing the reader about landslide classification, mechanics, trigger mechanisms and failure events in the geographical region of Northern Apennines, i.e. in the Taro Valley (Parma).

2.1 Northern Apennine Landslides

As mentioned above, landslide is a form of mass movement process (Cruden 1991; Varnes 1978) and the term describes inland, coastal and submarine landslide. Since a lot of landslide classification schemes exist, Cruden and Varnes (1996) and Varnes (1978) have attempted to standardize classification so that slope instability events can be described briefly and unambiguously.

Therefore, the classification criteria are: variety of movement (falls, topples, slide spread, flows) and type of material involved in the movement (rock, debris, earth). A combination of the type of movement and material enables to formulate an appropriately descriptive landslide name.

Geological and gravitational processes that occur on the slopes of different structures and morphologies, are the expression of an interaction of various geological factors, both of endogenous and exogenous origin.

Materials are broadly categorized as either *rock* or *soil*, or a combination of these two types of material.

Rock refers to hard or firm bedrock that is intact and in place before the slope movement occurs. *Soil* is distinguished further on the basis of texture.

Earthflows

Earthflow is a mass movement of fine-grained soils and the term includes both the slow earthflows which are common in plastic and fine grained soils, and the wetter rapid earthflows which occur in highly sensitive clay deposits (Sharpe 1938; Varnes 1978; Cruden and Varnes, 1996).

A lot of investigators studied individual earthflows, their geology, and underlying physical processes since the early twentieth century, when the term earthflow was recognized as a distinct type of a mass movement (e.g., Keefer and Johnson, 1983; Torrance 1987; LeFebvre 1996).

In the modern landslide classification schemes, the term earthflow includes earthflows, earth slides, composite earth slide-earthflows, as well as liquefaction spreads, and some debris slides (Varnes, 1978; Cruden and Varnes, 1996). Earthflows are common in areas where there are outcrops of clay-bearing sedimentary rocks and weathered volcanic rocks, as well as some areas of weathered metamorphic and plutonic rocks. Slow earthflows occur both in the fine-grained soils that consist dominantly of plastic silt or clay, and in the rocky soils that are supported by a plastic silt-clay matrix. The Atterberg Limits of an earthflow material range widely between individual earthflows, but generally are consistent with moderate to high plasticity values.

The materials involved have a low to moderate shear strength, as well as a low sensitivity.

Slow earthflows commonly have: a teardrop or bulbous shape in a map view, a sinusoidal profile, are elongate in the direction of the down slope movement and are several times wider than thick (Keefer and Johnson, 1983).

Active earthflows exhibit seasonal movement patterns primarily governed by precipitation and groundwater levels, and they can require several weeks of cumulative rainfall before the onset of movement (Kelsey 1978; Iverson and Major, 1987). Earthflows can potentially dominate sediment delivery to

channels in erosive landscapes (Putnam and Sharp, 1940; Swanson and Swanston, 1977; Kelsey 1978), and despite this, they seldom can made disasters (Iverson 2005). Therefore It is possible to distinguish earthflows from large displacement and catastrophic single-event failures, such as rockslides, translational bedrock slides, debris flows and rotational slumps (Cruden and Varnes, 1996).

Large ancient earthflows are quite common in the Emilia-Romagna Apennines. From a plan view, these landslides show: a large crown, a relatively narrower middle "channel" (corresponding to the area of the flow) and a wide basal fan reaching the valley floor, with a modest or none slope inclination. The thickness is usually no more than a few tens of meters.

Most of them (52%) reaches a depth ranging from 10 to 30m (Bertolini and Pizziolo, 2008). About 10% of them show a depth exceeding 40m; therefore the depth has seldom reached a magnitude of 80-100m.

The internal structure shows several superimposed "strata" which are formed in different periods of time in the past and from different parts of the slope.

In terms of shear strength properties, these materials show a spatially and temporally high degree of variability that is difficult to quantify. The minimum shear strength values are found in argillaceous materials with montmorillonite minerals (for example, Argille di Viano Formation; Bertolini, 2001b).

Slow earthflows respond quickly to hydrologic input, thus implying that the basal shear surfaces respond quickly to a positive pore water pressures. This type of landslide is particularly prone to a long term instability and it is commonly reactivate either during intense rainfall periods and processes such as earthquakes (Skempton et al., 1985). Moreover, the increase of the water content in flow deposits increases the unit weight and, therefore, the driving stresses that encourage the slope failure. This can be explained because the pore water pressures together with the soil moisture content increase and cause a decrease in the soil effective shear strength which may lead to mobilize the material. Pore pressure fluctuations and shear surface roughness influence the rate of the earthflow displacement (Iverson 2000; Coe et al., 2003).

Since the earthflow thickness is often a function of the depth of the weathering profile and the depth to competent bedrock, the bedrock weathering rate may limit the earthflow activity (Mackay and Roering, 2011).

In the Northern Apennines there are many historical villages which are of great value and represent a cultural heritage of great importance. The territory of the Emilia Romagna Region (Northern Italy) pertaining to the Northern Apennines involves a large number of landslides (Figure 2.1) of different types and sizes: the latest inventory (Regione Emilia Romagna, 1999) reports more than 30.000 landslides that cover about 20% of the mountainous and hilly terrain. Therefore, as the italian territory is greatly affected by the landslide hazard, the need to solve problems of land management and to act for the preservation of historical monuments arose (Chelli et al., 2005).

The large number of landslides is linked, mainly, to the geological features of the Northern Apennines, i.e. a fold and thrust belt which started to develop in the Late Cretaceous (Bettelli and De Nardo, 2001). The complex tectonic history of the chain have determined the superimposition of many stratigraphic units containing heterogeneous and/or chaotic rocks characterized by poor geomechanical properties which cause the strong tendency for the slope movements (Bertolini and Pellegrini, 2001). The large landslides are mostly of complex type, combining roto-translational movements (that prevail in the crown area) with long flows which generally reach the base of the slope. In the middle and lower zones frequently it may happen that a complete deformation of the material (typical of the flow) is accompanied by a sliding movement to the base.

An example of this type of landslide is that studied in this work, the Case Pennetta landslide, which has similarities with other landslides belonging to the Northern Apennines, such as Roncovetro, Casa Ravera and Corniglio landslides. Roncovetro landslide is located in the mid-Apennines of the Reggio Emilia provinces (River Enza Valley), between the hamlets of Roncovetro and Vedriano and presents rather particular morphometric and kinematics features: it is 2.5km long with a maximum width of 300m; the depletion and accumulation

zones are separated by a long and narrow landslide body which is wide about 30 or 40m (Bertolini and Gorgoni, 2001).

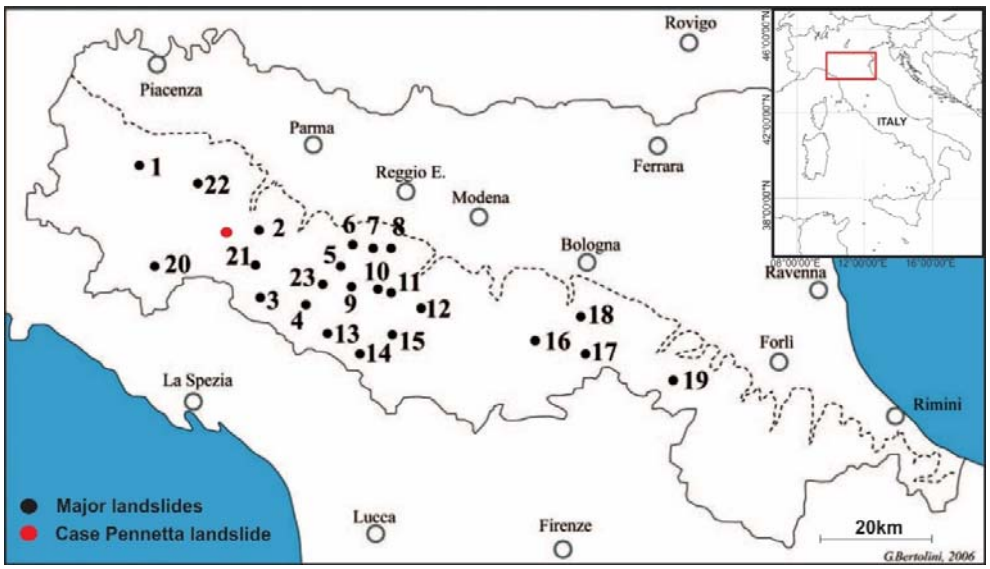

Figure 2.1. Map of Emilia-Romagna region, annotated with major landslides. (Bertolini and Pizziolo, 2008. Red dot: Location of Case Pennetta landslide. Black dot: location of major landslide; 1-Valleia (PC), 2-Signatico (PR), 3-Corniglio (PR), 4-Poviglio (RE), 5-Roncovetro (RE), 6-Rossena (RE), 7-Canossa (RE), 8-Casoletta (RE), 9-Garfagnolo (RE), 10-Magliatica (RE), 11-Ca' Lita (RE), 12-Morano (MO), 13-Cerre' Sologno (RE), 14-Febbio (RE), 15-Boschi di Valoria (MO), 16-Rocca Pitigliana (BO), 17-Ca' di Sotto (BO), 18-Gole di Scascoli (BO), 19-Borgo Tossignano (BO), 20-Ca' Terzaga (PR), 21-Costa Casaselvatica (PR), 22-Casa Revera (PR), 23-Groppo (RE).

The lower portions of the landslide maintain its static nature, whereas the crown portion may be considered as newly formed, because it is characterized by complex movements. The middle portion of the Roncovetro landslide is characterized by fluid-viscous flows and the geological formations affected by the movement, belong to the Ligurian and epi-Ligurian Sequences and shows a complex structure.

The Casa Ravera landslide (Pellegrino Parmense, Province of Parma), in the Northern Apennines, esumed its activity in January 1997 after intense rainfalls and a period of inactivity. The rock types affected by the slide belong to the allochthonous outer Ligurian Unit of the marly-calcareaous Mt. Cassio Flysch, which widely outcrops in the study area together with the clay shales of the Argille di Aviano Formation.

The mass movement is slow and characterized by an intermittent displacement; despite its considerable dimensions (length 1650m, difference of altitude 220m, presumed volume $12.6x10^6m^3$), no evidence was found concerning previous reactivations phases and it is classified as a complex landslide. In the source area retrogressive processes are observed with rotational-translational failure mechanisms; the material displaced causes the earthflows which, after a movement through the narrow landslide channel, overload and destabilze the soil of the old and wide accumulation zone. Displacements are around some tens of meters in the upper slope sector, whereas they progressively decrease downstream: in the foot area the inclinometers have recorded displacements up to 1mm a month at a depth of 28m.

The Corniglio landslides is located in the Northern Apennines (Parma, Italy) and it is a large mass movement which has affected the old village of Corniglio (700m m.s.l.) several times during the past 400 years. Global reactivations of this landslide have been historically recorded in the years 1612, 1740 and 1902, but the evidences collected have shown that other movements had occurred in the previous times (Larini et al., 2001). The Corniglio landslide dimensions are considerable: over 3000m long, 1000m wide and 120m deep, from an altitude of 1150m m.s.l. to an area at 550m m.s.l., near the Torrent Parma riverbed which is characterized by an annual mean rainfall of 1500mm.

In the middle of November 1994, after a long period of dormancy lasting nearly a century, the Corniglio landslides, which is classified as a slow, intermittent, complex and composite landslide, resumed its activity striking once more the village of Corniglio. The landslide that develops within arenaceous and calcareous flysches overlying chaotically arranged clay shales and limestone, consists of multiple rotational-translational slides in the upper and middle portions and of translational slide in the toe portion, associated with an earthflow.

The transformation into a real "casting" of land occurs only if the event lasts for a long time (months or years) and only if there are large quantities of water (Bertolini et al, 2005). The average depth of the landslide is between 10 and 30

meters. About half of the investigated landslide bodies falls within this depth class, i.e. 10-30 meters (Bertolini et al, 2005), but not lacking landslides that exceed 40 meters (10%), and few cases with landslides that are close to 100 meters.

Prediction of landslide occurrence is not only a fundamental goal of hazard management but also a test of how well the process is understood. Precipitation is one of the most important landslide triggering mechanisms, in fact temporal landslide activity is often associated with seasonal rainfall patterns (Van Asch et al., 1999). Forewarning of landslides may be provided in different ways but the most common approach is the recognition of landslide susceptibility from a spatial perspective (Crozier 1995). This way generally involves an investigation of geotechnical or geomorphic factors with the aim of ranking terrain units considering their potential to produce landslides. However, as Varnes (1984) has observed, the spatial susceptibility only partly represents the landslide hazard. The greatest challenge is the need to predict the occurrence of landslides in time: if sufficient rainfall data are present together with precisely dated landslide events the critical daily rainfall thresholds and the antecedent rainfall amounts that trigger slope instability can be determined. Therefore, the stability analysis of the unsaturated slopes requires an extensive and detailed seepage study, because slope failures in unsaturated conditions are closely related to heavy rainfall and infiltration. The mechanism that leads to slope failures is that the negative pore-water pressures start to increase when water starts to infiltrate the unsaturated soil. The loss of negative pore-water pressures decreases the shear strength of the soil below the mobilized shear strength along the potential slip surface.

2.2 Electrical Resistivity Tomography on Landslide System

Electrical resistivity tomography is a geoelectrical technique used to obtain an image of the subsurface electrical properties distribution and the the principal investigative tool of this project. In Section 2.3 the physical principles of

resistivity surveying and modelling techniques which are used in this work, as well as the current state-of-art of the electrical resistivity monitoring, are described.

2.2.1 Electrical Properties of Electrical Materials

The purpose of electrical surveying is to map the subsurface resistivity distribution by taking measurements performed at the surface or in borehole. From these measurements, the true resistivity of the subsurface can be estimated. Terrain resistivity depends on various geological parameters, such as mineral and fluid contents, porosity and degree of water saturation in the rock. Since electrical surveying was used for many decades in hydrogeological, mining and geotechnical investigations, more recently, it is also used for environmental surveys. The resistivity measurements are normally made by injecting current into the ground with two electrodes, and then measuring the artificial potential with two other electrodes (P1 and P2). From the current (I) and voltage (V) values, an apparent resistivity (*pa*) value is calculated:

$$p_a = \mathrm{k}\ \mathrm{V} / \mathrm{I}$$

where k is the geometric factor which depends on the arrangement of the four electrodes. Resistivity meters normally give a resistance value, i.e. R = V/I, so the apparent resistivity value is calculated by:

$$pa = \mathrm{k}\ \mathrm{R}$$

Equation 2.1. Ohm's Law for the apparent resistivity of a homogeneous material.

The calculated resistivity value is not the true resistivity value of the subsurface, but it is rather an "apparent" value, i.e. the resistivity of a homogeneous ground which may give the same resistance value for a same electrodes arrangement. The relationship between the "apparent" resistivity and the "true" resistivity is

complex; the true subsurface resistivity was determined by an inversion of the measured "apparent" resistivity values by using a computer program.

The resistivity method was born in the 1920's thanks to the work of the Schlumberger brothers. In the next 60 years, conventional sounding surveys (Koefoed 1979) were been normally used for quantitative interpretation. In the resistivity method, the center point of the electrode array remains fixed, but the spacing between the electrodes is increased to obtain more information about the deeper sections of the subsurface. Despite the limitations of this method, there are two main reasons that make common the 1-D resistivity sounding surveys. The first reason was the lack of an appropriate equipment to carry out 2-D and 3-D surveys. The second reason was the lack of practical interpretation tools, useful to handle the more complex 2-D and 3-D models (Griffiths et al., 1990; Figure 2.2). However, the relatively recent development of multi-electrode resistivity meters (Griffiths et al., 1990) and the use a fast computer inversion software (Loke 1994) have made 2-D and even 3-D electrical surveys as practical commercial techniques.

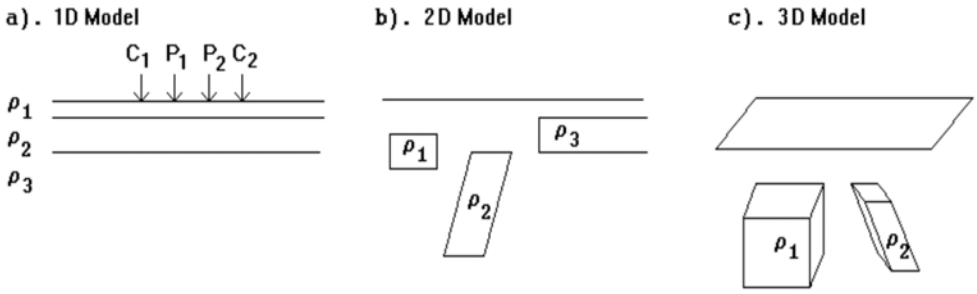

Figure 2.2. The three different models used in the interpretation of resistivity measurements (Loke 1999).

Before dealing with the 2-D and 3-D resistivity surveys, the resistivity values of some common rocks, soils and other materials will be briefly discussed. As mentioned above, resistivity surveys give a picture of the subsurface resistivity distribution; typical resistivity values for different types of subsurface materials and the geology of the area surveyed should to be known, in order to convert the resistivity picture into a geological picture.

Table 2.1 gives the resistivity values of common rocks, soil materials and chemicals (Keller and Frischknecht, 1966; Daniels and Alberty 1966). Igneous and metamorphic rocks have, generally, high resistivity values. The resistivity of these rocks greatly depends on the degree of fracturing and the percentage of the fractures filled with groundwater. Sedimentary rocks, which usually are more porous and have a higher water content than the igneous rocks, normally have low resistivity values. Clayey soil normally has a lower resistivity value than sandy soil. However, as is shown in Table 2.1, an overlap in the resistivity values of the different classes of rocks and soils occurs. This can be explained because the resistivity of a particular rock or soil sample depends on several factors, such as the porosity, the degree of water saturation and the concentration of dissolved salts: the sea water which has an high salt content, shows low resistivity value (about 0.2Ωm), while in the groundwater, more poor in salts, varies from 10 to 100Ωm. This makes the resistivity method an ideal technique for mapping the saline and fresh water interface in coastal areas.

In Table 2.1, also the resistivity values of several industrial contaminants are reported. Metals, such as iron, have extremely low resistivity values. Chemicals, such as potassium chloride and sodium chloride, are strong electrolytes and, even if they are present at fairly low concentrations, can greatly reduce the groundwater resistivity up to a value less than 1Ωm. The effect of weak electrolytes, such as acetic acid, is comparatively smaller. Hydrocarbons, such as xylene, have generally very high resistivity values.

Moreover, resistivity values can vary widely:, the resistivity of rocks and soils in a survey area can vary by several orders of magnitude. In comparison, density values used by gravity surveys, usually change by less than a factor of 2, and seismic velocities, usually do not change by more than a factor of 10. This makes the resistivity and other electrical or electromagnetic methods as very versatile geophysical techniques.

Material	Resistivity (Ω*m)	Conductivity (Siemen/m)
Igneous and Metamorphic Rocks		
Granite	$5x10^3$ - 10^6	10^{-6} - $2x10^{-4}$
Basalt	10^3 - 10^6	10^{-6} - 10^{-3}
Slate	$6x10^2$ - $4x10^7$	$2.5x10^{-8}$. $1.7x10^{-3}$
Marble	10^2 - $2.5x10^8$	$4x10^{-9}$ - 10^{-2}
Quartzite	10^2 - $2.x10^8$	$5x10^{-9}$ - 10^{-2}
Sedimentary Rocks		
Sandstone	8 - $4x10^3$	$2.5x10^{-4}$ - 0.125
Shale	20 - $2x10^3$	$5x10^{-4}$ - 0.05
Limestone	50 - $4x10^2$	$2.5x10^{-3}$ - 0.02
Soil and Water		
Clay	1 - 100	0.01 - 1
Alluvium	10 - 800	$1.25x10^{-3}$ - 0.1
Groundwater (frash)	10 - 100	0.01 - 0.1
Sea water	0.2	5
Chemicals		
Iron	$9.074x10^8$	$1.102x10^7$
0.01 M Potassium chloride	0.708	1.413
0.1 M Sodium chloride	0.843	1.185
0.1 M acetic acid	6.13	0.163
Xylene	$6.998x10^{16}$	$1.429x10^{-17}$

Table 2.1. Resistivities of some common rocks, minerals and chemicals (Loke 1999).

Clay minerals are capable of attracting more charge than other minerals, therefore they have an ion absorption capabilities which depends on their small particle size and their resulting large surface area. Moreover the species of clay minerals are several and have many different crystal lattice structures.

2.2.2 Electrical Resistivity Tomography (ERT)

The Electrical resistivity tomography (ERT) technique is considered as one of the most significant geophysical methodology; furthermore, new application areas are developed in the last years (Perrone et al., 2014). ERT is now widely used for environmental, engineering and groundwater resource mapping. The development of the technology associated with automatically multiplexed electrode arrangements and automatic measuring systems, facilitate the acquisition of a large number of measurements in a limited time. Furthermore, the advent of fast computers have allowed the development of the automated resistivity inversion schemes that aim to construct an estimate of a subsurface

resistivity distribution which is consistent with the experimental data (Perrone et al., 2014; Chambers et al., 2014; Chambers et al., 2011b; Loke et al., 2014).

The purpose of electrical resistivity surveys is to determine the resistivity distribution of the sounding soil volume. Artificially generated electric currents are supplied to the soil and the resulting potential differences are measured. Potential difference patterns provide information on the form of subsurface heterogeneities and of their electrical properties (Kearey et al., 2002). The greater the electrical contrast between the soil matrix and heterogeneity, the easier is the detection. Electrical resistivity of the soil can be considered as a proxy for the variability of soil physical properties (Banton et al., 1997). The current flow line distributions depend on the medium under investigation; they are concentrated in conductive volumes. The fundamental physical law exploited by resistivity surveying is the Ohm's Law, which describes the flow of current in the ground (Loke 2002). The Ohm's Law consider a single current electrode on the surface of a medium of uniform resistivity, as shown in Figure 2.3 and as described previously (Paragraph 2.2.1).

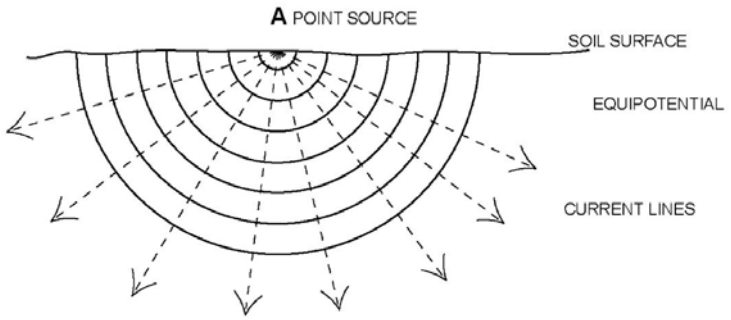

Figure 2.3. Distribution of the current flow in a homogeneous soil (Samouëlian et al., 2005).

As shown in Figure 2.5, in a homogeneous and isotropic half-space, electrical equipotentials are hemispherical when the current electrodes are located at the soil surface, (Scollar et al., 1990; Kearey et al., 2002; Sharma 1997; Reynolds 1997).

The current density J (A/m^2) has then to be calculated for all the radial directions with:

$$J = \frac{I}{2\pi r^2}$$

Equation 2.2. Current density for the radial directions.

where $2\pi r^2$ is the surface of a hemispherical sphere of radius r. The potential V can then be expressed as follows:

$$V = \frac{\rho I}{2\pi r}$$

Equation 2.3. Potential.

The potential difference DV measured between the electrodes M and N is given by the equation:

$$\Delta V = \frac{\rho I}{2\pi}\left[\frac{1}{AM} - \frac{1}{BM} - \frac{1}{AN} + \frac{1}{BN}\right]$$

Equation 2.4. Potential difference (Loke et al., 2013).

where AM, BM, AN and BN represent the geometrical distance between the electrodes A and M, B and M, A and N, and B and N, respectively. The electrical resistivity is then calculated using:

$$\rho a = \left[\frac{2\pi}{(1/AM) - (1/BM) - (1/AN) + (1/BN)}\right]\frac{\Delta V}{I} = K\frac{\Delta V}{I}$$

Equation 2.5. Apparent resistivity for any electrode configuration (Loke et al., 2013).

where K is a geometrical coefficient that depends on the arrangement of the four electrodes A, B, M and N. The current electrodes A, B, and the potential electrodes M and N can be placed in the field at the soil surface, or in boreholes. The subsurface field measured resistivity is not true subsurface resistivity but an

apparent resistivity, or a resistivity value that is the resistance of a homogeneous ground for the same electrode arrangement (Loke et al., 2002). As compared with the surface methods, the cross-borehole methods present the advantage of a high resolution with depth (Slater et al., 2000). This technique requires nevertheless intrusion into the studied bodies for the insertion of the electrodes. At the laboratory scale this technique can also be applied by placing the electrodes around the soil sample at various depths (Olsen et al., 1999).

Two-dimensional multi-electrode arrays provide a two-dimensional vertical picture of the sounding medium and carried out using several electrodes, connected to a resistivity meter system via multi-core cable (Loke 2002). The current and potential electrodes are maintained at a regular fixed distance from each other and are progressively moved along a line at the soil surface. At each step, one measurement is recorded (Figure 2.4).

The set of all these measurements at this first inter-electrode spacing gives a horizontal profile of resistivity values. The inter-electrode spacing is increased then by a factor n=2, and a second measurement line is done. This process (increasing the factor n) is repeated until the maximum spacing between electrodes is reached. The larger the n-values, the greater the depths of investigation as the distribution of the current also depends on the resistivity contrasts of the medium, the depth of investigation deduced from the spacing is called the "pseudo-depth". The data are then arranged in a 2-D "pseudo-section" plot that gives a simultaneous display of both horizontal and vertical variations in resistivity (Edwards 1977). The conventional graphic representation, introduced by Hallof (1957), puts each measured value at the intersection of two 458 lines through the center of the quadrupole. Each horizontal line is then associated with a specific value of n and gives a pseudo-depth of investigation.

Depending on the position of the potential electrodes with respect to the current electrodes, several array configurations can be defined: Wenner, Wenner-Schlumberger, dipole-dipole, pole-pole or pole-dipole arrays are the most commonly used. The latter configuration is an asymmetrical array, in which two directions (forward and reversed) are considered.

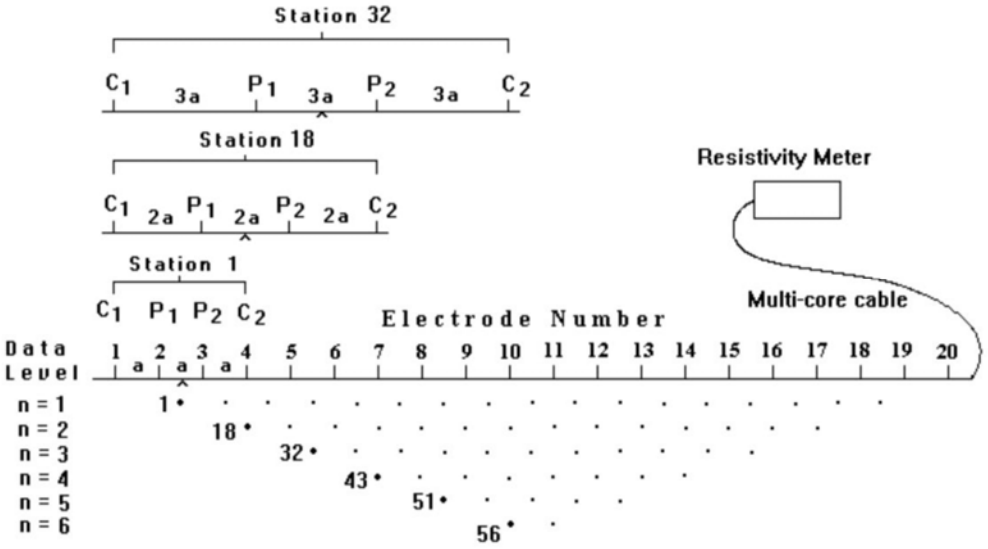

Figure 2.4. Layout of field equipment for a 2D ERT survey using the Wenner array (Loke and Barker, 1995).

Depending on the array configuration, the geometrical factor K differs; Seaton and Burbey (2002) reported that the array configuration has a substantial influence on the resolution, sensitivity and depth of investigation.

Most authors agree that the Wenner array has the best signal response and high resolution of horizontal structures but a relatively shallow depth of investigation and somewhat limited ability to detect vertical structures (Ward, 1990; Sharma, 1997; Loke, 2001). The Wenner-Schlumberger configuration is considered to have good signal response, the ability to resolve horizontal and vertical structures relatively well, and greater depth of investigation than the Wenner configuration (Ward 1990; Sharma 1997; Reynolds 1997; Loke, 2001). When a dipole-dipole array is configured with increasing n and a values, it has greater depth penetration than the Wenner and Wenner-Schlumberger methods (Loke 2001; Reynolds 1997). The dipole-dipole array produces the lowest signal response of all the arrays (Ward 1990; Sharma 1997; Reynolds 1997; Loke 2001) making it more subject to telluric noise than the Wenner and Wenner-Schlumberger arrays. The dipole-dipole configuration is considered inferior to the Wenner and Wenner-Schlumberger configurations for the resolution of horizontal and steeply dipping structures (Ward 1990; Sharma 1997; Reynolds

1997). The pole-pole configuration has the deepest penetration of all arrays and the widest horizontal coverage for a given array length but the poorest resolution (Loke 2001; Robain et al., 1999). The pole-pole method is also subject to telluric noise because of the long distance between the potential electrodes (Loke 2001). The pole-pole configuration is commonly used in shallow archaeological studies and three dimensional resistivity surveys requiring short spacing between electrodes. Table 2.2, summarizes for different 2D array configurations and compares the following characteristics for all the arrays: (i) the sensitivity of the array to horizontal and vertical heterogeneities, (ii) the depth of investigation, (iii) the horizontal data coverage and (iv) the signal strength (Loke 2001; Griffiths and Barker, 1993). The different orientations of heterogeneity can be vertical for heterogeneities such as dykes, cavities, preferential or horizontal flow, such as sedimentary layers; depth of investigation is determined for a homogeneous ground, but gives an a priori indication of the depth of investigation in a heterogeneous ground.

	Wenner	Wenner-Schlumberger	Dipole-Dipole	Pole-Pole	Pole-dipole
Sensitivity of the array horizontal structures	●●●●	●●	●	●●	●●
Sensitivity of the array vertical structures	●	●●	●●●●	●●	●
Depth of investigation	●	●●	●●●	●●●●	●●●
Horizontal data coverage	●	●●	●●●	●●●●	●●●
Signal Strength	●●●●	●●●	●	●●●●	●●

Table 2.2. Features of different 2-D arrays configurations types. The labels are classified from (●), which corresponds to poor sensitivity for the different arrays configurations to (●●●●), which represents the larger sensitivity for the different arrays configurations (from Samouëlian et al., 2005).

The horizontal data coverage is related to the electrode array configuration. The signal strength is related to the joint signal-response of the measurement. It is inversely proportional to the geometric factor K and is an important factor if the survey is carried out in areas with high background noise. All the different array types have specific advantages and limitations. The choice of the array configuration depends on the type of heterogeneity to be mapped and also on the background noise level; the characteristics of an array have to be taken into account. Hesse et al. (1986) emphasized that in specific cases the use of multiple

configurations can improve the chances of reading different features of the subsoil and leads to a better interpretation.

Although the Wenner- Schlumberger electrode configuration was used in this work, in the following section will be briefly described advantages and disadvantages about the different electrode array configurations.

The classical Schlumberger array is one of the array most commonly used for resistivity sounding surveys. In Figure 2.5 is shown a modified form of this array that can be used on a system with the electrodes arranged with a constant spacing.

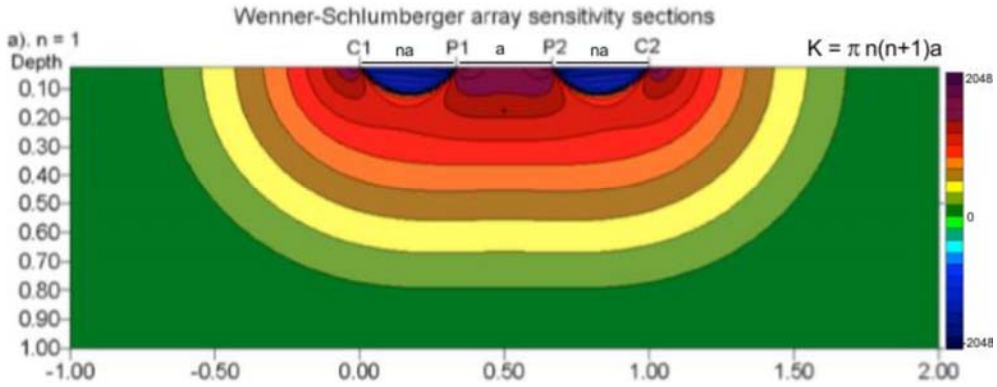

Figure 2.5. 2-D sensitivity in a Wenner-Schlumberger electrode configuration. (Loke 1997).

The "n" factor for this array is the ratio of the distance between the C1-P1 (or P2-C2) electrodes to the spacing between the P1-P2 potential pair. The sensitivity pattern for the Schlumberger array is slightly different from the Wenner array with a slight vertical curvature below the center of the array, and slightly lower sensitivity values in the regions between the C1 and P1 (and also C2 and P2) electrodes. There is a slightly greater concentration of high sensitivity values below the P1-P2 electrodes. This means that this array is moderately sensitive to both horizontal and vertical structures. In areas where both types of geological structures are expected, this array might be a good compromise between the Wenner and the dipole-dipole array. The median depth of investigation for this array is about 10% larger than that for the Wenner array

for the same distance between the outer (C1 and C2) electrodes. The signal strength for this array is smaller than that for the Wenner array, but it is higher than the dipole-dipole array. The Wenner array is a special case of this array where the "n" factor is equals to 1. The Wenner-Schlumberger array has a slightly better horizontal coverage compared with the Wenner array. For the Wenner array each deeper data level has 3 data points less than the previous data level, while for the Wenner-Schlumberger array there is a loss of 2 data points with each deeper data level. The horizontal data coverage is slightly wider than the Wenner array (Figures 2.6), but narrower than that obtained with the dipole-dipole array.

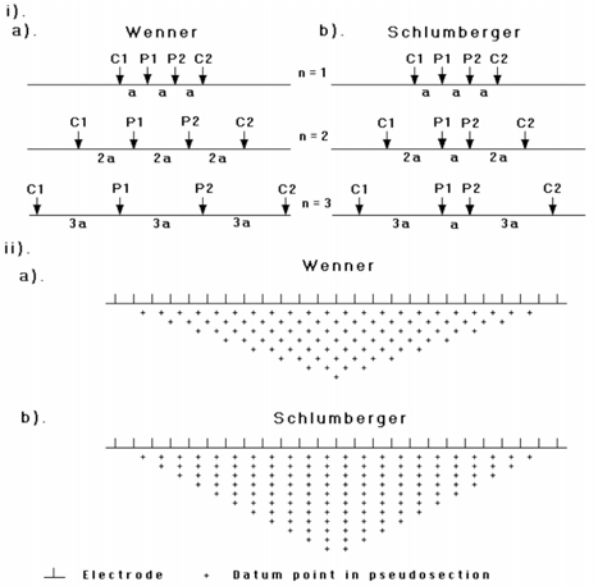

Figure 2.6. A comparison of the (i) electrode arrangement and (ii) pseudo-section data pattern for the Wenner and Wenner-Schlumberger arrays (Loke and Barker, 1995).

The pole-dipole array also has relatively good horizontal coverage, but it has a significantly higher signal strength compared with the dipole-dipole array and it is not as sensitive as the pole-pole array. Unlike the other common arrays, the pole-dipole array is an asymmetrical array and over symmetrical structures the apparent resistivity anomalies in the pseudo-section are asymmetrical. In some situations, the asymmetry in the measured apparent resistivity values could influence the model obtained after inversion (Loke and Barker, 1995). One

method to eliminate the effect of this asymmetry is to repeat the measurements with the electrodes arranged in the reverse manner (Seaton and Burbey, 2002, Loke and Barker, 1995). By combining the measurements with the "forward" and "reverse" pole-dipole arrays, any bias in the model due to the asymmetrical nature of this array would be removed. The pole-dipole array also requires a remote electrode, the C2 electrode, which must be placed sufficiently far from the survey line. For the pole-dipole array, the effect of the C2 electrode is approximately proportional to the *square* of ratio of the C1-P1 distance to the C2- P1 distance. Thus the pole-dipole array is less affected by the C2 remote electrode compared with the pole-pole array. If the distance of the C2 electrode is more than 5 times the largest C1-P1 distance used, the error caused by neglecting the effect of the C2 electrode is less than 5% (the exact error also depends on the location of the P2 electrode for the particular measurement and the subsurface resistivity distribution). Due to its good horizontal coverage, this is an attractive array for multi-electrode resistivity meter systems with a relatively small number of nodes. The signal strength is lower compared with the Wenner and Wenner-Schlumberger arrays but higher than the dipole-dipole array. For IP surveys, the higher signal strength (compared with the dipole-dipole array) combined with the lower coupling (compared with the Wenner and Wenner-Schlumberger arrays) due to the separation of the circuitry of the current and potential electrodes makes this array an attractive alternative.

The first step of a resistivity tomography survey (using the Wenner array) is to take all the electrical measurements using adjacent electrodes as current and potential electrodes. After all measurements with a=1 are performed, electrical measurements using every other electrode, or with a=2 are made. This process is repeated until all resistance measurements have been taken and often a maximum of n=6 is reached. Electrical measurements are performed in a systematic order to minimize the effects of electrode polarization which can hinder the quality of resistance measurements. Reciprocal measurements are often taken and are used as a measure of data quality, with a reciprocal error of

5% or 10% often being used as an arbitrary cut-off between good and bad data (Dahlin and Loke, 1998).

2.2.3 Modelling of ERT monitoring data

Several 2D smoothness constrained inversion algorithms for ERT data have been presented in literature (Sasaki 1989; Xu 1993; Elis and Oldenburg, 1994; Tsourlos 1995; Loke and Barker, 1996a). Further, since many of the problems associated with geophysical exploration are of a three dimensional nature several algorithms for treating the ERT problem in three-dimensions have been presented (among others Park and Van, 1991; Loke and Barker 1996b; Tsourlos and Ogilvy, 1999).

The transformation of a pseudo apparent resistivity map in a real resistivity map passes through an inversion process. This operation generates the subsurface real resistivity model able to supply in output a pseudo-map of apparent resistivity as much as possible similar to that measured in the field. The theoretical result of this measure can be mathematically determined (model) for define electrical properties with the appropriate initial and boundary conditions. This defines the "direct model" that allows to calculate theoretically the resistances measured for a given resistivity distribution and it is a predictive model because, given the distribution, it is possible to provide data. However, to investigate the subsurface, the "inverse model" must be solved, i.e. given a measurements set (data), the electrical properties distribution (model) must be" coherent" with the resistances actually measured (Figure 2.7).

As mentioned before, the direct problem (forward modeling) refers to a problem whose solution consists in finding an effect to a specific cause, using an appropriate physical model. It is described by a differential equation which can be solved analytically, or with digital techniques in general situations, but always been concerned to a unique solution, even if affected by the limits that all physical modeling entail. The region is discretized into cells (elements) with nodes that define the vertices (Dahlin and Zhou, 2004).

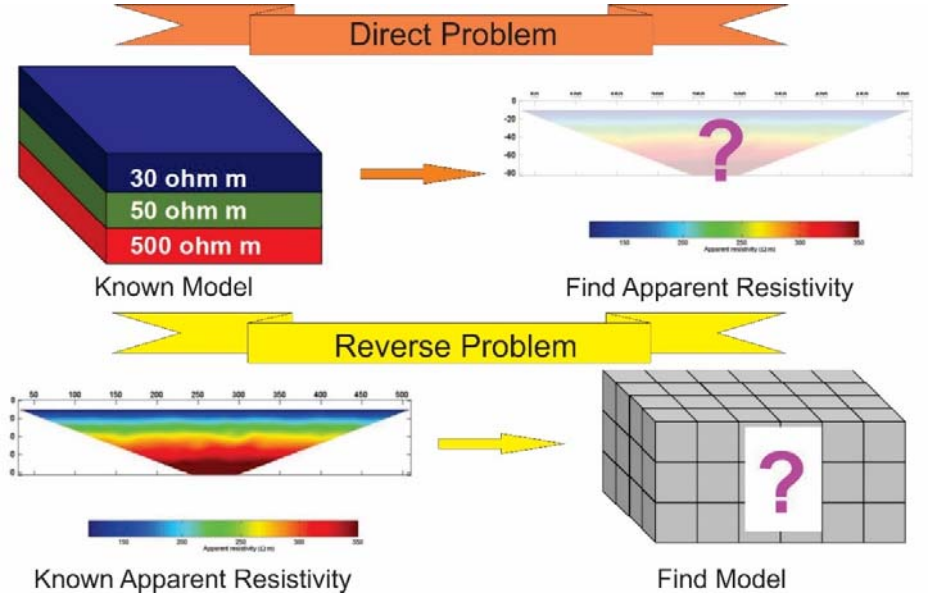

Figure 2.7. Definition of direct and reverse problems.

For each cell is assigned a different resistivity value and the potential is calculated at the nodes. The section consists of a precise number of cells (blocks), the dimensions are automatically calculated (as a function of the spacing of the electrodes) or manually by the operator. The cell sizes are reduced (more dense) near the electrodes, where there is greater sensitivity and increase with the depth towards the edge of the section, due to the decrease of the same sensitivity in these areas and the consequent lower resolution needed to describe the system (Dahlin and Zhou, 2004). The two most common techniques used to solve these problems are the finite difference methods and the methods to finite element (generally the most widely used because it is much more flexible). Both methods replace the original differential equations with a set of easily solvable algebraic equations (Griffiths et al., 1990)

In 2D modelling the change in resistivity is considered to be two dimensional but the current flow pattern is a three dimensional one. In other words, the measured values correspond to a three dimensional subsurface where the resistivity is allowed to vary in only two dimensions and remains constant in the strike direction (Tsourlos and Ogilvy, 1999). A cosine Fourier transformation is applied to include the potential variability in the strike (y) direction.

The Finite Element Methods treats the problem by discretizing the earth into homogeneous triangular (in this case) regions called elements (Figure 2.8). The potential within each element is approximated by a simple interpolation function (basis function). In order to minimize the error between the approximated and real potential, the Galerkin minimization criterion is applied (Papadopoulos et al., 2006). After applying the Galerkin minimization scheme to every element, the individual element equations can be assembled in to one global system which has the following form:

$$K \cdot A = F$$

Equation 2.6. Individual element.

where A is the unknown transformed nodal potential vector, F is the vector describing the sources and K is a matrix which is related to the nodal coordinates. After applying the homogeneous Dirichlet and Neumann boundary conditions (Bayliss et al., 1982) the system of equation (Equation 2.6) is being solved and the transformed nodal potential is obtained. After solving equation (Equation 2.6) for several wavenumbers the total potential is recovered by applying the inverse Fourier transform. Since the nodal potential is known, point to point potential differences and apparent resistivities are easily obtained.

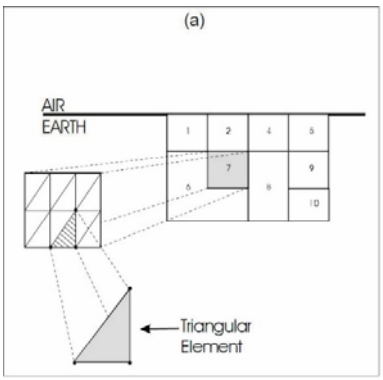

Figure 2.8. Triangular elements in which the cell is divided during the inversion process (Tsourlos, 2004).

The inversion core algorithm is the same for both the 2D and 3D case. A non-linear smoothness constrained inversion algorithm was used by the *ERTlab*

software (Sasaki 1992). The inversion is iterative and the resistivity xk+1 at the k+1th iteration is given by:

$$x_{k+1} = x_k + dx_k = x_k + [(W_d J_k)^T (W_d J_k) + \mu_k (C_x^T C_x + C_z^T C_z)]^{-1} (W_d J_k)^T W_d dy_k$$

where C_x, C_z are matrices which describe the smoothness pattern of the model in the x and z axes respectively (deGroot-Hedlin and Constable, 1990), dy_k is the vector of differences between the observed data d^{obs} and the modeled data d_k^{calc} (calculated using the forward modeling technique 2D), J_k and μ_k is the Jacobian matrix estimate and the Lagrangian multiplier respectively for the k_{th} iteration, W_d is the diagonal matrix of the data variances, and T denotes the transpose. The equation approach (McGillivray and Oldenburg, 1990) was incorporated into the FEM scheme in order to calculate the Jacobian matrix J (Tsourlos 1995). Depending on the dimensions of our problem the Jacobian matrix is calculated either by the 2D forward solver.

The subsoil is divided into cells, each with its resistivity, in order to obtain the inverse model (inverse modeling). Being "d" the vector that contains the measures of apparent resistivity, "m" the vector of the model parameters with constant resistivity in which the soil was discretized and "h"(m) the correspondence which solves the direct problem, the aim of the inversion is the search of the "m*" vector reproducing the measures "d":

$$D = h\ (m^*)$$

The inverse problem is defined according Hadamard (Lai and Rix, 1998) an ill-posed problem:

- for all data the solution is not unique, i.e there is the possibility that there are more solutions, possibly infinite;
- the solution does not depend on a continuous manner from data.

Among the main methods used for solving reverse problems, there is the Gauss-Newton least squares method. To solve this problem is introduced the concept of regularization techniques, replacing the "misplaced problem" with an equivalent problem that it is stable (Tikhonov et al., 1995).

The algorithm that implements the Tikhonov regularization geoelectric inversion is the Occam algorithm. This algorithm produces a beveled pattern, compatible with the experimental data within a predetermined margin of error.

2.3 Time-Lapse Electrical Resistivity Tomography

The advantage of time-lapse measurements over a single and static survey is that the first provide a means of imaging of the subsurface properties, but also of the dynamic changes in these properties which, in turn, can provide information about ongoing subsurface processes. Time-lapse geophysical measurements have been shown to be successful in monitoring and understanding physical processes in the subsurface (Ramirez et al., 1993, 1995; Lumley 2001; Tsourlos et al., 2003; Singha and Gorelick, 2005; Lane et al., 2006; MacBeth et al., 2006; Anno and Routh, 2007). In a general way, time-lapse methodologies can be utilized to determine the rate at which a process occurs, define the volume of subsurface region affected by a particular process, and understand the complex interactions between various subsurface processes. Time-lapse is especially important for near-surface studies since the medium is more dynamic due to the proximity of the air-earth interface. This is highlighted by increase in time-lapse applications for near-surface geophysical problems (Day-Lewis et al., 2002, 2003; Singha and Gorelick, 2005).

Time-lapse geophysical measurements can help to enhance our understanding of a particular site but can also make more challenging the planning of temporal and spatial sampling schemes. Ultimately, the rate at which a process of interest occurs, determines the time required for data collection. Day-Lewis et al. (2002, 2003) demonstrate the importance of accounting for the finite time in data collection because data may be change fast and and, anyway, certainly faster than the ability to complete a subset of measurements when inverting time-lapse cross radar data from a tracer test.

Since there are long-term studies where the properties of interest vary over diurnal, seasonal, or over even longer time scales, in this type of investigations,

there is an adequate time to collect data with little concern as to short-timescale variations in the subsurface.

Electrical resistance tomography data are useful in imaging properties and processes associated with groundwater and unsaturated zone systems (Müller et al., 2003; Mohnke et al., 2006; Oldenborger et al., 2007a, b; Descloitres et al., 2007). The ERT data are sensitive to the subsurface geoelectrical structure, which is, in turn, sensitive to subsurface variations in water saturation and pore water salinity (Archie, 1942; Mualem and Friedman, 1991; Henry 1997; Ewing and Hunt, 2006). This makes ERT particularly useful for characterizing infiltration into bedrock, where conventional methods of soil moisture, fail.

De Franco et al. (2009) presented a new experiment of time lapse electrical resistivity tomography (ERT-TL) that aims to track the dynamics of the saltwater intrusion into the South bounding coast Venetian Lagoon. They developed a device maintained for about nine months starting from November 2005.

The system has acquired ten resistivity tomographies per day, five of them with high resolution with a spacing of 97.5m long ERT line and 2.5m electrodes, the other five tomographies are long 300m with an electrodes distance of 5m and with a depth up to 50-60m. A seasonal fluctuation of resistivity is observed, with the front of salt water that intrudes landward during the fall-winter season and moves back to the sea in the spring one. This experience suggests that the TL-ERT is a powerful technique to perform a multi-scale monitoring of contaminants in different time scales.

Kuras et al. (2009) have presented the results of a recent study in which they used controlled hydraulic experiments in two test cells at reduced field scale, in order to explore the limiting conditions for a process monitoring with cross-borehole ERT measurements. They investigated different strategies for a practical data acquisition and show that simple reorganisation of ERT measurement schemes can help to harmonize data collection with the nature of the monitored process. The methodology of automated time-lapse ERT was found to perform well in different monitoring scenarios (2D/3D plus time) at time scales associated with realistic subsurface processes. The limiting factor is

the finite time needed for the acquisition of sufficiently comprehensive datasets. Authors have found that, given the complexity of monitoring scenarios, it is possible to obtain typical frame rates of at least 1.5–3 images per hour without compromising image quality.

Lebourg et al. (2010) have conducted a temporal imagery of water circulation in a landslide by Electrical Resistivity Tomography (ERT) to identify, spatially and temporally, the relationship between rainfalls, consecutive water inflows in a sliding mass and induced resistivity variations. Their work is based on a multi-scale experimental approach applied on the "Vence" landslide (South-eastern France) which is characterized by a sandy-clay sliding mass on a marly limestone substratum mostly controlled by high rainfall events. The Vence landslide is considered as a translational landslide including 106m^3 of material, affecting an area large about 250m and long 350m, with a slope of 12°/14°. On the basis of obtained results, a permanent time lapse ERT survey was designed on a specific part of the landslide, coupled with water level acquisitions (piezometric levels) and rain fall events. The statistical analyses of all the physical parameters measured during the three months of investigation have shown strong correlations between rainfall, piezometric elevation and resistivity. Therefore thanks to the time lapse technique the results show an accurate resistivity/piezometric elevation answer that can be considered a precursor of the reactivation of the landslide.

The understanding of the structure of the large, deep-seated La Clapiere landslide system in South East French Alps have been improved using 3D-ERT, which characterized its geometry, as well as ascertain the locations and nature of slip surfaces and vertical drainage system (Lebourg et al., 2005; Jomard et al., 2006). The top of the landslide is a 120m high scarp that extends over a width of 800m at an elevation of 1600m. In addition, groundwater evolution was observed studying water percolating in shearing zones and along rock discontinuities over a period of six months within three repeat 2D-ERT surveys performed on La Clapiere landslide. Repeated 2D-ERT surveys were displayed as electrical resistivity profiles, utilizing a 2m electrode spacing, but were not

performed during landslide activity and were not temperature corrected. They highlighted the sensitivity of ERT in order to identify the importance of different flow paths.

Dahlin et al. (2014) have presented the results of a geoelectric monitoring, done to trace water transport during a three-year irrigation study performed on a willow coppice. The results proved the potential of this method to monitor changes in soil water and ion content as well as for imaging development of the plant root.

Chambers et al. (2014) have developed a geoelectric monitoring as a non-invasive tool in order to characterize and observe earth embankments. The work illustrates the possibility of monitoring seasonal changes in moisture content. Time-lapse inversion experiments show that the 3D effects are significant and, in particular, the water level changes result in a spurious near-surface layer represented by different images. The results were corrected considering temperature, soil moisture monitoring, geotechnical testing and core of the samples.

Chapter 3
Ground Model Development of Field Site

In this Chapter will be presented and critically discussed the ground model used to study the Case Pennetta landslide system and based on an integrated approach that regards geology, geomorphology, 2D geophysical and geotechnical properties.

The study was performed on a site which was previously investigated with geophysical techniques (Quagliarini et al., 2016). The aim of this site investigation is to consider the geoelectrical method used in the previous study and then apply it for the development of the landslide ground model.

Site-scale 2D ERT surveys, reported in Quagliarini et al. (2016) are accompanied by additional, high-resolution, 2D ERT images of the most active regions of the landslide. High-resolution ERT results are integrated with detailed core logging and direct calibration of field ERT survey results. These data were correlated with mineralogical laboratory analysis of clay minerales sampled from the landslide, and geomorphological maps. Geoelectrical techniques can be used also to understand temporal and spatial landslide hydrogeological processes (presented in Chapter 5).

3.1 Site Background

The Northern Apennines are a fold and thrust belt of complex origin and evolution and are the result of the collision between the Adria Plate and the European Plate, that was started in the Late Cretaceous with the consequent closure of the Ligurian-Piemontese ocean basin (Molli 2008).

The different spatial distribution of landslides reveals their close dependence from predominantly clay formations and structurally complex lithologies. In the Northern Apennines, intense and prolonged rainfalls were claimed to be as the main trigger factors; therefore reactivations of the large complex landslides occur especially in autumn and spring, when also the snowmelt (April) may locally contribute to the groundwater circulating within the slopes (Bertolini and Pellegrini, 2001; Chelli et al., 2006, 2015). Among trigger factors, also the erosion caused by rivers and earthquakes must to be considered, although a clear

correlation between this factor and the triggering of landslides was rarely observed (Tosatti et al., 2008).

The complex tectonics of the mountain chain determined the superimposition of many tectonic units containing heterogeneous and chaotic rocks characterized by poor geomechanical proprieties, which cause the strong tendency to slope movement. Moreover these rocks underwent deep physical and mechanical weathering during the cold periods of the late Quaternary, further increasing their susceptibility to landsliding. Since the early Pleistocene, large parts of the chain were involved in a generalized uplift (Bartolini et al., 1982; Carlini et al., 2016) that caused progressive deepening of the drainage pattern. The formation of steeply cut valleys lead to extensive slope instability (Figure 3.1).

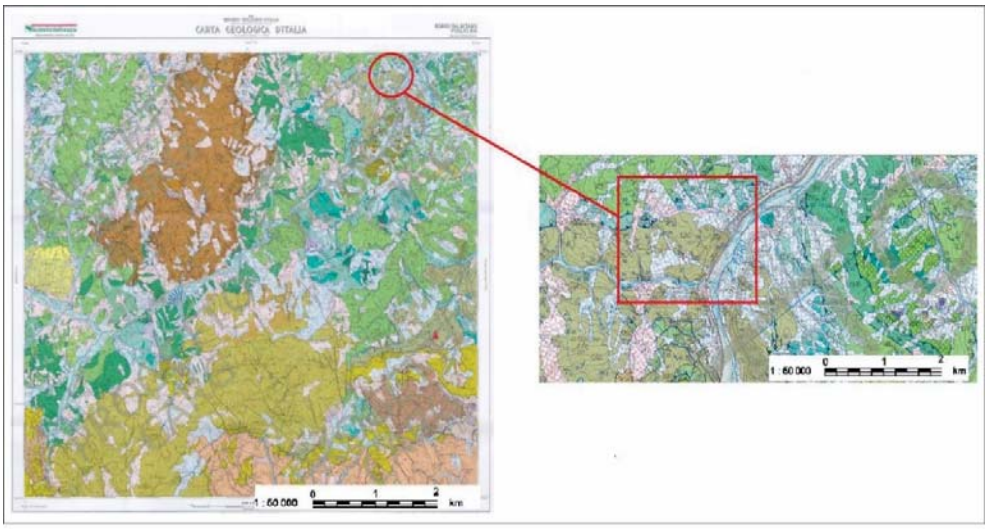

Figure 3.1. Geological Map of Italy, sheet N ° 216. (www.isprambiente.gov.it).

3.1.1 Climatology

Climatic conditions are studied by collecting rainfall data from ARPA site of the Emilia-Romagna region, which show the trends starting from 1991 to 2008 (Figure 3.2). As is shown in Figure 3.2, in the area of interest the setbacks were very intense, as also demonstrated by the average annual values that are between 1000mm and 1600mm.

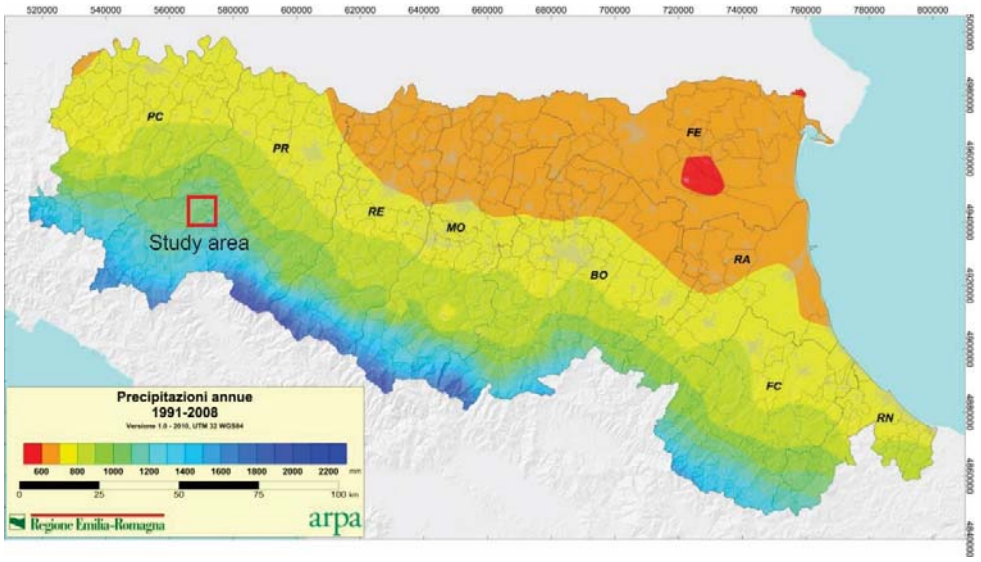

Figure 3.2. Rainfall patterns from 1991 to 2008. The ares of study is enclosed inside the red square. (www.arpae.it/).

In order to monitor the weather conditions, in particular rainfall in the area of Case Pennetta landslide, it was installed a weather station in the month of December 2015 (NESA s.r.l. Environmental monitoring systems, Figure 3.3); this was placed in the header area of the Case Pennetta landslide, near the Pennetta village.

3.1.2 Weather Station

A weather station measures rainfall, temperature and humidity of air and soil, located at 44°35'44.80"N - 9°53'38.89"E (Figure 4.1).

The weather station was installed in order to obtain reference data (Figure 3.3). It was purchased from NESA LTD (Environmental monitoring systems and remote controls) and consists of:

- a heated pluviometer (max 150W) in accordance with WMO class A with a collection mouth of 400cm^2;
- a sensor for combining measurements of air temperature and humidity, in accordance with WMO;

- a multichannel data logger mod. TMF100 Linux and a web server on board with 8 analogic inputs, 4 digital inputs, 4 analogic outputs, a display for data view and an internal battery charger with a direct input from solar panel. Server consists also of internal (32MB) and external (2GB on pen-drive USB) memories.
- a supply system that consists of a primary network with a mognetometric protection switch and a photovoltaic panel.

Figure 3.3. Position of the weather station installed at the Case Pennetta field site.

3.1.3 Geology

The Case Costa-Case Pennetta landslide complex is located near the confluence of the Mozzola Torrent and Taro River, as shown in Figure 3.4. The outcropping rocks are part of three different tectonic units (Ligurian Domain) Media Val Taro, Ottone and Mt. Caio units. Landslides cross the boundaries of these three units: the source of landslides material is mainly developed from Media Val Taro; this unit includes of Arenarie di Scabiazza (SCB; Coniaciano-Santoniano) Formation that consists of an alternation of fine and medium laminated sandstone, shales and grey-clay marl, and Argille a Palombini (APA; Hauteriviano-Aptiano) Formation that consists of beds of clay argillites intercalated with micritic grey limestone. Mt. Caio Flysch (CAO; Higher Campaniano-Maastrichtiano) Formation is constituted by a turbidite of

limestones and marls, intercalated with laminated grey sandstones, while the Argille a blocchi (ABC; Lower Campaniano) Formation, within of the Casanova Complex, consists of blackish clay with clasts of whitish calcilutites, serpentinites, basalts and laminated sandstones, alternating with calcareous-shales and marl (Geological Map of Italy, Borgo Val di Taro 216-1:50.000).

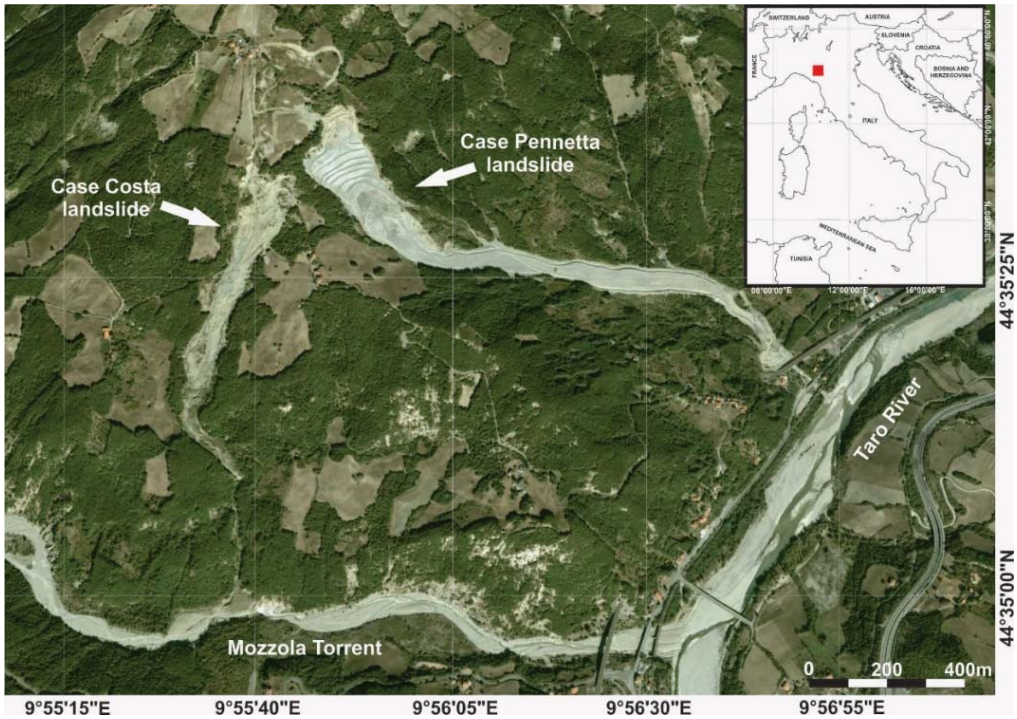

Figure 3.4. Case Costa and Case Pennetta location map (Parma, Italy). Google Earth image.

As mentioned above, the source of Case Costa-Case Pennetta landslide system is represented by Arenarie di Scabiazza Formation. The current configuration of the middle portion of Taro Valley is the results of the presence of differentially uplifted zones within the less uplifted areas (Bernini et al., 1997). Along the valley the latest tectonics are represented by high-angle extensional faults (exposed SE of the Taro River system, Vescovi 1988; Argnani et al., 2003) that give rise to prominent morphological features with three main orientations. Most of these are NW-SE-oriented following the strike of the belt, while others are

SW-NE oriented and, in some cases, the orientation becomes N-S (Carlini et al., 2016).

3.1.4 Geomorphology

Fieldwork carried out by the visualization of the main forms was initially performed by picking out slope features, such as changes or breaks in slope and sag ponds. Therefore, a georeferenced shape file (.shp) that could be imported directly into ArcGIS10 is created and interpreted. Once all geomorphological surface features are picked and catalogued in ArcGIS10, are interpreted in terms of landslide type, activity and distribution.
Identified landslide features include main and secondary scarps, head, crown and toes.

3.2 Methodology

Landslide system considered in this work, presents a remarkable complexity from the point of view of the variables involved, such as lithology, changes in the physical properties inside the landslide body, the soil mineralogical composition and groundwater levels. In order to realize a model able to handle the large number of variables which simultaneously are subjected to change, is necessary to put a control on lithology, by assuming that the monitoring site is installed within the same geological formation, i.e. Arenarie di Scabiazza Formation. For these reasons, Arenarie di Scabiazza Formation is characterized also by a mineralogical point of view (mineralogical analyzes are carried out on samples taken from Si1 and Si2 boreholes).

3.2.1 Surface Characterization

In order to characterize the landslide system investigated, some different data survey were done before the final choice of the site suitable for installation of the future geophysical monitoring system: i) a geological survey, in order to

ascertain the tectonic, lithological, geo-mechanical conditions; ii) a geomorphological survey, in order to represent erosion and accumulation forms that interest the slope; iii) a geophysical survey, in order to individuate and characterize possible buried sliding surfaces and preferential pathways of groundwater flow, and to understand how physical properties change within the investigated mass.

Case Costa and Case Pennetta landslides system was chosen for three reasons: i) absence of reclamation works that made invalid geophysical and geomorphological data; ii) activity of the landslide (as testified in the past by monitoring system) characterized by movement rates of the order of cm/y, in order to preserve the instrumentation that would be installed; iii) the potential relevant social impact that this landslide system represents, because they threaten two important communication networks that travel along the Taro Valley, as the Parma-La Spezia railway and the SS308 main road. Firstly, geological and geomorphological surveys were performed: therefore, it is possible to acquire and define the outcrops and the landforms to gain information on landslide types and on state, style and distribution of activity suitable for the planning of the geophysical, geotechnical and hydrogeological monitoring system. Based on these information, ERT survey configurations were designed with the aim of identifying preferential surface groundwater flow pathways and deep water associated with slope instabilities.

Based on geological and geomorphological data, the acquisition system of geophysical data was projected: the device used to obtain electrical tomographies consists of cable with lengths of 235 meters and consistuted by 48 electrodes with a spacing of 5 meters. In order to investigate the area between the two landslides a 960m pole-dipole ERT was installed (Figure 3.5). ERT array is sensitive to lithological heterogeneity, temperature and soil moisture content (Chambers et al., 2011a; 2011b; 2014, Shevnin et al., 2007).

In order to reconstruct the stratigraphy of landslide body, the coring Si1 (-35m m.s.l.) and Si2 (-30m m.s.l.) were carried out and data derived from core samples were then interpreted and compared with geophysical data (Figure 3.5).

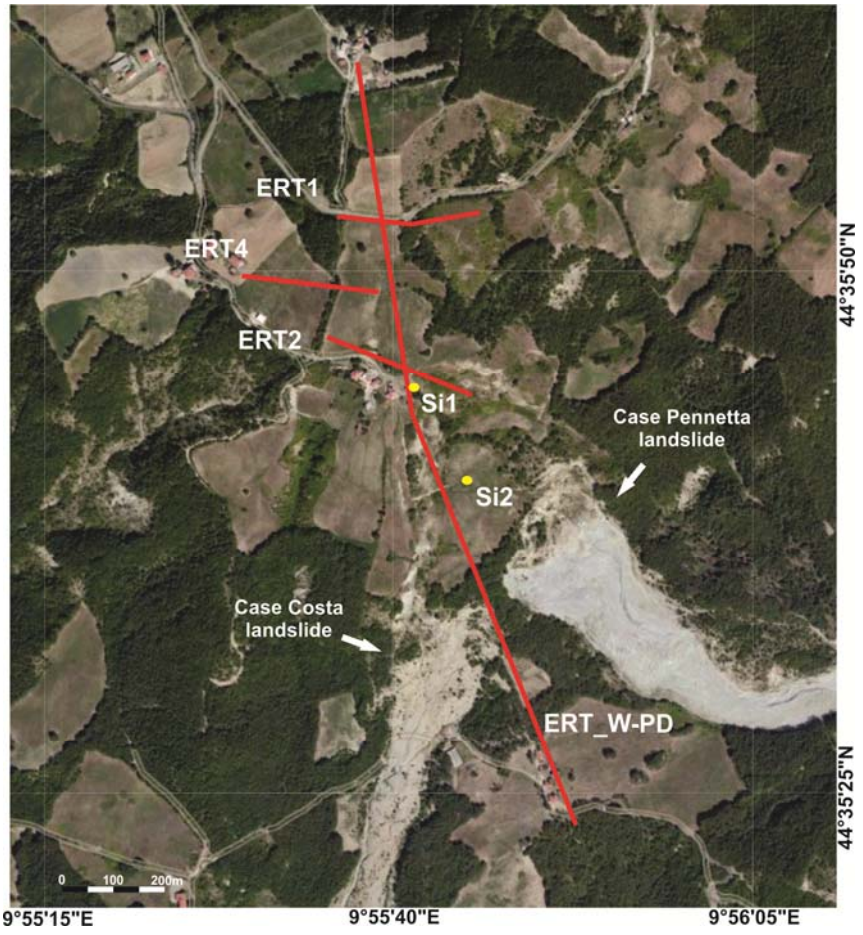

Figure 3.5. Map of the research site with the locations of monitoring equipment electrodes and identification names. (Google Earth image).

A mathematical inverse problem is solved to determine the subsurface distribution of resistivity from measurements of apparent resistivity performed at the surface (Loke et al., 2002). Inverse modelling of resistivity datasets find a subsurface model that gives a similar response to the observed apparent resistivity field measurements. Therefore, the model produces an idealized mathematical representation of the subsurface resistivity distribution that mostly agrees with field apparent resistivity measurements within certain restrictions. The model has a set of parameters that are the physical quantities we want to estimate from the observed field data (Loke 2002).

The inverse problem is solved in four stages. Firstly a forward model is developed starting from a homogeneous half-space. Secondly, the homogeneous

half-space is adjusted by creating synthetic apparent resistivities which are then compared to measured field data. Finally, apparent resistivities are adjusted and the model iteratively improved, in order to minimize the difference between the forward model and field data. Modelling process ceases when the model has a sufficient fit with field data (Dahlin and Zhou, 2004).

The software used in this PhD project is *ERTLab*^{TM} (by Multi-Phase Technologies and Geostudi Astier srl, Livorno, Italy). It consists of the resistivity and IP inversion modules that offer full three-dimensional topographical modelling and inversion. Its numerical core is based on tetrahedral FEM and allows to input complex topographic information; furthermore it inverts data set collected by using surface, borehole and surface-to-hole array configurations. Despite the aim of the inversion methods is to find a model whose response is equivalent to the set of measured data, it is never unique. Criteria for choosing the inversion methods in the range of models that approximate the actual data, is to minimize the difference between reality and model, that is quantified by the standard deviation. For each iteration we can try to minimize the reciprocal of vector of discrepancy and smoothing matrix, also called roughness of the resistivity model, which corresponds to the spatial changes of the square (Loke et al., 2002). This produces a model with a smooth variation of resistivity, valid when the resistivity of the subsurface varies gradually. It is possible to modify this method by changing the elements of the matrix, in order to emphasize vertical and horizontal variations of the resulting model, or, if data are much noise, you can weight the data using the weighting matrix. A finite-difference (Dey and Morrison, 1979) or finite-element (Silvester and Ferrari, 1990) forward modelling approach provides the mathematical link between these two values and is optimized in an iterative manner to minimize the sum of least-square error between model parameters and data (Day-Lewis et al., 2002).

Stratigraphic analysis, associated index testing and laboratory test, were combined with the two-dimensional electrical resistivity tomography. Moreover, by performing index testing and additional laboratory sample analysis it is possible to calibrate 2D ERT images- which suffer the issue of non-uniqueness

- in terms of geological formation and internal structures. The results of index testing and laboratory sample analysis are implemented to confirm what was achieved by ERT images.

3.2.3 Surface Expression

The geomorphological map produced at Case Costa-Case Pennetta landslide shows the distribution of landslide features, breaks in slope and other landforms throughout the field site.

Case Pennetta landslide originates at an altitude of 650m m.s.l. reaching the water course of Taro River at an altitude of 265m m.s.l.. Case Pennetta landslide shows a length of 1600 meters and a maximum width of 130 meters.

Case Costa landslide has, instead, a maximum length of 1300 meters with the main scarp located at 575 meters m.s.l. and reaches the thalweg of Mozzola T. at an altitude of 275 meters m.s.l.. Case Costa landslide presents an average width of 60 meters (Figure 3.6 - see, for more details, Appendix A1).

Case Pennetta landslide shows scarp with a climb of 50 meters and subject to continuous changes in time: there are fresh landforms completely lacking of vegetation. According to the identified geological and geomorphological features, Case Pennetta landslide is characterized by a roto-translational type movement. From the scarp, earthflows of Case Costa and Case Pennetta arise and then reach the riverbed of the Mozzola Torrent and Taro River, respectively. The two landslides are a series of elongated bodies in the direction of the maximum slope, and appear characterized by a roughnes surface due to flow structures oriented both in transverse and longitudinal directions.

The geological and geomorphological map of Case Pennetta is shown in Figure 3.6. In the north of the site there is an abrupt increase in slope angle that indicates the presence of the main scarp along with crown cracks, despite the landslide continues to move backwards. The backwards tilt of the head of the landslide is suggestive of slumping. Although the north-east region was seen to be the most active, the main scarp can be traced east-west across the site.

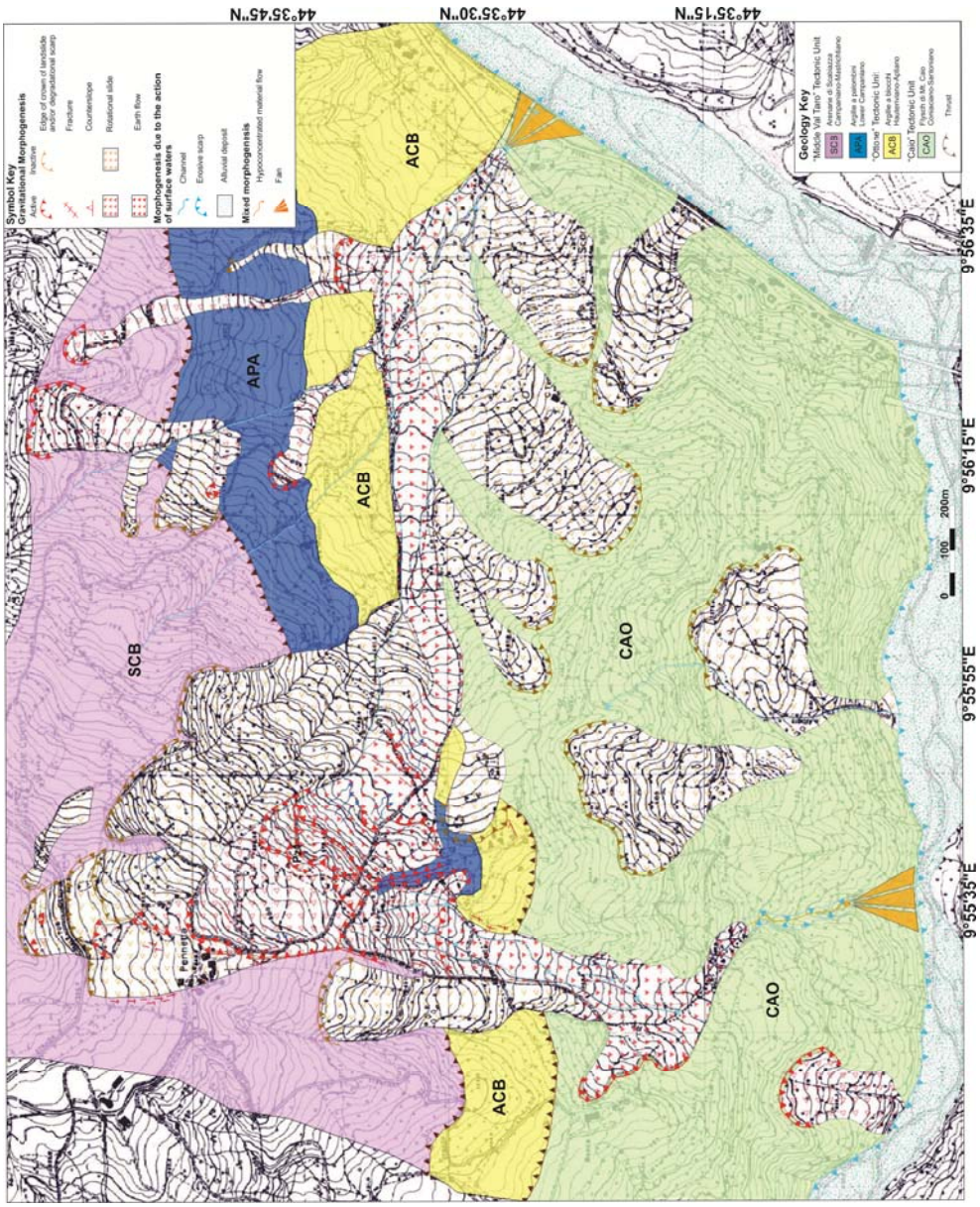

Figure 3.6. Geological and geomorphological map of the study area (presented using *ArcGIS 10.3*). Coordinate system is WGS84 UTM32N; for more details see Appendix A1.

Evidences of differing movement patterns are between the eastern and western area of the landslide. The northern region of the site has more visible fresh slumps than the west and this suggests that the northern area experiences slump activation more frequently and more recently if compared with the west part of the site. Slumps in the west site appear less frequently active; this is due to the

lack of fresh surfaces and the presence of more weathered, degraded appearance and morphology.

The main geomorphological expression of landslide evolution is the transfer of mass from denudation to accumulation areas. Soil denudation is due to the erosive action of water, and also as a consequence of slides and other mass movements. The mass movements are able to transfer considerable volumes of slope materials downslope under the action of gravity, and play an important role in the shaping of landslide features (Cendrero and Dramis, 1996).

Past activities of the Case Pennetta landslide date back to the early years of the last century. Beginning in the early 1900s, periods of activity were interrupted by inactivity phases. The phases in which the landslide body was subjected modifications date back to 1935, 1967, 1997 and 2001. In particular, the activity of 2001 was preceded by intense rainfall events that caused a reactivation of the landslide body which, in turn, caused damage to some of the railroad pylons connecting Parma-La Spezia.

The accumulation in the foot areas destroyed the Mezzoni Rio (north of the main casting) and a second southermost (unnamed) rio.

According to the information found in the archives of Servizio Tecnico dei Bacini degli Affluenti del Po (Basins Technical Service of Po Tributaries), the movement of 2001 caused a shift of the railway pylon of about 10m.

Case Pennetta landslide foot was put in security with works carried out in 2001 and is stabilized in the upper part of the landslide. In this area, for the presence of these important communication routes and after the event of 2001, during which the bridge of the highway was damaged and the railway was temporarily closed, works of making safe and cleaning up of the collapsed material were conducted. Case Pennetta landslide has a generally steep surface that delimits the undisturbed area which surrounds the upper part of the landslide originated by the loss of material slipped further downstream under the effect of gravity (Figure 3.7). In the northern area of the geomorphological chart, in the upper landslide sector, the main morphological element is a large perimeter scarp about 200m, over 35-45m high and bordering the most active area. The overall trend

of the scarp is about northwest-southeast. The average slope of this part of the scarp is about 45°-55°, the northwestern part of the scarp is steeper than the southeastern part. The mobilized material is collected in an almost flat area, located at the scarp's base, where its primary features are progressively lost and, owing to water absorption, it turns into a rather viscous mud.

Figure 3.7. Case Pennetta main slope. (View from Case Costa Village).

Further west of the main scarp, it was identified a second scarp (Figure 3.8), which indicates a reactivation of the slope and an enlargement of the Case Pennetta landslide towards the Costa Costa landslide; this has the size of about 35 meters in length and a height of about 20 meters.

Figure 3.8.Enlargement of the main slope of Case Pennetta.

In the upper part of the landslide body was identified an intermediate scarp which has a length of 70 meters and a height of about 5-10 meters; it is probably due to a likely morphological step below the blanket of detritus (Figure 3.9).

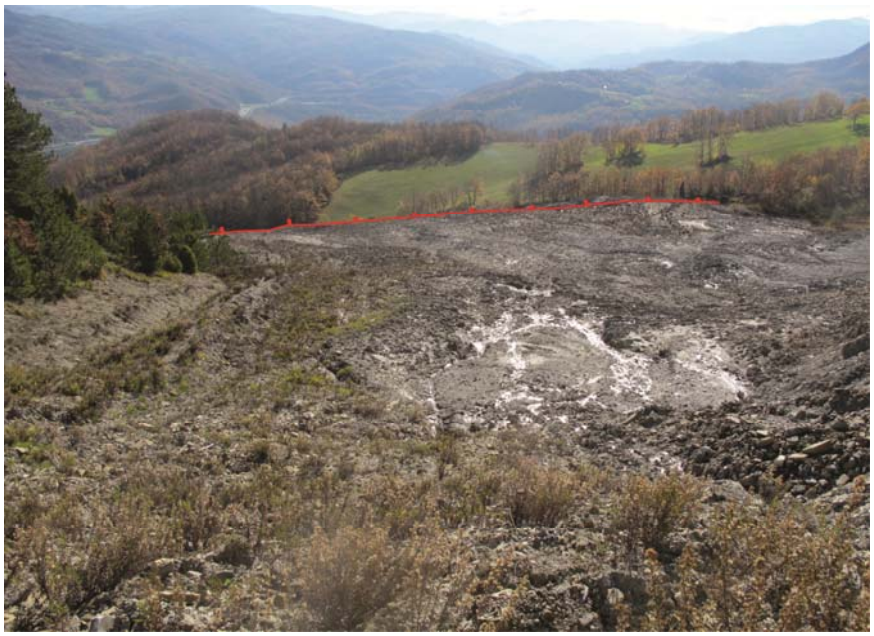

Figure 3.9. Taro Valley view from Case Pennetta main scarp.

In the area are present counterslopes of the ground that have an opposite slope respect to the considered slope, particularly in the main slope area of the landslide body (Figure 3.10). From 460m m.s.l. to the foot of the earthflow, along the south side, there are some landslide movements collected in the main body of Case Pennetta landslide.

Figure 3.10. Counterslope upstream the main scarp.

Fractures (Figure 3.11) and the areas surrounding the landslide body and representing the earthflow side portions, were mapped in the upstream of the main slope area. The uppermost fractures that have been mapped in the upper part near the village of Case Pennetta, have a variable length from about 1.5-2.0 meters and a width of about 30-40cm. Fractures are tension cracks and normal faults, both indicating stretching. The landslide material in the area of the fractures is a powdery clayey silt to silty clay that does not preserve fractures well. The features produced are caused by stretching and thinning of the ground in the upper part of the slide as well as in ground uphill from the slide. The most common fractures include tension and collapse cracks with their long axes

oriented in the same direction of movement. Several features that have the appearance of long linear furrows are interpreted to be depressions above tension cracks that opened at depth and propagated to the surface as collapse features.

Figure 3.11. Fractures in the upper part of the landslide body, near Case Pennetta village.

The earthflow source area is about 1415m long from 570m (m.s.l.) to 250m (m.s.l.). Throughout its length, the flow can be subdivided into three parts: the first from 570m (m.s.l.) to 450m (m.s.l.) and 280m orientated NE-SW long; the second from 450m (m.s.l.) to 320m (m.s.l.) and 705m long oriented E-W, and the third that reaches the Taro River from 320m (m.s.l.) at a height of 250m (m.s.l.) and that is 430m long orientated NE-SW. This latter part is the narrowest part of the landslide, where the flow is forced into a space of about 40-50m. The earthflow shows deposits with heterogeneous composition, consisting of variables size pebbles (from metric to centimetric), within a matrix (fine and very fine, Figure 3.12). Deposits are derived from the rocks weathering, belonging to the Arenarie di Scabiazza Formation that outcrops in the area.

Figure 3.12. Earthflow area of Case Pennetta landslide body.

As shown in Figure 3.13, In the upstream of the main escarpment is present a second scarp, characterized by recently activities, as evidenced by the presence of fresh shapes and lack of vegetation. This scarp extends for a length of about 70m and for a height of approximately 15-20m.

In the downstream part of the landslide body, the material is channeled in a natural watershed, until it is reached the main road SS9 and the railway Parma-La Spezia in the proximity of the Taro River. The entire area should be the foot of the landslide, but it was completely anthropized and is difficult to recognize depositional forms.

The erosive activity due to the sliding of surface water, is visible both on the landslide body and in upstream area, near Case Pennetta village. In the study area, ditches and cracks in the ground along which the water flow focuses, especially during heavy rain events, were mapped. These forms are originated along the landslide and in the northern area of the chart, and reach an approximately depth of 10-20m in the high part of the slope and about 1.5-2m upstream of the main scarp. Traces of surface runoff were also mapped; they are located in the northern part of the landslide body and are caused by the rainwater flow on the ground surface that being visible as a soil superficial collapse.

Figure 3.13. Secondary scarp under Case Pennetta village.

3.3 Subsurface Characterization

3.3.1 Core Logging

The subsurface characterization was performed in order to study the most active part of the landslide system within the field site, because exhibits the freshest landslide features, i.e. sharp crown and a main scarp with lightly vegetated flow deposits. The campaign was carried out during January 2016 (from Grendi s.r.l., Solignano, Parma) by a geotechnical drilling and using two boreholes advanced to a depth of 35m (Si1) and 30m (Si2) (see Figure 3.14).

Data obtained from Si1 and Si2 boreholes show a little consolidated predominantly silty-clay component with the presence of different sized clast.

In Si2 core, the bedrock was found at a depth of 25 meters (b.g.s.)

Based on geophysical and coring data, we have assumed a thickness of landslides material between 25 and 30m (b.g.s), mainly consisting of very wet clay, silty-clay with presence of clasts with dimensions from centimeter to meter.

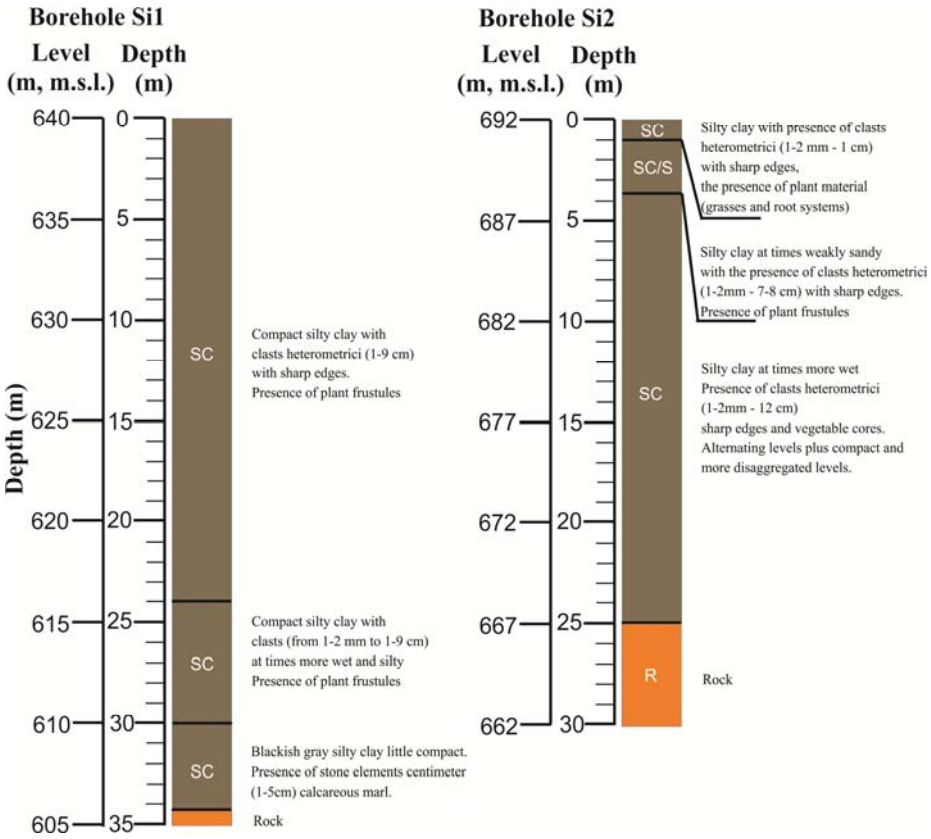

Figure 3.14. Si1 and Si2 core logs are interpreted in term of landslide deposit type (the position was reported in Figure 3.3).

3.3.2 Standard Penetrometer Test

A Standard Penetrometer Test was performed in Si1 core from Grenti S.r.l. (Solignano, Parma) during the drilling phase, at the depth of 9m and 19m (b.g.s.). Results obtained gave the following average values:

$N_1 = 9$
$N_2 = 11$
$N_3 = 17$
$N_{SPT} = 28$

3.3.3 Permeability Test

Permeability (k) in Earth Sciences and Fluid Mechanics is a measure of the ability of a porous material (often, a rock or an unconsolidated material) to allow passing of the fluids through it. In order to obtain the soil permeability

measurements, four tests of variable load permeability within the borehole Si2, were carried out. The variable load test, carried out within the site, have allowed to measure the local permeability coefficient of the ground, for many layers thick at the base of the borehole.

The test is divided into two phases: i) in the first phase a filtering section at the base of the hole was arranged; ii) subsequently, a hydraulic gradient between the internal part of the hole and the groundwater level, was produced. The hydraulic gradient is made to vary over time after an initial rise of the water level inside the core, compared to that of groundwater.

In this manner the coefficient of permeability K was calculated from Darcy's Law and considering the geometry of the filter base, through a CF form coefficient, and the values of the groundwater level inside the hole as a function of time.

The values obtained and the formulas used are described in certificates issued by Grenti S.r.l. company in Appendix A2.

3.3.4 Mechanical Characterization of Samples

Four samples named Si1A (10.30-10.63m, b.g.s.), Si1B (16.50-17.00m, b.g.s.), Si2A (6.70-7.30m, b.g.s.) and Si2B (8.20-8.80m, b.g.s.), were taken during drilling operations, with the aim of reliably assessing the mechanical parameters of the soil.

Tests were performed on undisturbed samples of Case Pennetta landslide, after the extraction of them from their frames by means of the extruder. Firstly, a visual analysis was made: the homogeneity in relation to its entire length, the presence of frustules of vegetable origin and the color were described, using Munsell tables (Munsell Book of Color-Matte Finish Collection). Secondly, on sediment cores, the pocket test to determine the resistance to penetration was performed (Appendix A3). Subsequently, in order to evaluate the texture of the soil, physical analysis were conducted: i.e. granulometrical analysis which involves the step of dry sieve and the step of sedimentation with a hydrometer,

and water content analysis; were also determined the specific weight of the grains, density and Atterberg limits using the Casagrande spoon. The direct shear test was then performed with the use of reconstructed samples.
Furthermore, for the same reason why it was not possible to perform tri-axial tests, it was decided to execute a free lateral expansion test on one sample, then used as a reference for the evaluation of the resistance to the undrained shear.

3.3.5 Granulometric Curve

Results obtained after tests, were reported in a semi-logarithmic graph that shows, in the ordinate (natural scale), the percentage P% of material smaller than a certain diameter (passer), and in the abscissa (logarithmic scale to decimal base), the corresponding diameter *d* in millimeters.
The legislation provides for the correction of the first two sedimentation values to 60s and 1min, respectively, for the soils that have a consistent quantity of gravel, in order to make the performance of the more continuous curve.
The final certificates for this test were prepared for each sample (Si1A, Si1B, Si2A, Si2B) and contain, in addition to the grading curve, the division of the land as a percentage by pebbles (diameter> 60mm), gravel (diameter between 2-60mm), sand (diameter of between 0, 06- 2mm), silt (0,002- diameter of between 2mm) and clay (diameter <0.002mm).
The graphs obtained are described in Appendix A4.

3.3.6 Atterberg Limits

The determination of the granulometric curve allows to get information on the sands and gravels but nothing on the features of the fine portion (clay), and the type of minerals contained in it. Mechanical behavior of the ground depends on minerals which determine water content that tends to be absorbed by particles and, therefore, the strength of the bond between water and ground.
The graphs obtained are described in Appendix A5.

3.3.7 Casagrande Plasticity Chart

Fine-grained soils can be classified by entering values obtained by Atterberg limits, within the Casagrande Plasticity Chart (Casagrande 1948; Figure 3.15). This is divided into six regions by three straight lines:

- the straight line A identified by the equation: $I_p = 0.73 \cdot (W_L - 20)$;
- the straight line $W_L = 30$;
- the straight line $W_L = 50$;

The soils that are above the straight line A relates to inorganic clays and are divided into three types with low, medium and high plasticity.

The soils that are below the straight line A are divided into:

- inorganic silts
- organic silts
- organic clays

As is shown in Figure 315, the four samples studied in this work were reported within the Casagrande Plasticity Chart.

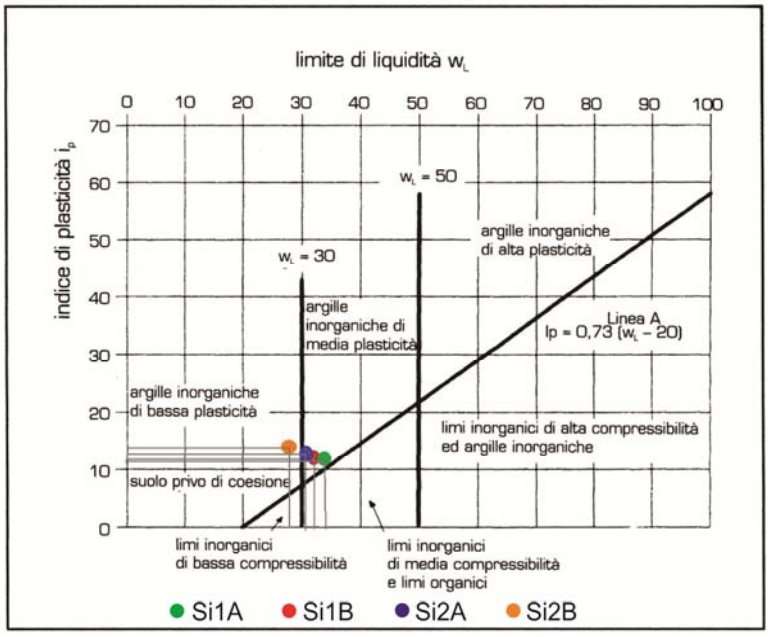

Figure 3.15. Casagrande Plasticity Chart and classification of the four soil samples (Si1A, Si1B, Si2A, Si2B).

Moreover, the USGS classification (Unified Soil Classification System) which is developed by Casagrande, shows that samples can be classified in inorganic clays with medium-low plasticity, as reported in in Figure 3.16.

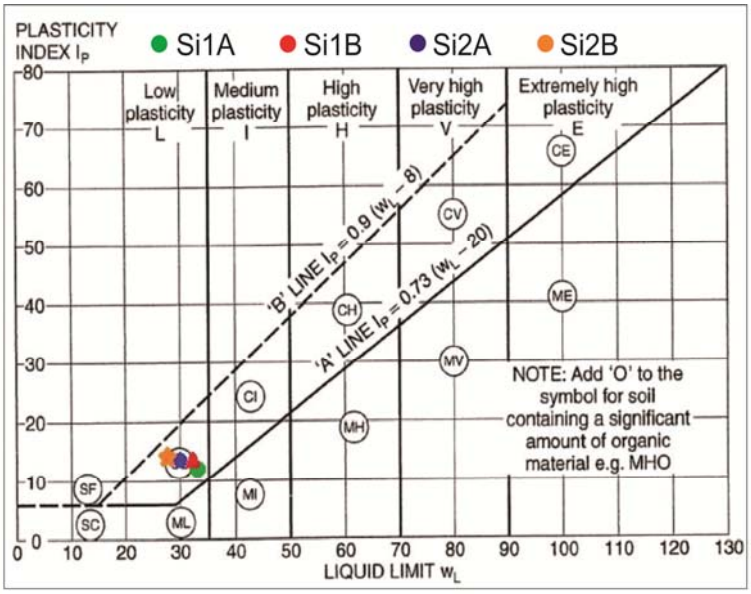

Figure 3.16. USGS classification of the four samples Si1A, Si1B, Si2A, Si2B.

3.3.8. Direct Shear Test

The direct shear test is a laboratory testing methods used to determinate the shear strength parameters of the soil. Results of different tests for the same soil are presented in a chart with peak stress reported on vertical axis and normal (confining) stress reported on the horizontal axis. A linear curve fitting is often made on the result test points. The intercept of this line with the vertical axis gives the Cohesion and its slope gives the peak friction angle.
The graphs obtained are described in Appendix A6.

3.3.9 Mineralogical Soil Composition

The close association of landslide phenomena with the clay minerals has led to an investigation of their mineralogical composition. The widespread presence of clay minerals in the rocks, with chaotic structure, results in a strong surface

degradation. Clay minerals easily absorb water modifying their physical structure, resulting in a decrease of the resistance between the particles. Since the matrix material of the chaotic unit is particularly unstable, an attempt was made to determine its mineralogical characteristics. Tests were performed on the four selected samples Si1A, Si1B, Si2A and Si2B (Table 3.1).

ID sample	ID Core logging	Depth (m, b.g.s.)
Si1A	Si1	10.30-10.60
Si1B	Si1	16.50-17.00
Si2A	Si2	6.70-7.30
Si2B	Si2	8.20-8.80

Table 3.1. Undisturbed four samples used for mineralogical analysis.

Powder X-ray diffraction was performed by using a Bruker D2 PHASER diffractometer equipped with a solid-state thermo electron detector, operating with CuKα1 radiation (λ= 1.5406Å) and installed at the Department of Chemistry, Life Sciences and Environmental Sustainability (Earth of Sciences Building), University of Parma, Italy.

Samples selected for X-ray diffraction were prepared by grinding them in a porcelain mortar until the material passed a 230 mesh screen. Clay mineral composition was determined by X-ray diffraction, using a SIEMENS automatic unit. The aggregates were analyzed at room temperature, after a special treatment with blue methylene.

As is shown in the diffraction pattern of Si1B sample (Figure 3.17), it contains montmorillonite and illite, in order of decreasing abundance. However, mineralogical characterization of the samples revealed a heterogeneous composition. The material can be characterized as a clastic formation which consists of thin, tectonically disturbed alternations of clayey, siltstone and sandstone with minor limestone inclusions. It is mainly composed by grainy and lamellar minerals including quartz, feldspars, calcite, chlorite, muscovite,

biotite, illite and montmorillonite, in various proportions forming a fine layered and granular texture.

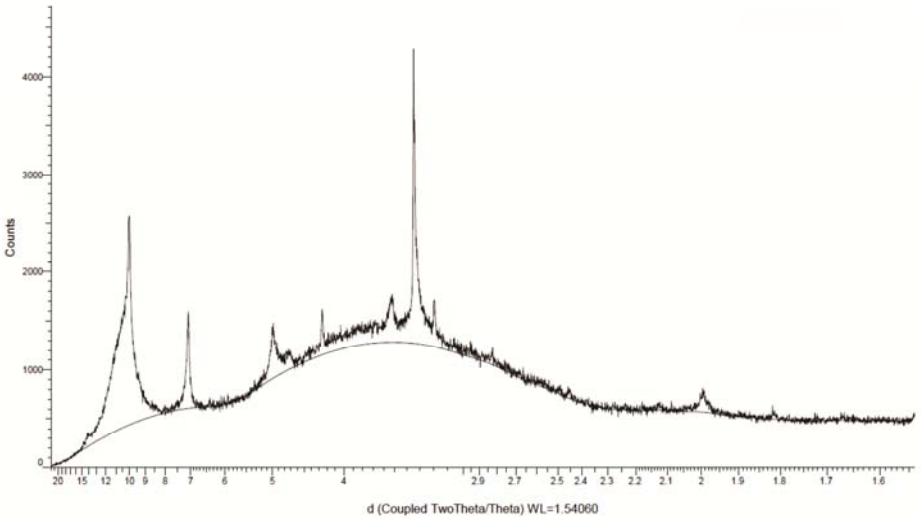

Figure 3.17. X-ray diffraction patterns of Si1B sample.

3.3.10 Geoelectrical Characterization

Geoelectrical methods such as ERT can be usefully applied in order to perform landslide investigations where it is necessary to provide information of the ground and when several lithological formations with constrasting values of resistivity, are present within the area of interest.

The investigation presented here provided a high level of detail about the subsurface conditions within the hill slope by drawing upon many complementary information streams. Wherever one data set is lacked of the ability or resolution necessary to inform about a feature or property, another data set could be used to provide such information. An example that can be considered is the inability of the large-scale ERT, to differentiate between mobilized material and in-situ material.

The choice of the location of the monitoring system can be mainly made on the basis of data obtained from geoelectric surveys.

The interpretation of geophysical data have highlighted low resistivity contrasts, from 15 to 75Ωm, and therefore have indicated a poor lithological variability that goes from wet clay to more dry clays.

Globular anomaly of high-resistivity between the electrode 15 and electrode 24 in ERT_1, probably concern a body made by debris within wetter clayey sediment. The low resistivity body in ERT_4 with values from 15 to 20Ωm, is related to a channelized groundwater flow in fractured zones. This groundwater circulation pattern is typical of this grain size. The body with more high resistivity anomaly (25-30Ωm), can be connected with the anomaly of ERT_1 section between electrode 15 and electrode 24, thus represents a debris body within wetter clay. The ERT_2 shows two low resistivity rounded bodies near the houses of Case Pennetta (Figure 3.18), which probably indicate the preferential surface and deep water pathways.

Data of core Si1 and Si2 samples, made in this area to better constrain and interpret geoelectric data acquired by monitoring system, shows a little consolidated predominantly silty-clay component with the presence of different sized clasts. In the Si2 core the bedrock was found at a depth of 25 meters (b.g.s.).

Based on geophysical and coring data, it is possible to assume a thickness of landslides between 25 and 30m, mainly consisting of very wet clay, silty-clay with presence of clasts with dimensions from centimeter to meter. This hypothesis is also confirmed by geophysical data that provide information on water circulation pathways in the survey area. Zones characterized by low resistivity values are probably associated with the water circulation within the debris deposit. The low apparent resistivites observed in the monitoring area suggest that groundwater circulation may be relatively shallow, i.e. until 15m (b.g.s.). Probably this groundwater characterizes the area from the higher part of the slope up to the earthflow source area, where water flow out in numerous springs and possibly continues into the body landslide, downstream to the Case Pennetta village.

Laboratory results of mineralogical analysis indicate a close correlation between landslide phenomena within the chaotic unit of the Pindos flysch Formation, and the existence of clay minerals. Expandable minerals like montmorillonite are present within the fine grained matrix of the Pindos flysch Formation. Semi-quantitative mineral analysis indicates proportions as high as 10% for montmorillonite. These minerals have the ability to exert expansive pressures. Small percentages of swelling clays can cause relatively great increases in the plastic properties of the material. The structure of montmorillonite is such that, when it is interlayered with other clay minerals, it forms planes of weakness that permit a breakdown of the clay particles with an attendant great increase in plasticity. Smectite absorbs water between the individual silicate layers with resulting high swelling. Illite and chlorite comprise the bulk of the clay minerals present. Clays, in general, exert a significant influence upon the Atterberg limits, swelling properties, water adsorption and shrinkage of the material. The water adsorption and the repeated swelling-shrinkage process of clays facilitate the cracking and deterioration of the rock mass, changing the physical characteristics and mechanical behavior of the host material. The rock surface thus, becomes much more sensitive to weathering, lowering its durability value. Continuous evolution of this process results in decomposition of the exposed rock and the formation of a surface cover that becomes very unstable, so that landslide phenomena start to generate under favourite climatic conditions.

A preliminary inspection of ERT_W-PD allow us to obtain resistivity images and to identify resistivity values lower than 50Ωm. The images show a good homogeneity of the near surface material and presence of clay lenses that can be associated to lateral and vertical boundary of permeability; as shown by the stratigraphic analysis, this could affect the groundwater pathway and circulation of the slope. Moreover, the very low apparent resistivity values (from 10 to 30Ωm) observed at a depth ranging from 1m to 25m (Figure 3.19) in the inverse model resistivity sections, could correspond to the landslide material which is characterized by clay, weathered marl, and water. The conductive zone has an irregular shape and could correspond to the mobilized body but could be also

related to more consolidated portion of landslide body (material typical of the Arenarie di Scabiazza formation).

Elongated zones of lower resistivity from 10 to 25Ωm, parallel to the ground surface, is interpreted as wet zones of clay material. Broad zones of low resistivity values under the profile ERT_W-PD are of particular interest for our interpretation and also for the future monitoring system. Several of these features can be correlated directly with landslide zones observed in the geomorphological survey, like the small landslides adjacent to the two main bodies of Case Costa and Case Pennetta (Figure 3.6). In literature there are several examples of correlations between low resistivity values and water-bearing fractures (Ramirez and Daily, 2001; Cavinato et al., 2006) that appear to influence the topography.

All the techniques mentioned above, allow to investigate the landslide and to develop the subsequent ground model, because each technique informs and directs the next technique to be utilized. It is generally good practice to start with surface characterization and geomorphological map production followed by subsurface characterization through the application of 2D geophysics and intrusive investigations.

According to the landslide morphology, characterized by a stepped slope profile, one traverse line was conducted approximately in the middle of the two landslides, using a combination of Wenner array configurations. We present results obtained from Wenner (ERT_1, ERT_2, ERT_4, Figure 3.18 and ERT_WPD) acquisitions between May and December 2015, but similar results were obtained also for other dates. Data showed a low variation of the resistivity values from 40 to 100 Ωm, that, in sedimentological terms, results in a poor lithological variability, being in the clay field.

The ERT_1 image resistivity profile (Figure 3.18) shows a layered sequence of low resistivityvalues ranging from 15 to 30Ωm (Low Resistivity Boundary, LBR) and medium resistivity material with values up to 50-75Ωm (High Resistivity Boundary, HRB). The first meters show values of 10-20Ωm. The landslide mass has a similar resistivity. The most interesting feature of the section is a globular anomaly of high-resistivity between the electrode 15 and

the electrode 24. The ERT_4 section highlights a low resistive body (from 15 to 20Ωm), and, in the central part of the section, a high resistive body (from 25 to 30Ωm). In the north of the Case Pennetta village, the section ERT_2 shows little variation in resistivity values, from 10 to 40 Ωm (LRB, Low Resistivity Body), with the presence of two bodies with resistivity between 30 and 40 Ωm, (HRB, High Resistivity Boundary) which are separated by a lower resistive body.

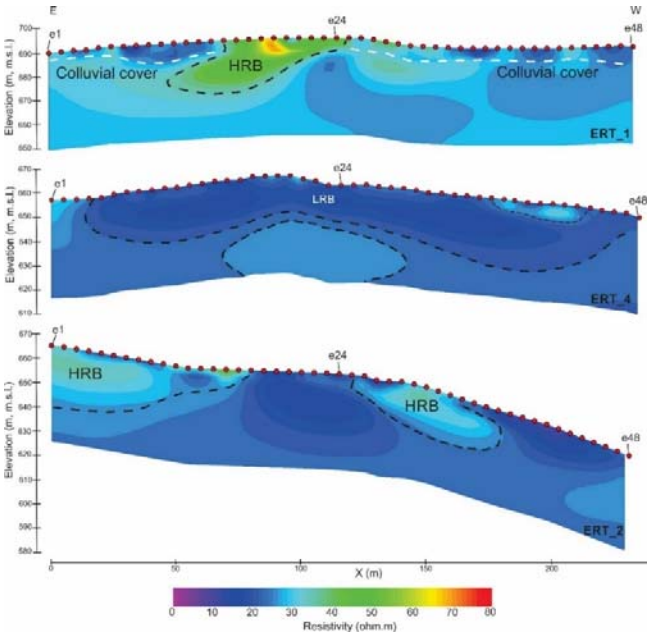

Figure 3.18. 2D image of resistivity obtained from the high-resolution ERT survey. ERT_1, ERT_2 and ERT_3 (showed in Figure 3.5) profiles collected during ERT survey in May 2015.

In Figure 3.19 is shown the ERT_WPD acquisition carried out in December 2015. This type of geoelectric acquisition is made up of seven blocks, each of which includes three different acquisitions, one Pole-Dipole and two Wenner array configuration. These acquisitions overlapping each other, ensuring good data coverage. The profile is 960m long and extends from 715m to 580m (m.s.l.) passing through the area that separates the Case Pennetta and Case Costa landslides. The geoelectric section can be divided into areas with greater and less resistivity. The most interesting areas in this work are those in Case Pennetta, which have resistance values between 20 and 50Ωm. In contrast, upstream and

downstream areas are characterized by higher values of resistivity that reaches about 100 Ωm.

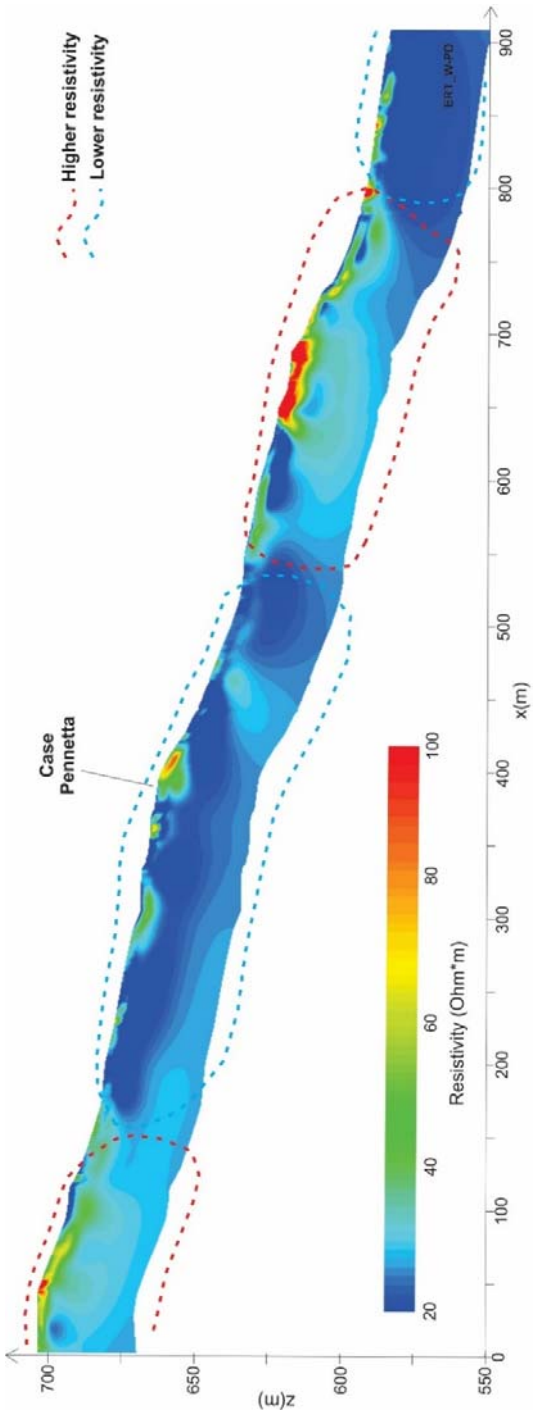

Figure 3.19. 2D image of resistivity obtained from the high-resolution ERT survey. ERT_WPD profile collected during ERT survey in December 2015.

3.4.1 Ground Model Development

The model of the study area, that is near the the village of Case Pennetta and the namesake landslide, was reported in Figure 3.20. It was realized using all the information obtained from geological, geomorphological, geotechnical and geophysical data. Therefore, this section provides a detailed understanding of the structure of the Case Pennetta landslide system.

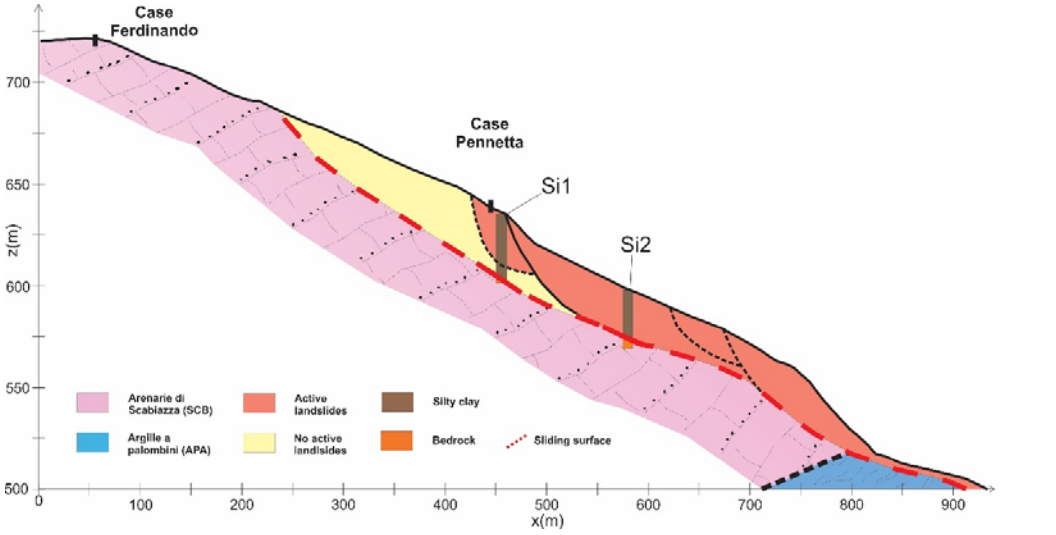

Figure 3.20. Geological and geomorphological model. Boreholes Si1-Si2.

This detailed ground model was developed using additional high resolution ERT information, remote sensing datasets and thorough interpretation of results obtained from core logging, geotechnical testing and laboratory analyses of the core samples. This was achieved by calibration of the geophysical results with direct physical property measurements of materials taken from the landslide and its surroundings and allowed to define the depth of the sliding surface.

Therefore, it was suggested that the sliding surface of the landslide is located at a depth of 30-35m (b.g.s.), and it is shown by the Si1 and Si2 core.

Furthermore, a different landslide was identified within the main body.

As is shown in Figure 3.20, the upper part of the profile above the Case Pennetta village, is characterized by resistivity values of 5-15Ωm, that indicate a good ground-water circulation.

In correspondence of the Si1 core, it was hypothesized the presence of a landslide body that may be considered as a active body. From inclinometer data it is possible to determine that, depth of the sliding surface of this active body, varies between 20 and 25m from the ground surface.

As revealed by stratigraphic analysis, under the sliding surface, for a thickness of 80-100m, it is possible to identify the Arenarie di Scabiazza Formation that feeds the Case Pennetta landslide (Figure 3.20). In the deepest part of the model and close to the ground surface, appear the Argille a palombini Formation (Figure 3.20), for a thickness not well defined and in correspondence of the jumping slope.

Chapter 4
Methodology for Slope Monitoring

The issues related to landslides are important in the management of the territory, in the definition of risk scenarios and in the preparation of opportune measures of forecasting and prevention (Propper et al., 2014). For this reason, it is essential to develop methods based on the collection of survey data and monitoring in order to define scenarios and implement warning system and/or civil protection plans (Borie et al., 2011). These methods should include installing of tools directly in the study area and provide information on the type-punctual variables measured (i.e. resistivity, groundwater level, displacement; Borie et al., 2011; Ogilvy et al., 2009). Exposure to hazardous conditions, long times required for the installation of the equipment, site accessibility, weather conditions and high costs of management and maintenance are to be considered for the selection of adequate instruments. Several permanent monitoring systems, which record a range of physical and environmental parameters, like resistivity, groundwater levels and displacement for more points, are installed at the Case Pennetta site. These subsurface properties can vary due to both environmental conditions and landslide activity.

In this chapter the methodology for monitoring site campaign is presented: in order to understand how physical properties changes within the landslide body, multi-factors were simultaneously monitored.

4.1 Monitoring Techniques

The system was deployed to get periodic measurements of electrical properties on the subsurface, with the aim of linking trends obtained in the electrical properties to landslide processes, i.e. rainfall infiltration and soil moisture accumulation. Since the mechanisms that occur inside the landslide body can not be studied and reported by installing only a geophysical monitoring array on the landslide, several monitoring systems should be used to record information to validate and complete the geophysical monitoring data.

ERT monitoring results are corrected for the seasonal effect of sub-surface temperature distribution. This is recorded at the field site but potentially hides the little soil moisture variations, and this may affect the success or failure of the

survey. ERT data are modelled using an appropriate heat equation. This equation is used to normalize to a constant subsurface temperature, all ERT model results. Other sensors are installed to get an integrated interpretation of the landslide geophysical monitoring data; a weather station and six piezometers to monitoring water level changes, two inclinometers to monitoring displacements, and two geo-electrical cables to measure the resistivity were installed at the site. The rainfall data were required to assess frequency and amount of water entering the sub-surface. The locations and extents of all sensors and monitoring arrays installed at the Case Pennetta field site are shown in Figure 4.1, which is the field site map. In this chapter the base map is presented as an aerial photograph; in addition, to each type of sensor is assigned a color and a reference code.

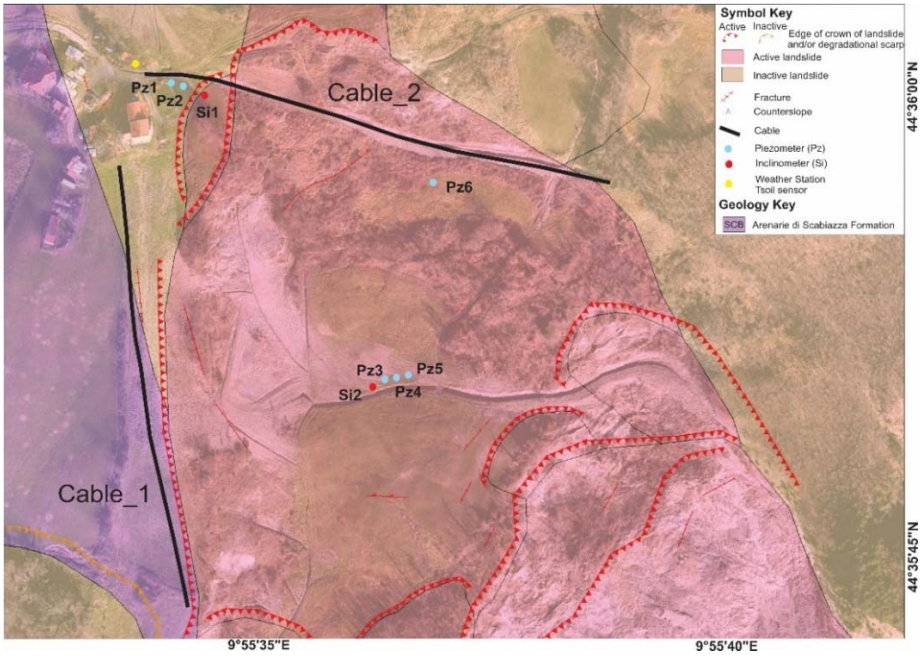

Figure 4.1. Case Pennetta base-map showing monitoring system installed at the Case Pennetta field site (geoelectrical cables, piezometers, inclinometers and weather station).

Subsurface temperature at the field site was monitored to correct geophysical monitoring datasets for the effect of subsurface temperature fluctuations.

Subsurface temperature is monitored by a sensors TT-N of the Nesa s.r.l. which gives discrete point source temperature information from surface up to a depth

of 2m. Since a break in temperature logging by sensor due to technical issues such as data logger malfunction and defective temperature sensors, is occurred, logger and sensors were replaced in the next monitoring in order to minimize data gaps. Between 01/10/2016 and 15/10/2016 the data loggers for measuring the air temperature are failed and manual daily air temperature measurements were done to supplement the logger data.

Seasonal subsurface temperature variation greatly affects the resistivity response of the ground. Therefore, to eliminate this effect, subsurface temperature was modelled. Seasonal temperature changes in the subsurface can be described by the Equation 4.1 (Brunet et al., 2010; Chambers et al., 2013) and is valid where temperature at the surface varies sinusoidally with a period of six months:

$$T(z,t) = T_{mean}(air) + Ae^{-(z/d)} \sin\left(\omega t + \varphi - -\frac{z}{d}\right)$$

Equation 4.1. Model to describe subsurface seasonal temperature variation where T(z,t) is the subsurface temperature at day t and depth z, (meters), $T_{mean}(air)$ is the mean yearly air temperature, A is the yearly amplitude of the air temperature variation, d is the characteristic depth of the temperature variation, m, φ is the constant phase offset, radians, and ω is the angular frequency (2π/360).

The constant phase offset ensures that the maximum temperature at the surface occurs at the hottest time of the monitoring. The overall phase lag (φ – z/d) describes that the maximum subsurface temperature occurs later in time and more in depth than the maximum surface temperature, because the heat has further to travel through the ground (Uhlemann et al., 2017). From the field data, it was obtained that T_{mean}=13.94°C, ΔT=7.89°C, d=1.72m, and ϕ=2.03.

The characteristic depth highlights how quickly the temperature variation decrease with depth and is related to the thermal properties of the ground, by the expression:

$$d = \sqrt{\frac{2k}{\omega \rho c}}$$

Equation 4.2. Characteristic depth, d, parameter of heat equation.

where k is the thermal conductivity ($Wm^{-1}K^{-1}$), ρ is density ($kg \cdot m^3$) and c is the specific heat capacity (JK^{-1}) at constant pressure.

Temperature data from subsurface sensor collected for six months (recorded every 15 minutes), i.e. from autumn 2016 (October) to spring 2017 (May), were used for modelling the subsurface seasonal temperature distribution.

The fitted model determines the four parameters T*mean*, Δt, d and φ. The fitted parameters from temperature modelling are presented in Table 4.1.

Model Parameters	Values
T_m	13,9479°C
ΔT	7,8905°C
d	1,72184m
φ	-2,03778

Table 4.1. Temperature-model parameters.

In Figure 4.2 a very good correlation between raw temperature data recorded by temperature sensor and the fitted temperature models is observed. The blue line represents field temperature measurements from sensor arrays while the green curves represent the fitted temperature model (Equation 4.2).

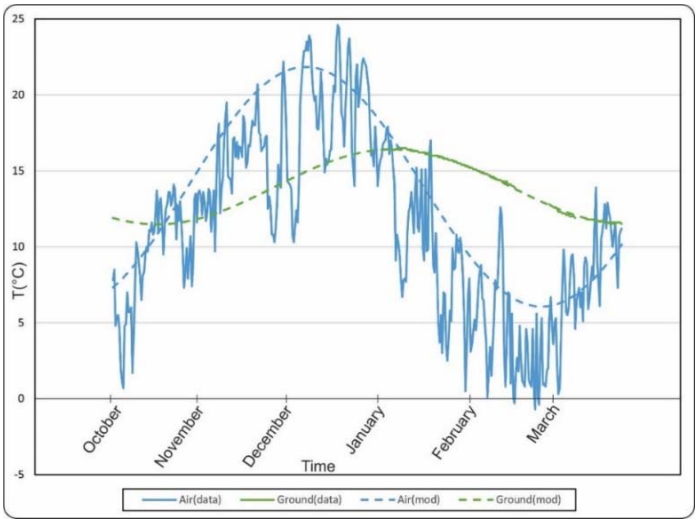

Figure 4.2. Temperature data plots and temperature model obtained from temperature sensor and collected from October 2016 to March 2017.

4.2 Rainfalls

Meteorological factor is certainly one of the most important that determine the activation of the earth mass. Intense and heavy rainfalls able to discharge a few millimeters of water to the ground in a very short time, frequently affect all the valleys of the Northern Apennines. Variations in the rainfall conditions can result in rainfall-induced landslides, depending on topographic, geological, climatic, and meteorological condition (Peruccacci et al., 2017).
Rainfalls were monitored at landslide site to get rainfall input information in order to complete the results obtained from the geoelectrical monitoring system. Knowledge of rainfall is essential for the investigation of the processes that occur within moisture-driven landslides, because it gives quantitative information about moisture inputs, and these information are linked to the water pressures and moisture content into the landslide system. Rainfalls were monitored at the field site from March 2016 to May 2017 and recorded every 15 minutes with the PL400-PL400R pluviometer (Raingauge 400cm^2 collection surface): for each step, pluviometer shows that the data logger recorded a single amount of rainfall of about 0.1mm. Therefore, rainfalls can be determined, first by summing the number of rainfalls whose amount is over 0.1mm, then by multiplying this value for the capacity of the rain gauges bucket. The output is a rainfall value in millimeters.

4.2.1 Piezometers

Six piezometers were installed within boreholes in several parts of the landslide site (Figure 4.1) which were properly covered by a plastic casing. Each piezometer is laterally open at different depths, in order to intercept variations of the groundwater level (Table 4.2). Piezometric level was monitored at the field site from 1st March 2016 to 31th May 2017 (ongoing). In Table 4.2 general properties of each piezometer are reported.

ID	Ground Surface (m, m.s.l.)	Depth (m, b.g.s.)	Screened from-to (m)
Pz1	645.61	35	30-35
Pz2	645.87	25	1-25
Pz3	589.05	30	25-30
Pz4	588.91	23	20-23
Pz5	588.75	15	3-15
Pz6	607.72	20	3-20

Table 4.2. Piezometers installed at Case Pennetta field site.

4.2.2 Inclinometers

The geotechnical monitoring allows to evaluate, with high accuracy and a high reliability degree, the horizontal displacements with respect to the read zero, and to obtain information about depth, direction and speed of landslide movements. The installation of the inclinometer casing was carried out within the two boreholes which are constituted by a tube of circular cross section which was permanently stucked in the ground. The tube has 4 grooves (guides), which allow the wheels of the inclinometer probe to slide, while maintaining a fixed orientation (Figure 4.3). The grooves are arranged at a 90 degrees angle to one another, to provide measurements along the orthogonal axes. The inclinometer casing in the study site has a diameter of 90mm and is made of PVC alloy with anticorrosion. The study performed on the sliding surface level, shows that the inclinometer casing is installed at a depth of 35m and 30m from the ground surface, for SI1 and SI2, respectively, i.e. below the bedrock.

In accordance with the operating procedure of the inclinometer probe, the first measurement made on the site, was the zero. A direction of the insertion of the A0 reference wheels was chosen: in particular, one for each survey and two for each inclinometer.

In the Si1 inclinometer was chosen an angle of 101 degree for the direction of the first Si1A measurement; for the second SI1B measurement, the direction is rotated by 90 degree angle with respect to the first measure. In the Si2

inclinometer, for Si2A and Si2B were choosen the angles of 95° and 185°, respectively. The directions of 0 was considered as the reference orientation both for the first measure and for all inclinometer surveying carried out subsequently. Therefore, particular attention was paid to the maintenance of the references.

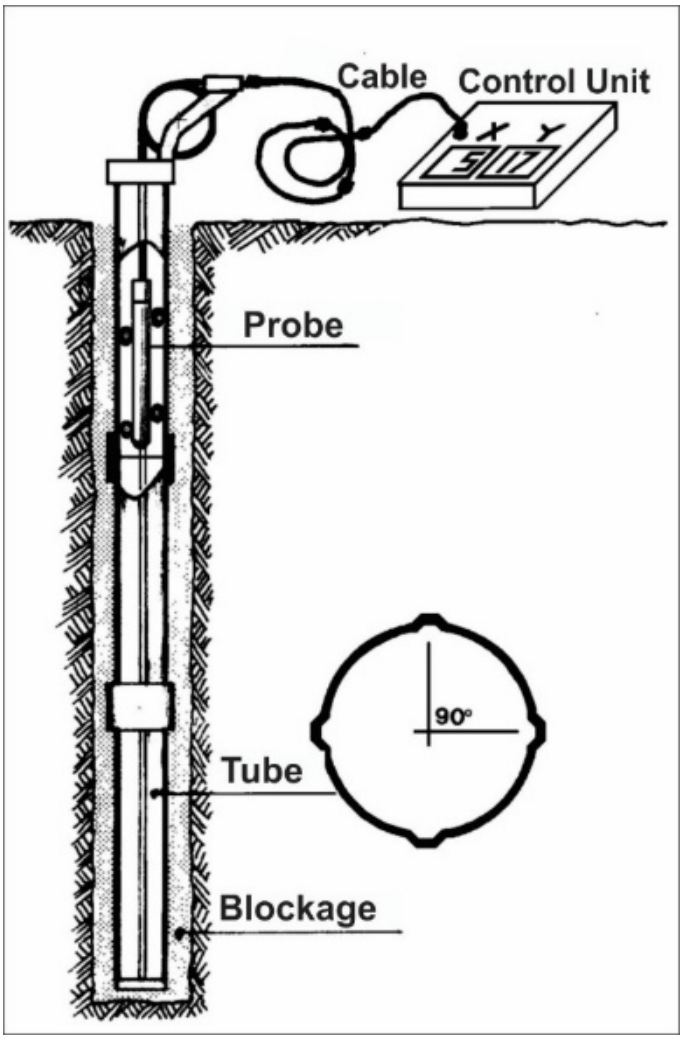

Figure 4.3. Inclinometer structure.

The acquisition instruments used are represented by the Digitilt Classic system that is constituted by a Digitilt inclinometer probe (Figure 4.4), a control cable and a DataMate (i.e. a control unit for reading and storing the inclinometer data). All equipment is designed and manufactured by DGSI (Durham Goe Slope indicator).

Figure 4.4. Digitilt Classic system (Slope Indicator).

4.3 Landslide Monitoring System by Electrical Resistivity Tomography (ERT)

The landslide system at Case Pennetta is monitored by a permanently-installed geoelectrical monitoring system that was designed, constructed and developed by Roberto Francese, Professor of Geophysics and Andrea Quagliarini, PhD student of the University of Parma. The system was installed on the landslide at the end of 2015 and the first resistance measurements was acquired during the summer of 2016. The investigations were carried out according to the technical-logistical requirements, intensifying the measures during the major rainfall events. For technical and logistical reasons, the Cable_1 presents some anomalies that have prevented the proper functioning. Therefore data obtained from Cable_1 will not be presented in this work.

4.3.1 The ERT System: how to construct it?

The ERT system consists of two cables (Cable_1 and Cable_2), each one long 235m and including 48 electrodes buried at a depth of 0.5m from the ground surface (Figure 4.1).
The realization of the geoelectrical cables was carried out at the University of Parma. This phase was developed step by step:

- Construction of cables consisting of 48 electrical wires (diameter of 0.5mm). Each wire represents a single electrode (Figure 4.5).

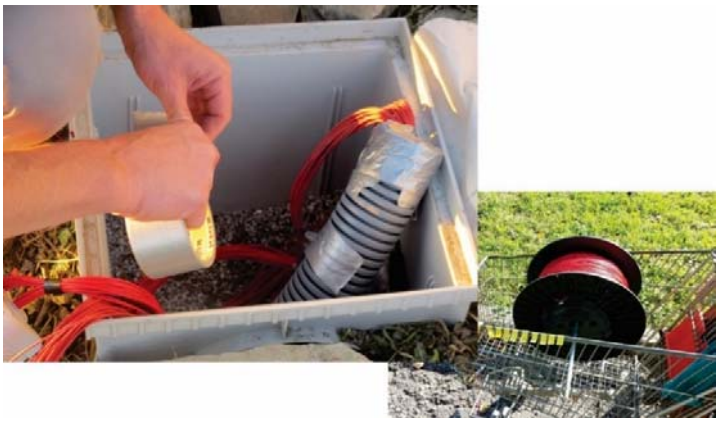

Figure 4.5. Realization of the cables.

- Transport of geoelectrical cables to the Case Pennetta study area and realization of the electrodes, as shown in Figures 4.6. Electrodes are made by steel plates (5x10x0.2cm) to ensure a greater contact with the ground, allowing the passage of the electric current.

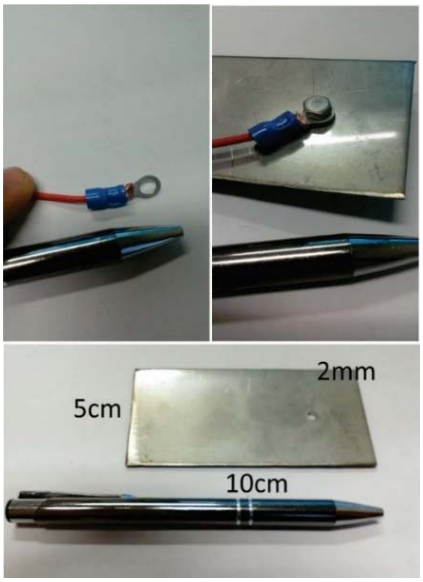

Figure 4.6. Realization of the electrodes. Notes: 2mm are referred to the tickness of the plate, 5 and 10cm represent the other two dimensions (height and length, respectively) of the plate.

- Waterproofing, with a silicon sheath, of the cable-electrode contact areas (Figure 4.7).

Figure 4.7. Electrodes waterproofing.

- Protection of the cable inside a tube to further protect the electric wires from water, excessive summer heat and animals (Figure 4.8). Each hole in which the electrode was buried, was made, with a percussion drill, by Andrea Quagliarini, PhD student.

Figure 4.8. Protection of the cable inside the tube.

- Finally, the electrodes were buried at a depth of about 40-50cm from the ground surface. The Cable_1 was buried, while Cable_2 was left in surface (Figure 4.9). This different choice was made to have greater control over Cable_2 in the case of necessary logistic and maintenance operations.

Figure 4.9. The electrode is buried under the ground.

4.4 Data Management

After the field survey, the resistance measurements were reduced to the apparent resistivity values. In this section, the steps involved to convert the apparent resistivity values into a resistivity model section, will be shown. The resistivity model section can be used to improve data interpretation.

In the Wenner-Schlumberger survey that is employed in this work, the sequence indicates that the first two electrodes are the first pair of current injection. Voltages are then recorded for the remaining electrode pairs for a number of predefined combinations. Since the instrument has 10 recording channels, 10 potential measurements for each current injection pair were collected.

Typically, ERT data quality is improved by stacking several measurements for each quadrupole transmitter-receiver pair. A data repeatability threshold, i.e. 1%-5% standard deviation, can then be used to remove noisy measurements

from the data. Alternatively, the noise data may be retained and, before to make inversion, can be assigned higher standard deviations. Points of measure are represented as a "*pseudo-section"* (apparent resistivity section), which provides, through an image of the underground stratigraphy and thus the sub-superficial geology, a first indication of the features of the resistivity spatial distribution in the investigated soil portion. The section is called a "*pseudo-section*" because the geometric position of the individual points is defined on the basis of the surface quadrupole and not as a function of the real distribution of ground resistivity (Figure 4.10). Apparent resistivity is a function of electrodes spacing and position, indirectly associated with the depth of investigation, being the depth of investigation 1/5 of the length of the cable.

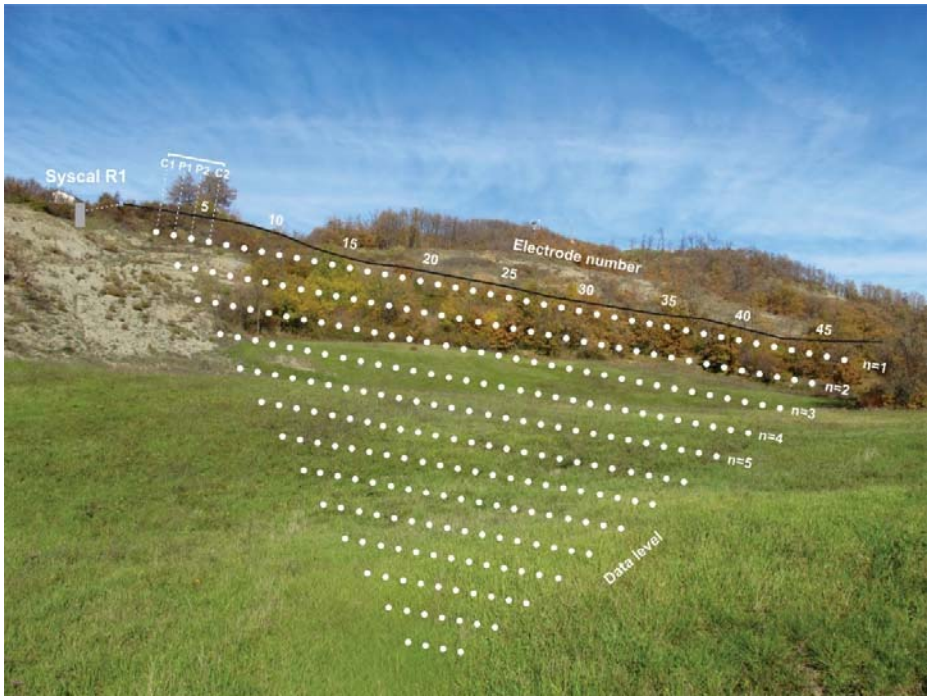

Figure 4.10. Sequence of measurements (Cable_2) made with a multi-electrodic device and their conventional representation in the form of *pseudo-section*. C1 and C2 are current electrodes, P1 and P2 are potential electrodes. "n" represents the pseudo proof which is a multiple of the distance between the electrodes.

Thus, it is possible to acquire a large number of measuring points to achieve a high degree of resolution. The pseudo-section provides a very approximate and

sometimes distorted view of the real distribution of ground resistivity, due to the fact that the shape of the iso-resistive curves depends heavily on the real distribution of resistivity and the type of loop used (Figure 4.11). Pseudo-section is a way to represent apparent resistivity measurements in a graphical form, which may prove useful as an initial guide for subsequent quantitative processing.

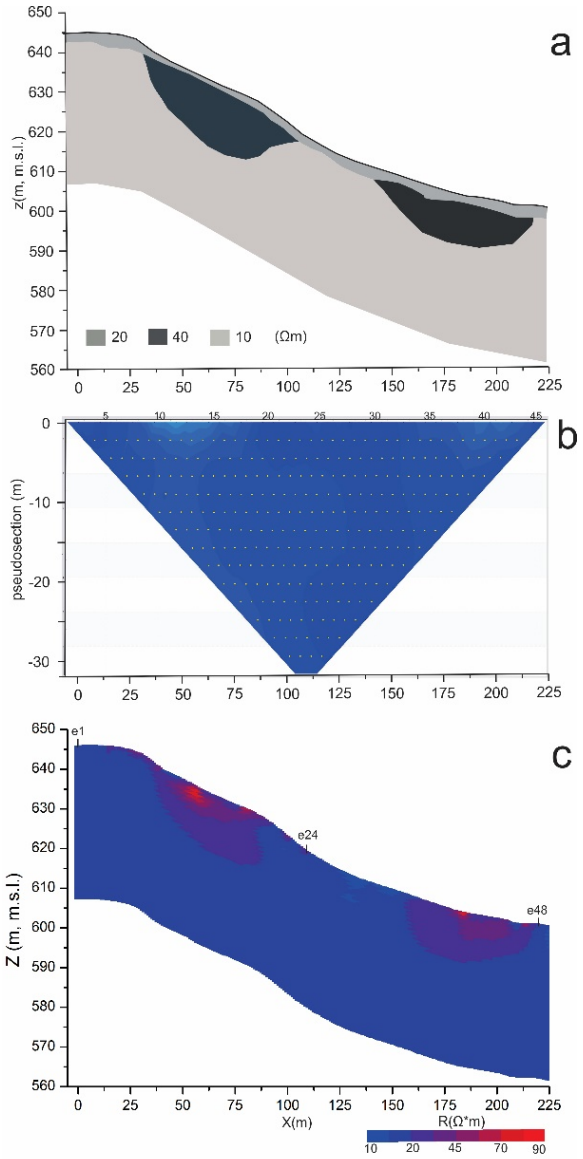

Figure 4.11. Resistivity modelling of a landslide model: a) the conceptual model, b) the apparent resistivity pseudo-section for a Wenner configuration, c) the resistivity tomogram obtained by inversion method.

4.4.1 Resistivity Measures and Data Analysis

Data from each 2D survey line (Cable_1 and Cable_2 as shown in Figure 4.1) was initially inverted, independently of the ERTlabTM software, to give 2D cross-sections. The forward problem was solved using the finite-element method (Silvester and Ferrari, 1990), in which node positions were adjusted to allow topography to be taken into account during the inversion process. Before performing the inversion process all resistivity data were examined and the "bad data points" were manually removed with Prosys II software (IRIS Instrument). All 2D apparent resistivity data were inverted with the l1-norm implementation (a robust constrained model) of the regularized least-squares optimization method and a finer model with a cells width of 1 meter. After the inversion was done, the Temperature Correction was applied.

4.4.2 Data Processing and Inversion

A model used to interpret the 2-D data set is shown in Figure 4.12. The subsurface is divided into several layers and each layer is further subdivided into a number of rectangular blocks. 2-D resistivity inversion program, ERTlab™ (Appendix B1)**,** used to interpret the data, attempts to determine the resistivity of the blocks in the inversion model, that most closely reproduce the measured apparent resistivity values from the field survey. Since the resolution of the resistivity method decreases rapidly with depth, it was found that subdividing the blocks is beneficial for the top two layers only. In many cases, subdividing the top layer only is enough. The inversion operation performed by ERTlab™ is a minimization of the differences between the calculated pseudo-section and the pseudo-section measured by the least squares method associated with regularization (Constable et al., 1987).

The first step is to associate the *.bin* file, obtained with the IRIS Syscal R1 (Appendix B2) instrument, with an ASCII *.prn* file that contains the real coordinates of each electrode. The reason for this passage is due to the fact that within the *.bin* file there are the Cartesian coordinates of the electrodes A, B, M

and N of each quadrupole. In this case, the electrodes of each quadrupole have a different reference system. By associating the .bin file with the *.prn* file, each electrode will be numbered consistently to the conversion table contained in the .prn file. For the inversion process a mesh is generated, i.e. a discretization of the subsoil in finite cells. It is very important to set the cell size. The optimal size of the cell is usually equal to half the spacing "a" used in the field. Cells were set at 1m side both in the foreground area and in the background area (Figure 4.12) and fit to topography. At first, during the processing of the geoelectric data, a cell size of 2.5m x 2.5m was chosen, but subsequently to increase the resolution degree and thus have a greater display detail, it was decided cell size of 1m x 1m.

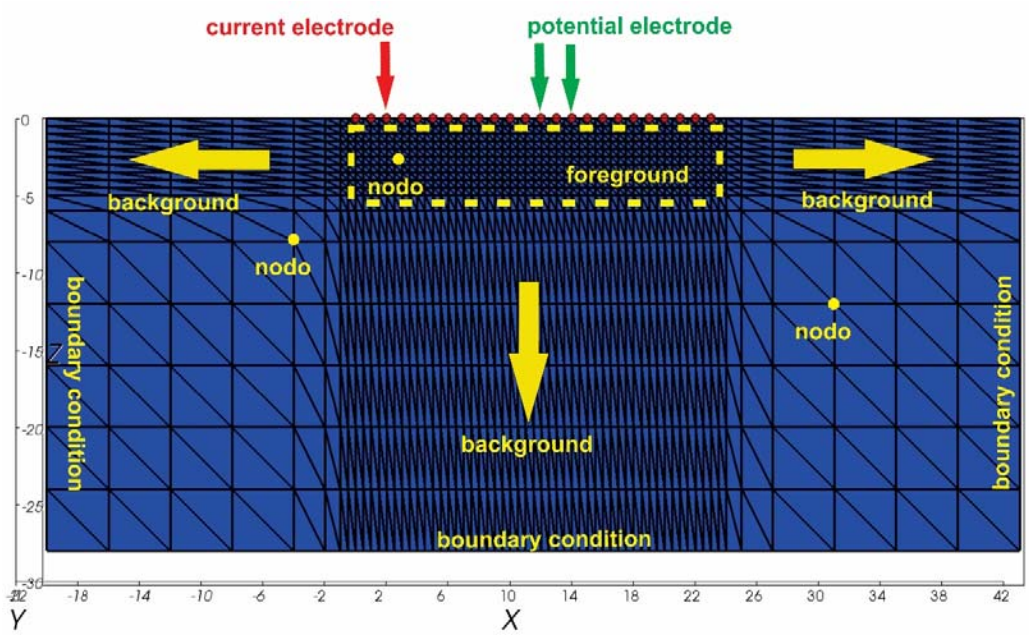

Figure 4.12. Forward 2D modelling-mesh.

Iterations during the inversion process terminate once the misfit (Figure 4.13) reaches the minimum value. In the case presented here, that represents one of the "many" inversions made during this work, the misfit is low for all inversions During the inversion process, error minimization iterations are made between measured field data and computed data. Iterations end when the misfit reaches

the minimum value or there is no more convergence to the iteration process (the misfit between two iterations varies by a few percentage points). In our case, the final misfit is low for almost all inversions (except for some outlier).

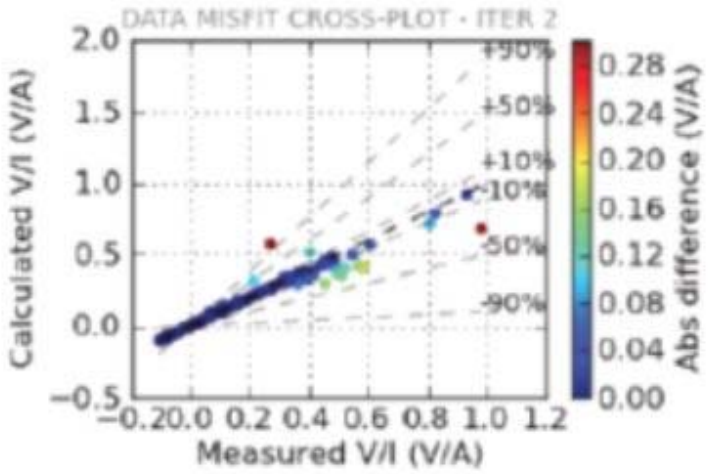

Figure 4.13. Minimization iteration of error during the data inversion. An example of tomography (05/04/2017) misfit.

The inversion produces an *InvDataOutput.data* file that contains the result of the inverse solution in terms of real resistivity, i.e. a value for each finite element in the grid. The file has five columns: the x, y and z coordinate elements, the resistivity and the log10 resistivity elements. Furthermore, as we will see in the next paragraph, a .xyz file useful for extrapolating data for the creation of charts, is produced.

4.4.3 Temperature Correction

One of the challenges in soil science is to understand the relationships between electrical resistivity and other soil properties. Indeed, electrical resistivity is a complex soil electrical property that is affected by various soil parameters that can interact with each other. Soil temperature plays a central role among all of the factors that significantly influence electrical conductivity.

Where time-lapse electrical resistivity data are compared over a time duration longer than the time it takes for subsurface temperature to migrate, it is important

to correct ERT results for the seasonal variation in subsurface temperature distribution. This is due to the effect that subsurface temperature variation has on the electrical properties of the subsurface, mainly its resistivity (ρ) or conductivity (σ). Therefore the principal target is to observe the effects of subsurface temperature on resistivity data.

The method of temperature correcting time-lapse electrical resistivity data is a two stage process. Firstly, raw ERT data are inverted. Secondly, the inversion results are corrected by adjusting them to a temperature constant homogeneous half-space (sometimes referred to as a standard temperature equivalent model). This is achieved by determining the subsurface temperature distribution as a function of the time, n, from the Case Pennetta temperature model and applying:

$$\rho_{cor} = \rho \left[1 + \frac{tc}{100}\right](T_{standard} - T_{model})$$

Equation 4.3. Temperature correction, with a temperature factor tc of -2.0°C^{-1}. ρ in the electrical resistivity and is a function of date and depth, ρ_{cor} is electrical resistivity at $T_{standard}$, mean air temperature, T_{model} is the modelled subsurface temperature and tc/100 denotes the empirical coefficient that is often between 0.02 and 0.025°C^{-1} (Hayley et al., 2007, Brunet et al., 2010).

Currently, the model used to correct temperature data is the model proposed by Hayley et al. (2007) and Brunet et al. (2010) that assume a flat, horizontally layered resistivity. This is, obviously, an approximation because the ground is not homogeneous. Nevertheless, the model fits data very well, having an RMS (Root Mean Square) error of only 1.1%. This model was used to estimate the temperature at each cell of the resistivity model and at each time step, and subsequently, to correct the model resistivities ρ to a standard temperature $T_{standard}$ = 20°C, using the ratio model (Hayashi, 2004; Ma et al., 2011).

It is necessary to have an understanding of both spatial and temporal subsurface temperature variation if electrical resistivity models are to be corrected for the effect of subsurface temperature. This can be achieved by normalizing all model resistivity values to a common temperature, most often to an arbitrary

temperature, for example 20°C (Brunet et al., 2010); however, in this investigation, a temperature-constant homogeneous half-space normalized to the mean air temperature ($T_{Standard}$ is 13.94°C) was used, as shown by the green curve in Figure 4.2 that represent the fitted temperature model.

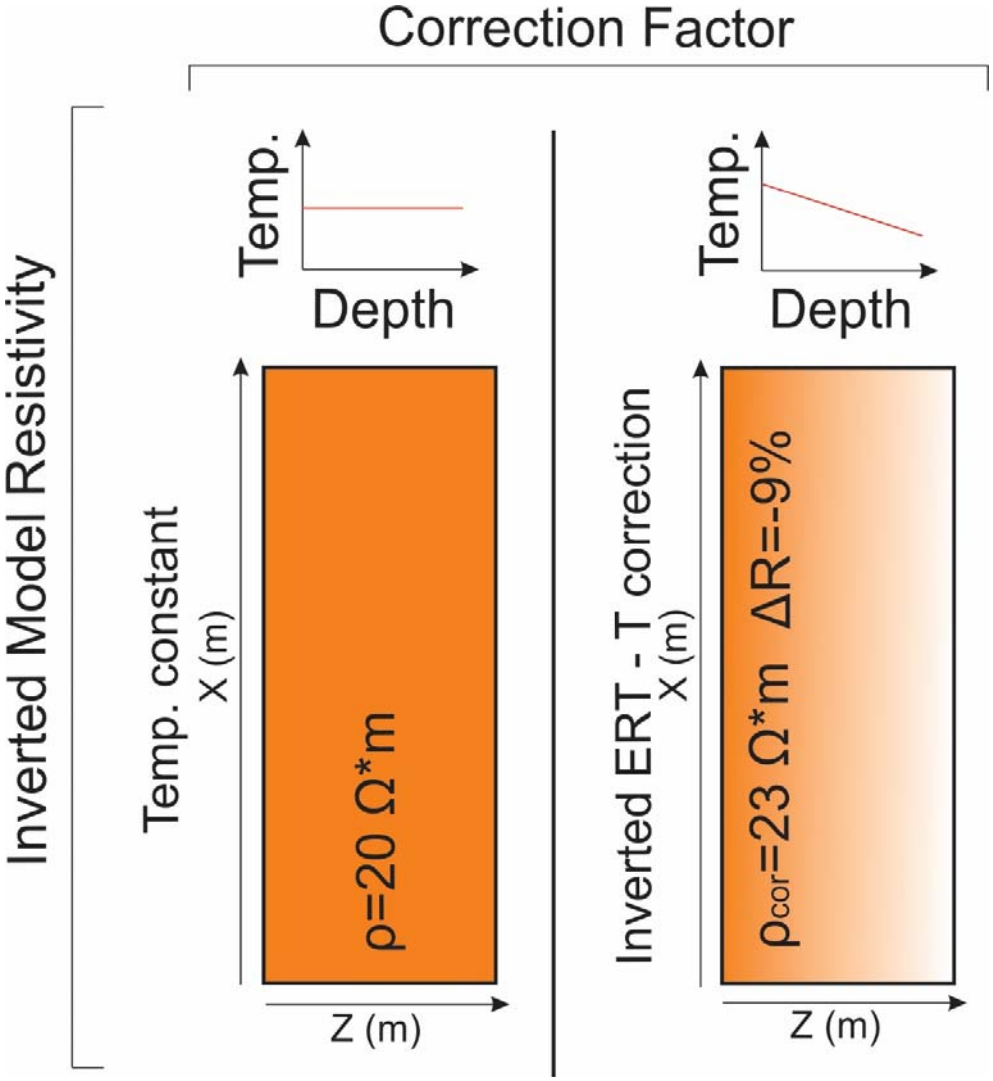

Figure 4.14. Diagram of the temperature correction of field transfer resistance measurements by 1D layered resistivity model.

An example of how the degree to which seasonal subsurface temperature variation affects the electrical resistivity of a model half-space is given in Figure 4.14. Here, the temperature model fitted for the Case Pennetta field site is obtained by applying the theoretical equation for temperature correction from

Hayley et al. (2007) and the temperature and resistivity distributions plotted for a period of six months.

4.4.4 Capability of the Analytical Method

The methodology proposed here has good prospects for providing reasonable estimates of future landslide activity by assessing the susceptibility of hazard and determining the geological and topographical conditions which may cause landsliding. Since different processes may modify the state of a landslide, it was necessary to consider all of them in order to achieve a more complete picture of the landslide activity. However, the most important controlling factors of landsliding that we have studied are hydrogeology, climate (rainfall records of a weather station) and resistivity variations.

This study show, once all the triggering factors were identified and combined, the development and the application of an integrated geoelectrical and geotechnical monitoring network on an active landslide of the Northern Italy. Therefore, it was possible to reveal the hydrogeological precursors to the movement and to develop new investigative and predictive tools for the study of the slope instability.

Furthermore, the system reveals bidimensional structures of the landslide and monitors temporal changes in the slope, including changes in water content and movements of the landslide.

The great strength of this methodology is that it provides subsurface information at the site scale, together with geotechnical and hydrogeological data; furthermore it characterizes lithological variability, monitors hydraulic changes associated with failure events, and produces calibrated 2D models of the subsurface water content variations from the timelapse resistivity data. Therefore, the technique described here can be used in the ongoing monitoring of the landslide, its dynamics and its hydrogeological processes.

Chapter 5

Monitoring System Result

In this chapter the results from the monitoring campaign are presented. The beginning of this chapter contains the results of conventional slope monitoring data, including rainfall and piezometric heads. In order to have a better understanding, the rainfall–groundwater relationships and the hydrogeological monitoring lapsed resistivities sections, have been carried out on Case Pennetta landslide. Resistivity data have been processed and inverted (4.3.1 and 4.3.2) and then presented in several interpretative layout. Subsequently, the resistivity outputs were related to the hydrogeological data. The datasets obtained have been integrated, analyzed and interpreted together.

5.1 Monitoring Results

5.1.1 Inclinometers and Sliding Surfaces

The inclinometer measurements have been done to assess the displacement along the inclinometer every 0.5m, onto the two planes orthogonal to each other, which are represented by the tube guides.

During the lithological interpretation, it was possible to hypothesize that in the study area, there is a rock substratum with fragile features at a depth of 35m and 25m for the Si1 and Si2 inclinometers, respectively. As is shown in the graphs of differential displacements, the main sliding surface which is into the silty-clay layer, is at about 23m depth in the Si1 inclinometer (b.g.s.; Figure 5.1a), and at about 14m depth in the Si2 one (b.g.s.; Figure 5.1b). The movement recorded on the sliding surface is slightly accentuated.

In the representation of stratigraphy that was carried out using samples extracted during the drillings, the layer which contains the sliding surface, was described as silty-clay with centimetric clasts. From the interpretation of the displacements of the sliding surface, I have attributed the silty-clay layer to a partially broken section of the Arenarie di Scabiazza Formation, where the disintegration in the result of the disturbance caused by the roto-translational movements of the landslide. The secondary sliding layer is more superficial and it can be considered as an indicator of the Earth-flow movement, which is located in the

downstream of the landslide body investigated. The most superficial layer is characterized by a continuous movement because the precipitations are absorbed by the first meters from the ground surface, even if the infiltration times are high because the ground surface is permeable. The secondary sliding surface is located at about 7 m depth (b.g.s.) in Si1 and 4m depth (b.g.s.) in Si2.

The inclinometer monitoring for the Si1 borehole began in March 2016 (read 0) and continued until May 2017, for a total of 15 measurements; for the Si2 inclinometer, the monitoring began in April 2016 (read 0) and continue until May 2017, for a total of 14 readings. The measurements for all installations have been performed every 30 days. As is shown in Figure 5.1, the displacement detected is about 2mm per month from March to August, and it decreases in September and for the next months, in which the movement is almost zero.

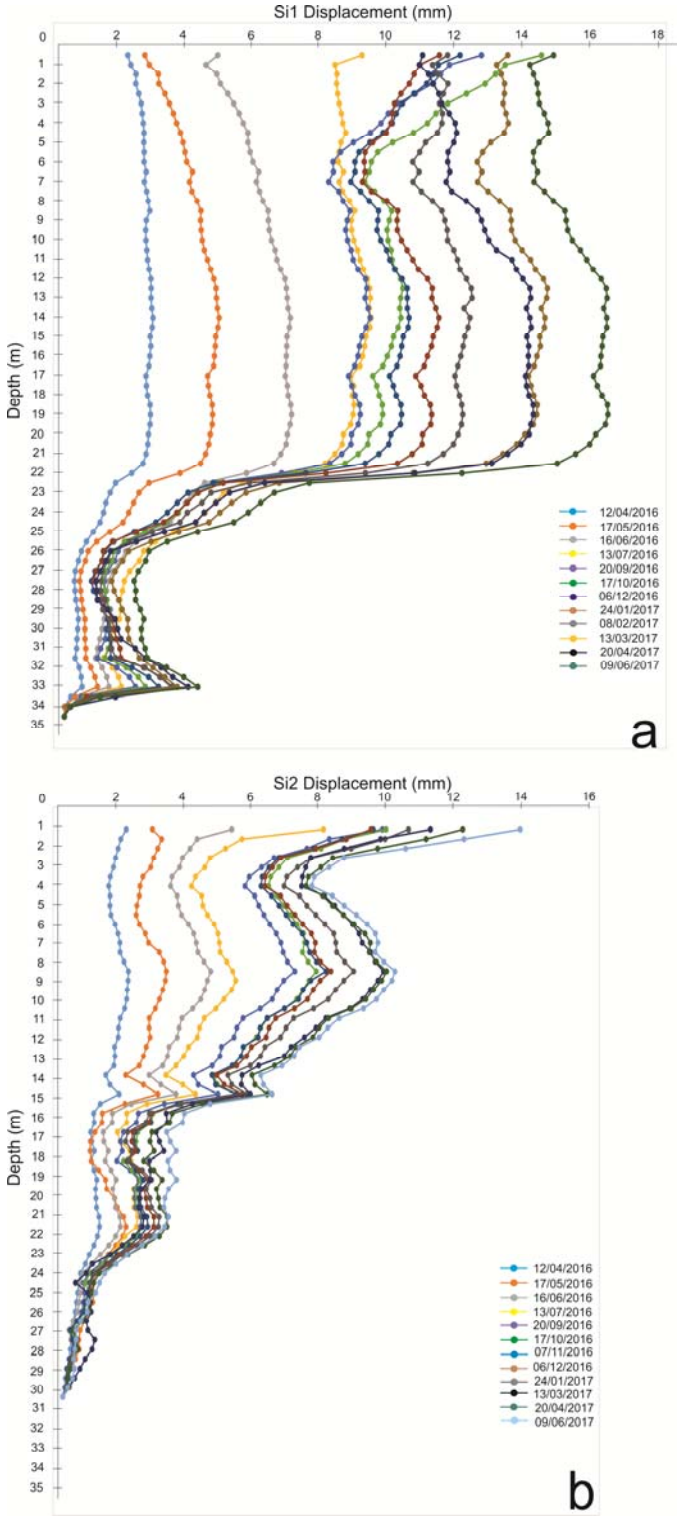

Figure 5.1. Si1(a) and Si2(b) inclinometric displacement from March 2016 to May 2017. The differential displacements are taken from the direction of the maximum slope.

5.1.2 Rainfalls

The water content inside the soil was measured and monitored by two methods. A pluviometer was installed on a weather station in order to provide the rainfall amounts and the intensity of each event. Rainfall results are presented in monthly and daily rainfalls with the aim to compare each event with the resistivity variations and to verify how it changes as a function of the infiltration.

Furthermore, rainfall data were compared with piezometer data and with subsurface electrical resistivity data in order to better understanding the interplay between the rainfall infiltrations and the variation on the underground physical properties. Rainfalls were monitored over a period of one years and three months and data were provided by meteorological station installed near Case Pennetta village (Figure 4.1, Chapter 4). Rainfall data are presented from 01/03/2016 to 30/05/2017, by including cumulative seasonally rainfalls and cumulative monthly rainfalls (Figure 5.2).

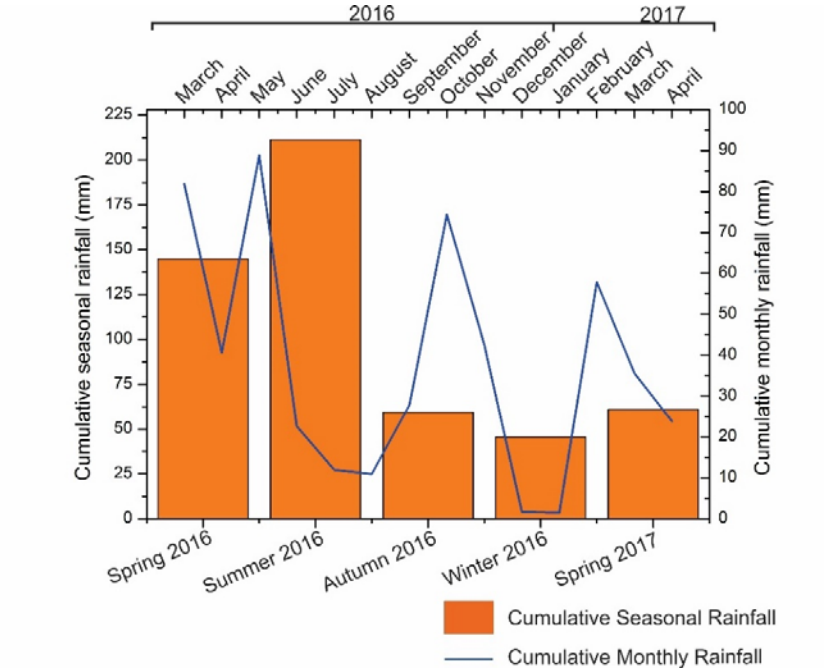

Figure 5.2. Rainfall data for Case Pennetta site. Presented are both monthly total rainfall and seasonal rainfall. (Spring: March, April, May- Summer: June, July, August- Autumn: September, October, November- Winter: December, January, February).

The first rainfall monitoring months over the spring season 2016 (March-April-May), have recorded a sequence of several weeks of rainfall events. In particular, March and May began with 80mm and 90mm of cumulative rainfalls, respectively, while, April was characterized by low cumulative rainfalls that reach 40mm. The summer season (June-July-August, 2016) was characterized by three months of lower monthly-rainfall events, ranging between 10mm and 22mm. In particular, June and July were characterized by quite short rainfall events (only a few hours). Between September and the end of October (2016) rainfall events were increased, reaching 65mm during the autumn period. Cumulative monthly rainfalls (25mm) over the winter season (December-January-February, 2016) have shown that rainfall events are fell more than half compared to the autumn season. The spring season 2017 is similar to the winter one 2016, with 30mm of cumulative rainfalls.

Therefore, the peaks that indicate the most rain months during the monitoring period, are May 2016 with 90 mm of cumulative rainfalls, October 2016 with 75mm of cumulative rainfalls and February 2017 with 60mm of cumulative rainfalls, of which 45mm are fell in the first three days of the month.

In order to compare data relating to geoelectric, piezometric and inclinometric acquisitions with pluviometric data, it should be considered the months of January and February 2017 because, in this period, a total of 60mm of rain fell in the monitored area. Therefore, as shown in Figure 5.3, the ten days that precede the four geoelectric acquisitions (24-01-2017, 08-02-2017, 09-02-2017, 10-02-2017 and 02-03-2017), were considered.

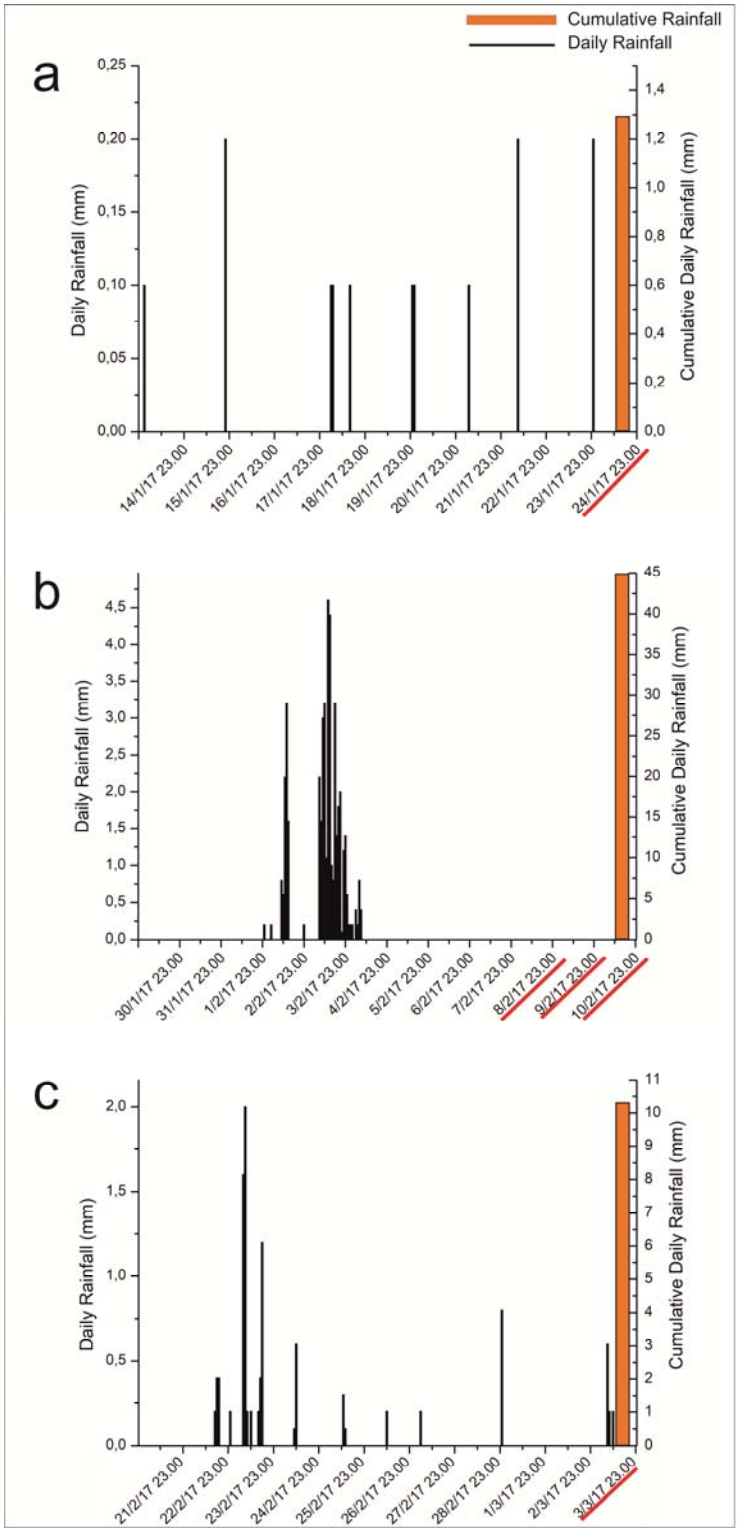

Figure 5.3. Daily rainfall. Ten days before the geoelectrical acquisitions: a) 24-01-2017, b) 08-01-2017, 09-01-2017, 10-01-2017 and c) 02-03-2017.

By the analysis of the graphs reported in Figure 5.3, it is observed that during the period prior to the acquisition of the 24 January 2017, cumulative precipitations of 1.3mm in 10 days were recorded (Figure 5.3a). Rainfalls increase significantly in the following period considered, i.e. before the series of geoelectric acquisitions of 8th, 9th and 10th February were performed (Figure 5.3b). In this period a cumulative rainfall amount equal to 44.9mm in 10 days was recorded. In the last time-interval ranging from 21st February to 3rd March 2017, precipitation data recorded by the weather station were about of 10.3mm. The entire monitored period produces various and interesting findings regarding resistivity variations, as will be widely described in the following Chapters.

5.1.3 Piezometers

The hydraulic heads have been represented within a two-dimensional plane (Figure 5.4): on the ordinate is represented the altitude above the sea level in meters (m.s.l.) while on the abscissa is represented the time expressed in dates of the acquisition. The curvilinear, which identifies the trend of the hydraulic heads measured in each piezometer, is the result of a fit curve through the piezometric values acquired during some of the dates represented in the graph. The piezometers Pz1 and Pz2 located in the northern part of the investigated area, had synchronous head fluctuations during the monitoring period.

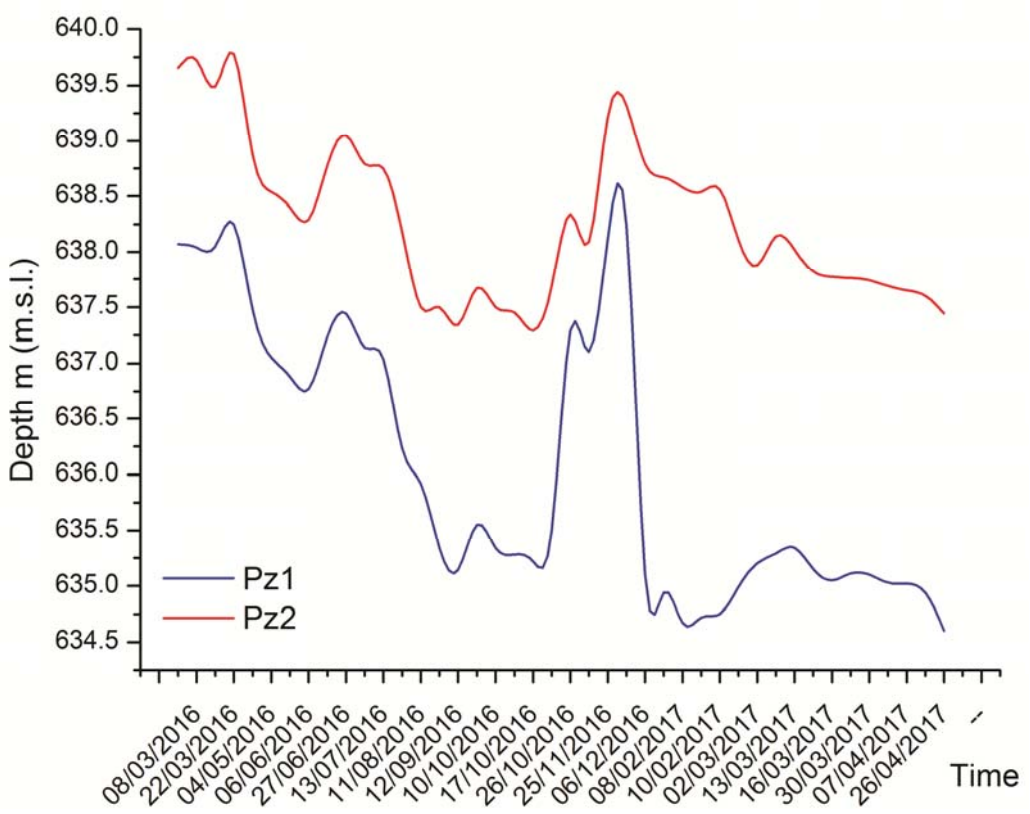

Figure 5.4. Trend of Pz1 (screened from 30m to 35m b.g.s.) and Pz2 (screened from 1m to 25m b.g.s,) from 01/03/2016 to 31/05/2017.

Figure 5.5 shows differences of hydraulic load in Pz3 (purple line), Pz4 (yellow line) and Pz5 (black line) piezometers, located in the southern part of the monitoring site. The trend helps to understand, how hydraulic loads measured at different depths (Pz3, Pz4, and Pz5) evolve over time along the same vertical. The range of piezometric level is between 583.40-583.56m (m.s.l.), for example between 10/09/2016 and 15/09/2016, and 588.46-588.76m (m.s.l.) that occurred between 20/03/2016 and 25/03/2016.

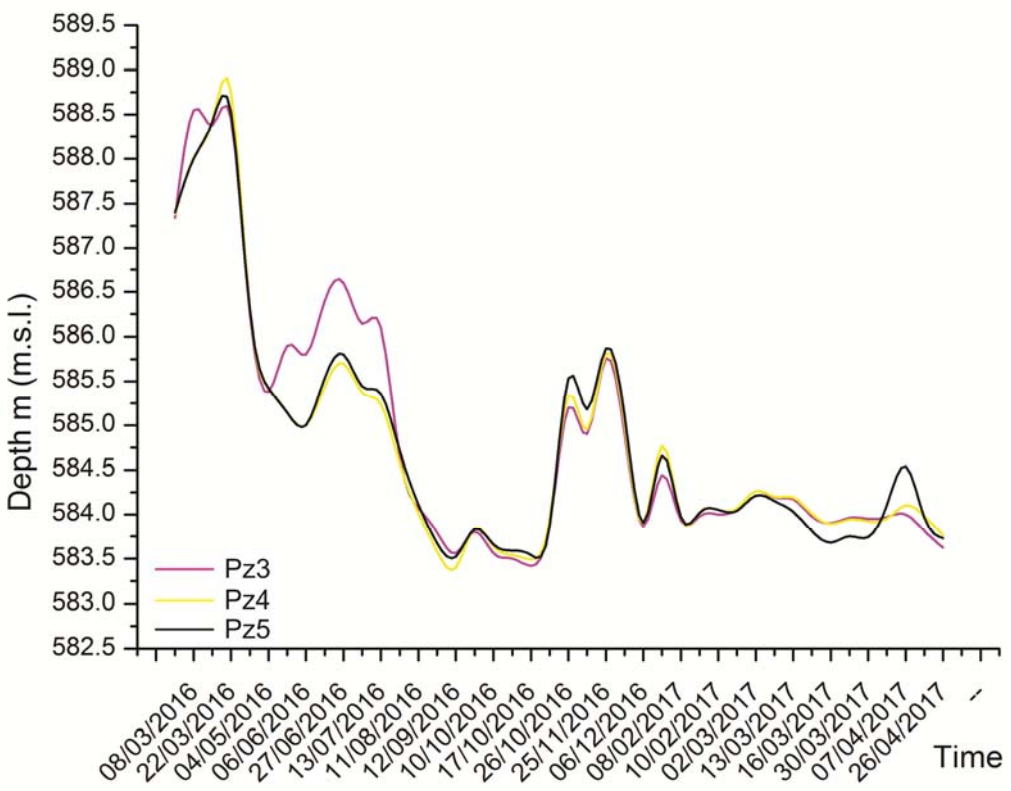

Figure 5.5. Trend of Pz3 (screened from 25m to 30m b.g.s.), Pz4 (screened from 20m to 23m b.g.s,) and Pz3 (screened from 3m to 15m b.g.s.) from 01/03/2016 to 31/05/2017.

The piezometer 6 (Pz6 green line), shown in Figure 5.6, and located in the middle region of the Cable_2 (Figure 4.1), started working on 16th February 2016. Although the peak of 600.21m (m.s.l.) recorded on 04/03/2016, for the first six months of the year, the piezometric level was relatively low, fluctuating from 596.51m (m.s.l.) to 597.95m (m.s.l.). This low relative level was followed by a high relative piezometric level on the November month, reaching 600.95m (m.s.l.) on 28/11/2016, with a consistently level up to 2 meters higher than the relative low level of the previous six months. After this event, the level rather sharply reduced over a period of three or four weeks, decreasing rapidly and reaching again a relative low piezometric level, as in the first months of 2016. A period of low piezometric level at 597.2m (m.s.l.) prevailed from February and May 2017.

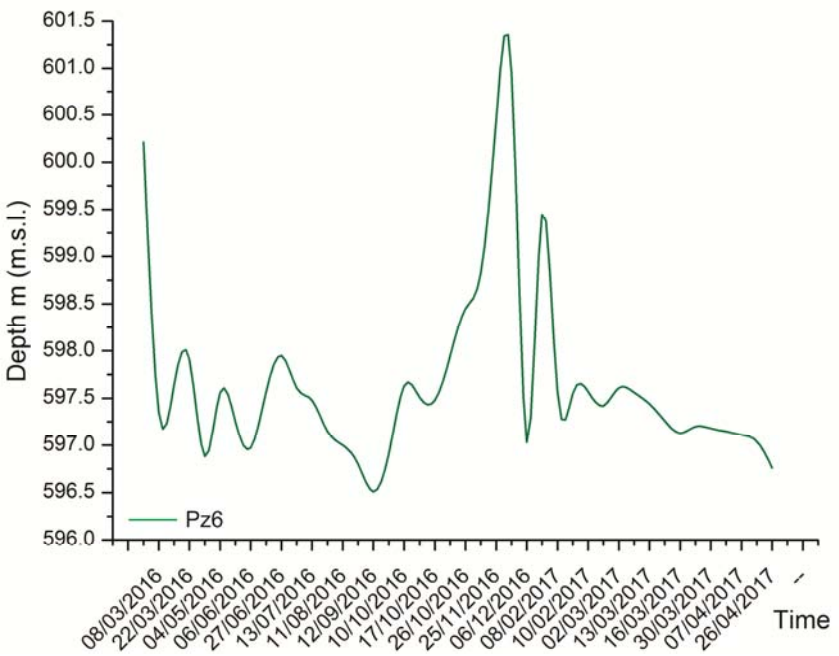

Figure 5.6. Trend of Pz6 (screened from 3m to 20m b.g.s.) from 01/03/2016 to 31/05/2017.

5.2 Resistivity Results

Data of the 29 ERT of Cable_2 surveys from 01/07/2016 to 31/05/2017 monitoring period, have been inverted, analyzed and then represented in Figure 5.7, in this figure is possible to see how only some ERT acquisition have been used for to monitoring the Case Pennetta landslide. As it has not been possible to obtain from the Cable_1 a complete monitoring which includes inclinometers and piezometers measurements, it is not represented in this thesis. The color scale was chosen to represent all resistivity models (the cool colors represent low resistivity area; the warm colors represent high resistivity area), and the inversion data are shown in Figure 5.7 (Cable_2).

In all ERT acquisitions of the Cable_2, a good convergence between the observed resistivity data and the resistivity model, have been achieved after 3 iterations as indicated by an RMS error lower than 1% for all the profiles.

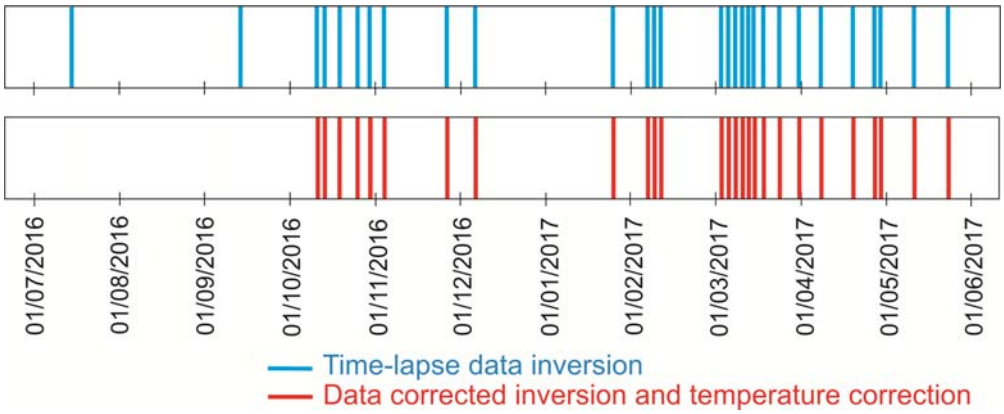

Figure 5.7. Cable_2 ERT survey data and the type of inversion performed.

The monitoring period was characterized by scarce and discontinuous rainfalls, so it was necessary to focus attention on the major rainfall events. On the 3rd of February (2017), 33mm of rain felt on the ground, and it allowed to acquire data before, during and after this meteorological phenomenon. Therefore in Figure 5.7, are represented only three of the 29 acquisitions performed with the Cable_2, which are: the acquisition of the 24th January 2017 (pre-event), the acquisition of the 8th, 9th and 10th February 2017 (immediately post-event) and the acquisition of the 3rd March, 2017 (post-event).

Furthermore, it should be noted that ERT models are smoothed images for which the resolution decreases with increasing depth of investigation because the model in these regions is less well constrained by the data. Therefore, the ERT images can provide only an approximate guide to the true resistivity and geometry of subsurface features (Olayinka and Yaramanci, 2000; Chambers et al., 2002). In all lines can be discriminated a more superficial level characterized by anomalies ascribable to the ground surface proximity. These anomalies can be clearly distinguished from the surrounding soil by means of resistivity contrasts.

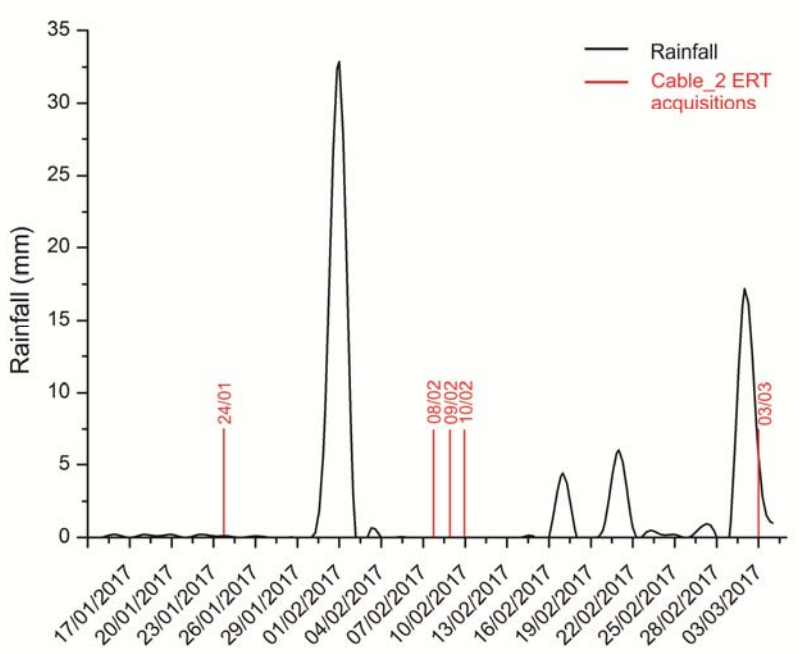

Figure 5.8. Rainfall monitoring from 15/01/2017 to 03/03/2017 and Cable_2 ERT acquisition.

These data have resistivity values ranging from 60 to 90Ωm (Figure 5.11, red-purple in colors) and are probably due to the denser structures with chaotic forms characterized by coarse grain size and centimetric size pebbles (40-50cm). The resistivity of the surrounding soils is lower than 50-60Ωm (blue in colors). The level containing the resistivity anomalies is found from the ground surface to approximately 2m depth, and it reached greater depths (about 3m) between the electrodes 12 and 16 and between the electrodes 35 and 40. Between the electrodes 22 and 27 are observed lower resistance values, i.e. between 10 and 20Ωm. The underlying level extends from the base of the upper layer to the maximum investigation depth which is of about 37m. Figure 5.8 shows, in detail, the rainfalls of February.

The acquisition of 24/01/2017 (Figure 5.9), carried out one week before rainfall event, shows resistance values of about 80-90Ωm both at the beginning and end areas of the profile. Similar values have been measured for the acquisitions of 08/02/2017 and 09/02/2017, although the latter two have been realized, respectively, four and five days after the weather phenomenon affected by 33mm

rainfall on the ground. Resistivity variations obtained from the 10/02/2017 acquisition, took place exactly six days after the described meteorological phenomenon. Rainfall event started on the 29th January and ending on the 4th February, resulting in a drop in the resistance values from 80-90Ωm to about 40-50Ωm in the two above mentioned areas. Three weeks later, during which are fallen 14mm of rain on the ground, another acquisition was done (i.e. 3th March). It was so possible to find resistivity values similar to those measured in the acquisition of January and in the firsts two days (i.e. 8th and 9th) of February. To confirm this, the acquisition of January 24th was made after a month characterized by the absence of liquid and solid precipitation. The first two acquisitions in the month of February, have been realized 3 days after the end of the meteorological phenomenon. Before this period no variation in resistivity values is observed in the soil. This delay in the resistivity response can be explained with the time required by rainwater to infiltrate into the ground portions underlying the most superficial layer.

In Figure 5.9 is shown on the left side apparent resistivity values of five ERT acquisitions (24/01/2017, 08/02/2017, 09/02/2017, 10/02/2017 and 02/03/2017) obtained after the inversion and on the right side, the calculation of the percentage difference between the same ERT survey. What emerges is that between the acquisitions of 24th January and 8th February, there is an increase in resistivity values of 0 and 5%, while in the area between the electrodes 12-16 and 35-40 there is a decrease between 10 and 20% in resistivity.

Major variations are observed in the percentage difference between the acquisition of February 10th and February 9th. A change of about -10% was recorded in correspondence of the electrode 22, while in the two areas characterized by lower conductivity values, there have been an increase of 40-50% of the resistivity. The percentage difference between the acquisitions of 02/03/2017 and 10/02/2017 follows the same trend, increasing the difference of the resistivity data in the areas between the electrodes 12-16 and 35-40 of a value of 20 -40%, and decreasing in the central part of the Cable_2 of about 10-20%.

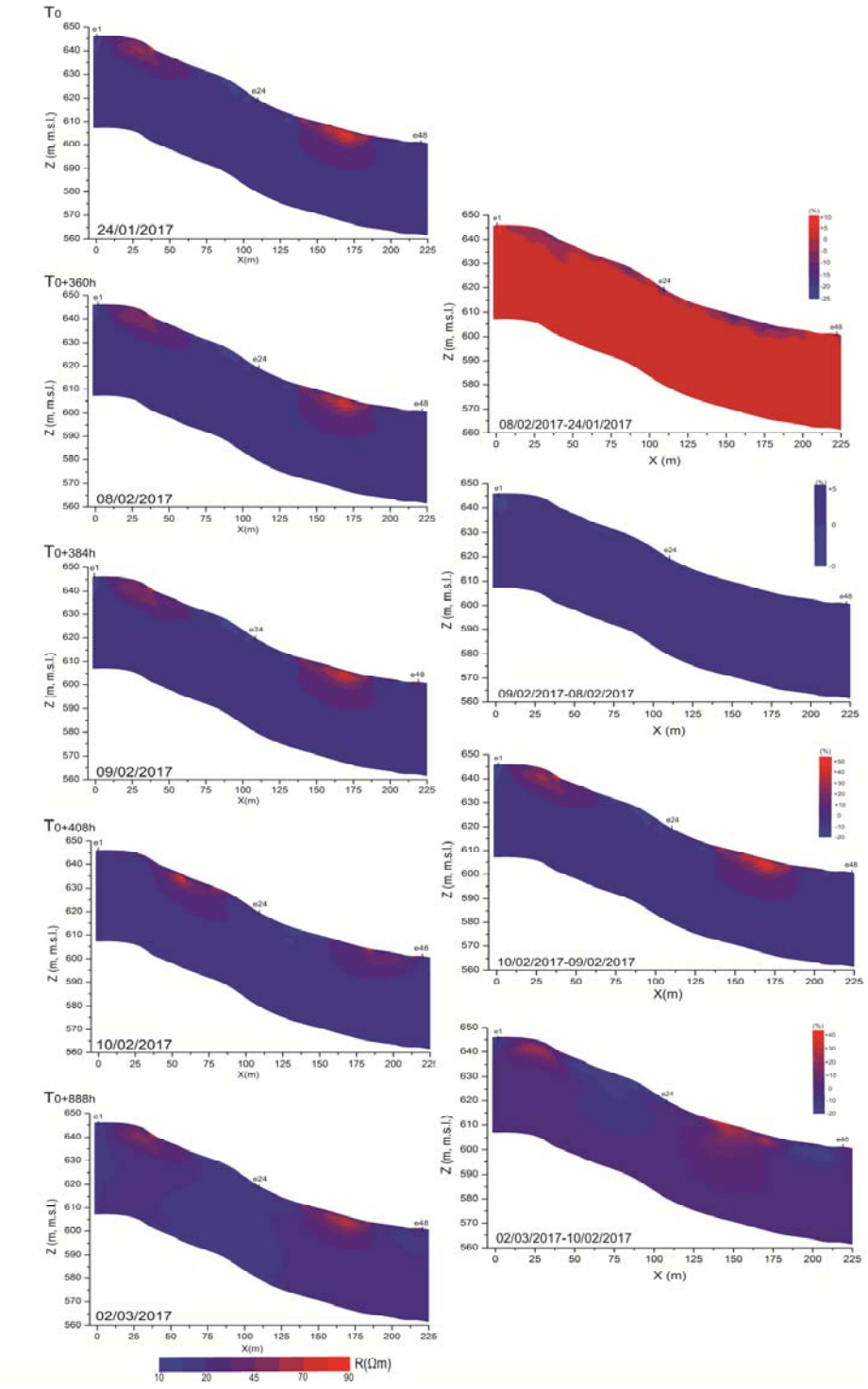

Figure 5.9. On the left side, Cable_2 ERT acquisition (24/01/2016, 08/02/2017, 09/02/2017, 10/02/2017, 02/03/2017). On the right side, percent difference between Cable_2 ERT acquisitions (24/01/2016, 08/02/2017, 09/02/2017, 10/02/2017, 02/03/2017).

5.3 Statistical Analysis of Resistivity Measures

Resistivity variations measurements were also statistically treated.

In Figure 5.10, rainfalls are compared with apparent resistivity data of the cells that constitute the mesh realized during the inversion process of geophysical data. Considering this comparison, it was possible to make two considerations. The first is that the value of the cells tends to uniform with the depth: it increases from the ground surface to the depth (the shallower cells show a more significant response than deeper cells). Moreover, comparing rainfalls with geophysical data, it was possible to observe a synchronous behavior for all layer, and that, the resistivity undergoes a variation about 7-10 days later a meteorological (rainfall) event.

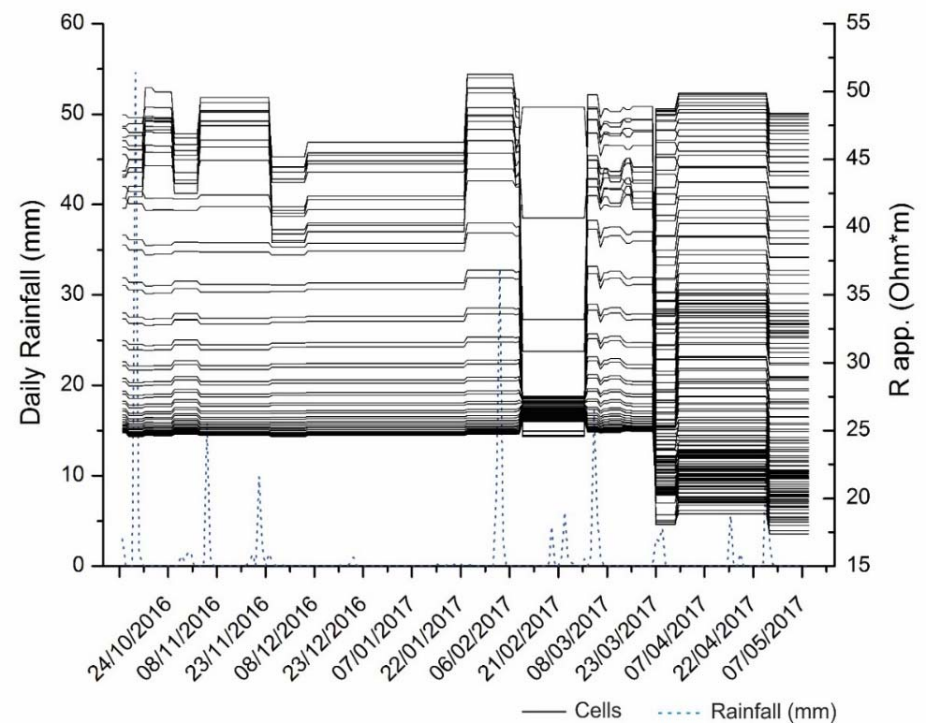

Figure 5.10. Cells apparent resistivity variation ranging from 24/10/2017 to 09/05/2017.

In order to analyze resistivity data and variation, the study was performed on five representative areas (Figure 5.9). Only five areas of the entire model were

considered because, from the analyses previously performed and as it is shown in Figure 5.10, in these areas a resistivity variation larger than in the other parts of the model, was observed. Therefore, in Figure 5.11 is represented the model obtained from ERT acquisition performed on February 2017 with the highlighted five representative areas. Each area includes 25 cells (each cell is 1m x 1m) for a total surface of 25m^2; this value was extracted from the mesh generated during the inversion process of the Cable_2 resistivity data. The positions of the five representative areas are reported in Table 5.1. As is shown in Figure 5.11, the five areas are located within a circumscribed band, i.e. between 2 and 20m from the ground surface; beyond this depth resistivity data can not be considered optimal for this study, because they tend to conform, without significant variations.

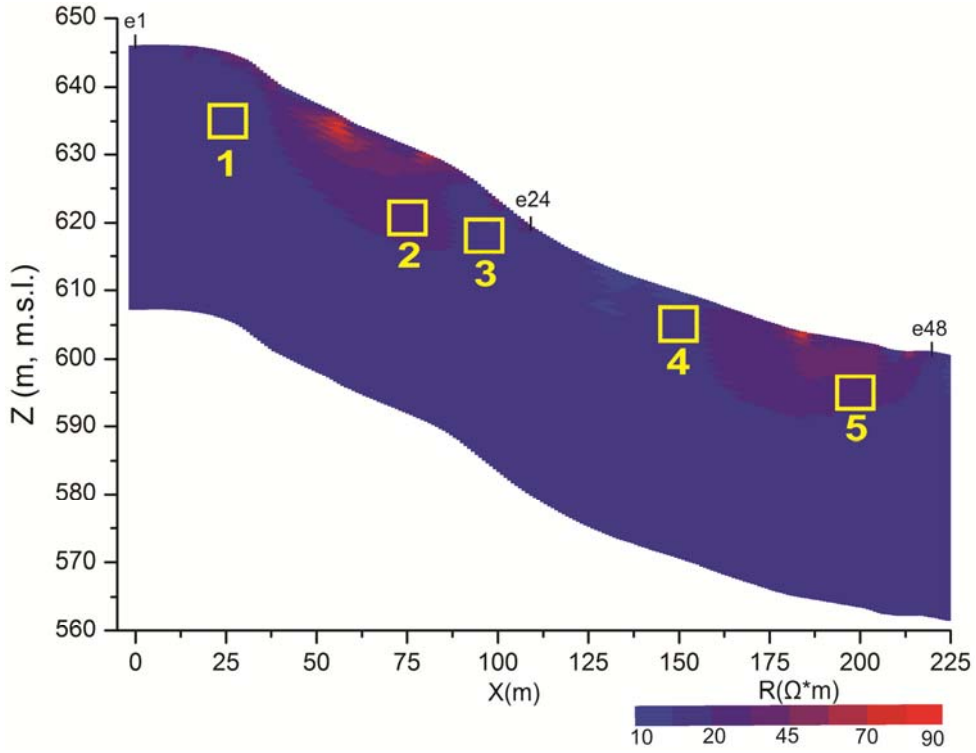

Figure 5.11. ERT Cable_2 with the indicated position of the five areas (example of 10/02/2017 ERT acquisition).

Area		
ID	**x (m, from-to)**	**z (m, m.s.l.)**
1	18-23	632-637
2	73-78	618-623
3	97-102	616-621
4	148-153	603-608
5	198-202	593-598

Table 5.1. Position of the five areas in the Electrical Resistivity Tomography of the Cable_2.

As is shown in Figure 5.12, rainfall events from October 2016 to May 2017 were compared with the average resistivity variations recordered in the five areas during the same period, in order to confirm that in these representative areas, resistivity greatly varies after abundant rainfalls, i.e. in the month of February 2017. This is better showed in the following figure.

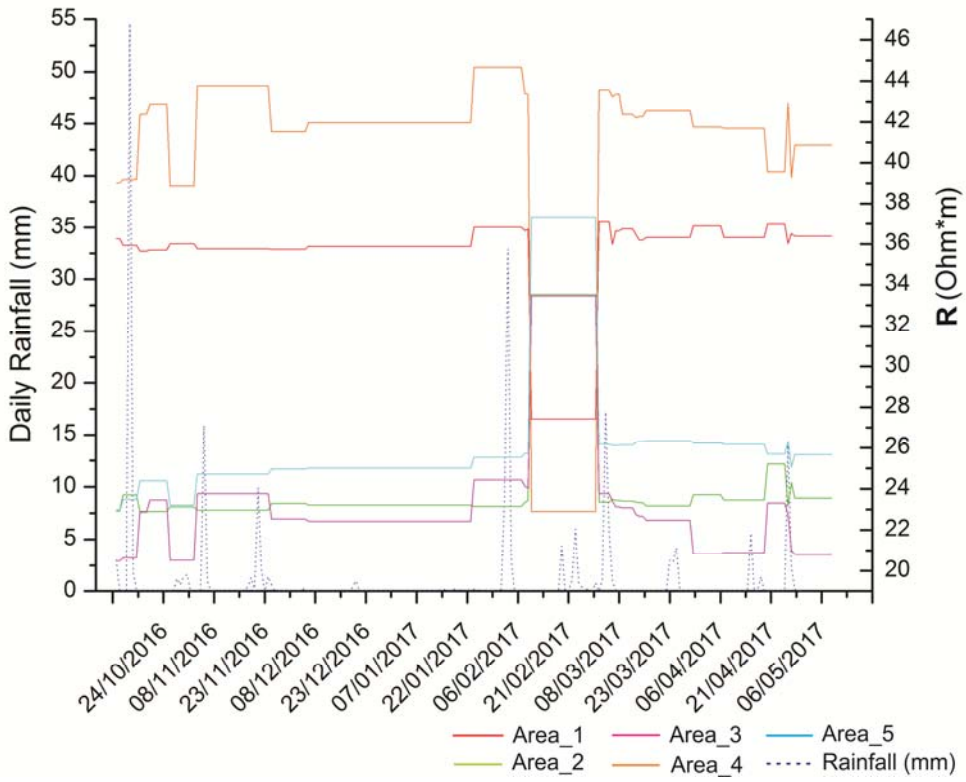

Figure 5.12. Average resistivity variation of the five representative areas from 24/10/2017 to 09/05/2017.

Therefore, in order to show more details, in Figure 5.13 resistivity variations in the five representative areas, from January 2017 to March 2017, are reported. It is shown that, after rainy events characterized by the fall of more than 15-20mm, there is a variation in the average resistivity of each area. Moreover, the event happened in February and already described above, which is represented by the fall of 33mm of rain, causes an important variation of the average resistivity of all the five areas.

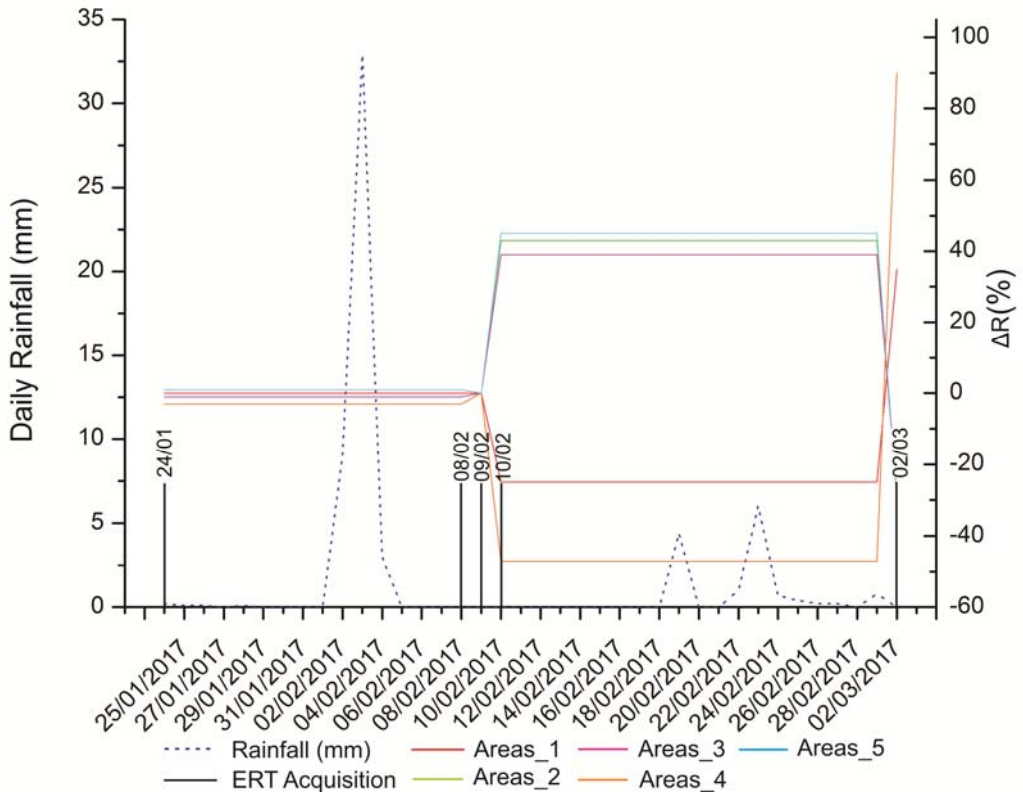

Figure 5.13. Resistivity variations in the five representative areas, from 24/01/2017 to 02/03/2017.

The resistivity variation was recorded about 4-5 days after the rainfall event, between the geoelectric acquisitions of 9th February and 10th February. Areas 2, 3 and 5 show an increase in the average resistivity variation of 43, 39 and 45% respectively, while areas 1 and 4 suffer a decrease in the average resistivity variation of 25 and 47% (Table 5.2).

The acquisition for the 2th of March showthat values are similar than those measured before the rainy day. In fact, the 2, 3 and 5 areas show a decrease of 30%, in the average resistivity variation, while the 1 and 4 areas display an increase of 35 and 90%. The different behavior can be explained considering the different positions of the five areas along the geoelectric profile. The decrease in the average resistivity values after the rainy event in the 1 and 4 areas can be explained by the presence of a groundwater flow. On the contrary, the percentage increase recorded in the 1, 2 and 5 areas may suggest the presence of zones whose behavior can be related to the non-passage of the groundwater flow.

Average resistivity variation in each area (Ωm)					
Time / ID	**1**	**2**	**3**	**4**	**5**
24/01/2017	35.53	24.24	23.54	42.65	26.03
08/02/2017	35.54	22.78	23.51	41.90	24.87
09/02/2017	37.43	22.65	22.28	42.54	24.98
10/02/2017	26.34	32.11	32.21	21.45	36.78
02/03/2017	36.87	22.34	22.65	42.02	25.11

Table 5.2. The average resistivity variation recorded from different geoelectric acquisitions during the event happened in February.

5.4 Results of Temperature Correction on Data Set

Raw transfer resistance field measurements are corrected for the effects of subsurface temperature distribution. Temperature corrected resistance data normalized to a baseline survey are shown in order to explain the influence of temperature on resistivity measurements (compared to a plotting of the absolute resistances). The resistance field measurements are corrected for the effects of the subsurface temperature distribution.

In order to display the temperature correction, the acquisition of 10/02/2017, that better than the others ERT acquisitions expresses the resistivity variations following the greater interest rainfall event and recorded during the monitoring period, was chosen. In this case, what emerges as a result of temperature correction (Figure 5.14), does not allow to appreciate the advantage of this technique, due to the low resistivity variation data which are, in turn, caused by the moderate environmental variations (precipitation and temperature).

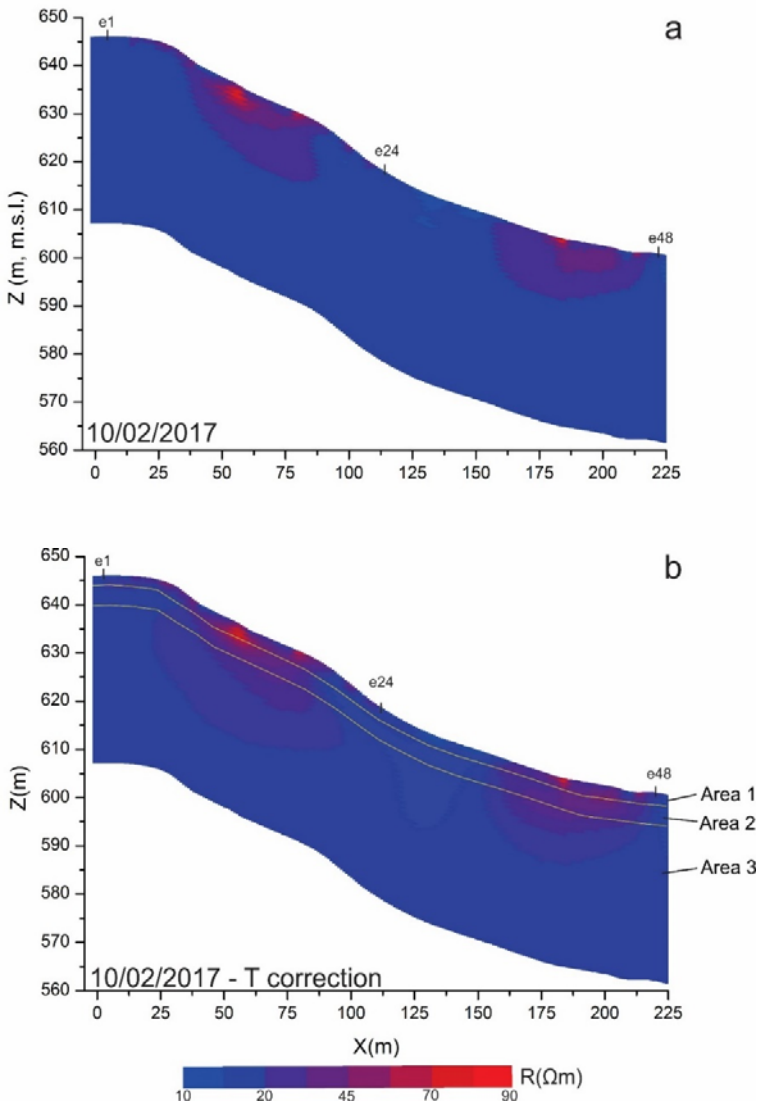

Figure 5.14. ERT temperature correction of the 10/02/2017 acquisition; a) inverted ERT without T correction; b) ERT with T correction.

In Figure 5.13, it can be noted that, after applying the temperature correction, the resistivity variation is extremely low. In the first 2 meters, i.e. in Area_1 (image b), a resistivity increase of 10% is observed from the ground surface with respect to the same area of the a image. In Area_2, which is at a depth ranging from 2m to 6m (b.g.s.), a resistance value 1.2% greater than superficial layer was measured; in Area_3, until to the section base, resistivity value is 1.5% and 0.5% minor than in Area_2 and Area_1, respectively.

Chapter 6

Discussion

This section describes the features observed in each of the monitoring data set, in the conventional hydraulic head measurements, and in the resistivity monitoring of the subsoil. The Chapter ends by summarizing the processes which take place within the Case Pennetta landslide and assessing the suitability of the implemented monitoring methods for the shallow earthflows.

The investigation had for its object the study of the groundwater level which depends on recharge from infiltration of precipitation; for this purpose installed piezometers are analyzed. They have demonstrated that the groundwater level response to rainfall differs considerably with respect to both overall hydrological conditions and groundwater mean depth level.

Although, during the wet periods and after some rainfall events, a rate increased up to 0.5cm/day of groundwater level was measured, a lower recharge rate and a delayed groundwater level response to rainfalls (usually from 1 weeks to 9-10 days) are observed at the beginning of the wet season and after considerable depression of the groundwater levels. This is probably due to a previous effective rainfall deficit. Comparison between hydrological conditions that have characterized the time period analyzed and intense rainfall events, allows to assume that the above-average precipitation, during the rainy season and after a prolonged wet period, may lead to an acceleration of movements (and to a possible failure of slopes). Long-term hydrological conditions (ranging from several seasons to several years) strongly affect the groundwater response to rainfall events in the Case Pennetta landslide. The variations over time of the groundwater profile are very similar in all of the six piezometers analyzed (Figures 5.3, 5.4, 5.5). This may indicate the presence of an aquifer, whose surface tends to follow the ground surface and with a height well-distributed from the surface to the rocky substrate. During the monitoring period, the recorded groundwater level reaches a maximum up to 0.5-1m (b.g.s.) depth. In April 2016 the level tends to a gradually decrease over time, dropping to depths of 4-5m (b.g.s.), but in May-July 2016 the levels reach the minimum of about 8m depth (b.g.s.).

6.1 Comparison between Hydraulic Heads and Rainfall Data

Although the monitoring period was characterized by prevailing dry and precipitation-free climatic phases, in order to analyze the interplay between rainfall events and piezometric level responses, a cross-check between two datasets, i.e. those belonging to the monitoring period ranging from 01/03/2016 to 31/05/2017, was made. The six piezometers used (Pz1-Pz2; Pz3-Pz4-Pz5; Pz6) are presented, separately, in three different figures. In Figure 6.1 is shown the groundwater level in the Pz1 and Pz2 piezometers from March 2016 to May 2017. As it can be seen from the graph, rainy events occurred in the following four dates, i.e. 05/03/2016, 19/05/2016, 14/10/2016 and 03/02/2017, have led to significant water inputs (i.e. 32mm, 26mm, 54mm and 32mm, respectively).

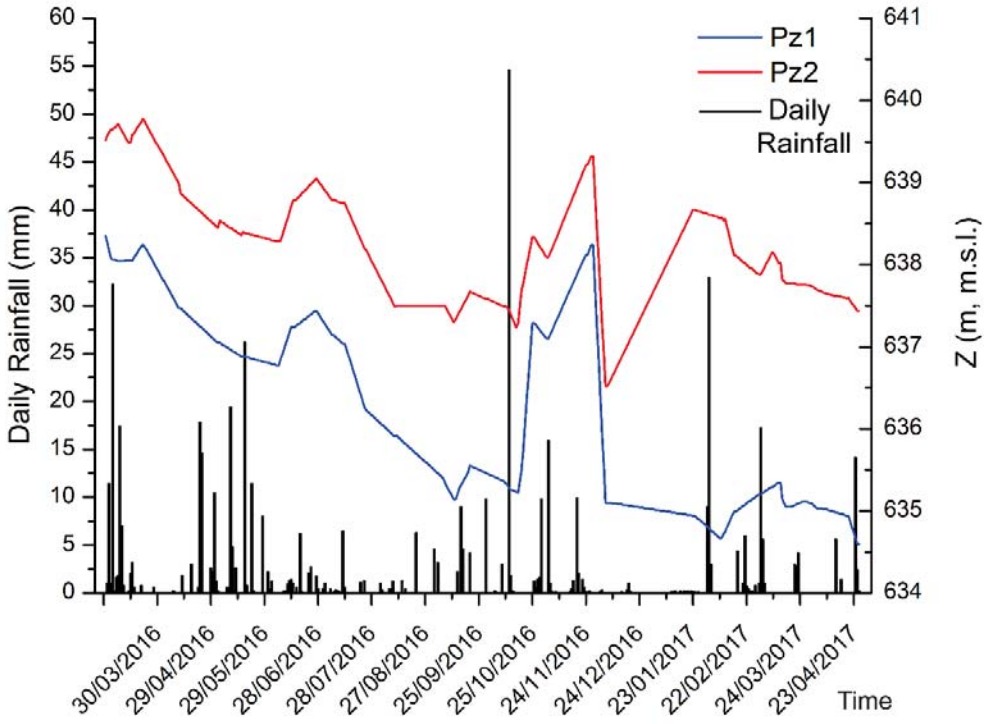

Figure 6.1. Comparison between Pz1-Pz2 and rainfalls from March 2016 to May 2017.

The Pz3-Pz4 and Pz5 piezometers shown in Figure 6.2, have the same trend for the entire monitored time period but it is possible to observe (as in Pz1 and Pz2)

that, a week after the abundant rainfall event of 14/10/2016 characterized by a cumulative daily rainfall of about 55mm, the groundwater level shows a rise of about 2m.

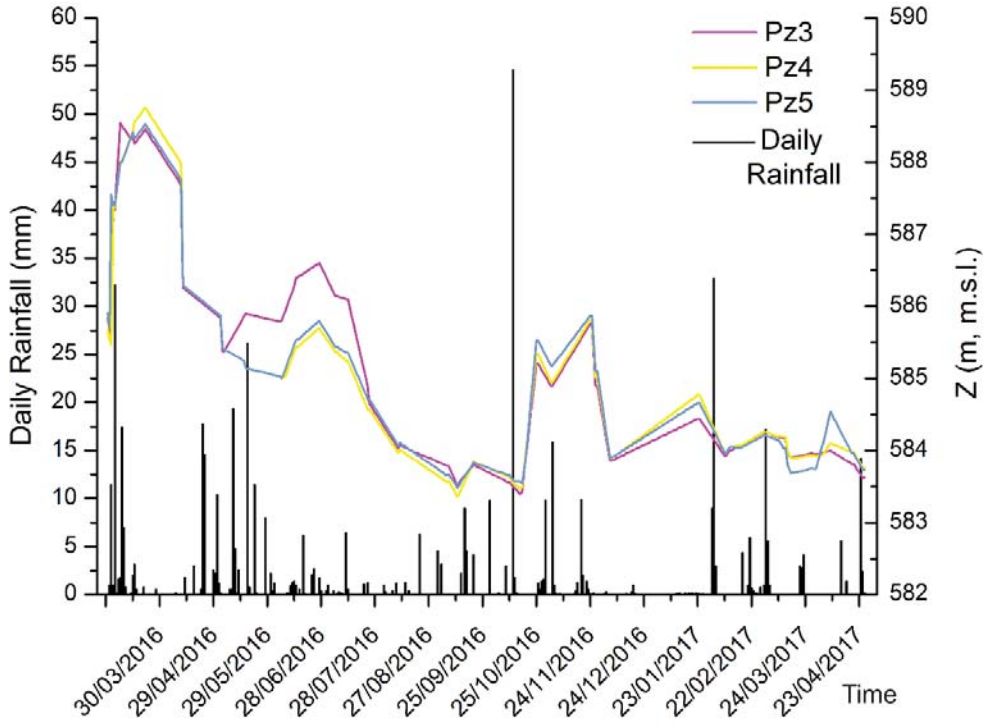

Figure 6.2. Comparison between Pz3-Pz4-Pz5 and rainfalls from March 2016 to May 2017.

Although Pz6 piezometer is located in a different area compared to the other five piezometers (Pz1, Pz2, Pz3, Pz4 and Pz5), it shows a response to the greater rainfall events similar to the other five piezometers (Figure 6.3).

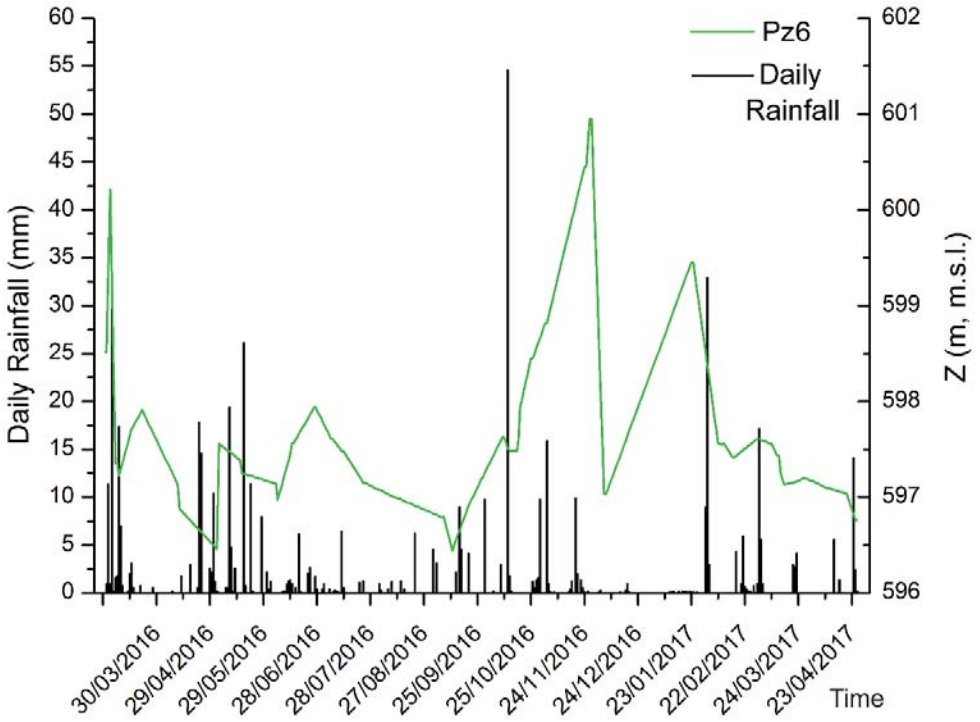

Figure 6.3. Comparison between Pz6 and rainfall from March 2016 to May 2017.

Although the measurements of hydraulic heads was performed in a discontinuous manner due to the logistical and technical problems, a comparison between hydraulic heads data and variation in groundwater level was done. This has provided important information on the aquifer recharge features within the landslide body: the aquifer tends to recharge itself as a result of the rainy periods, and, after the greater rainfall events, it provides a delayed response of about 1-2 weeks in time. This is probably due to the low permeability of the superficial soil layers which are rich in silt and clay.

6.2 Comparison between Rainfalls and Piezometric Data

Pz2 and Pz6 piezometers, which are close to the Cable_2, were considered in order to correlate piezometric and resistivity data, because their opening, in depth, allows to monitor the groundwater variations and, therefore, to make a good correlation between these variations and resistivity values. Since the scale

relative to z, which represents the depth (m) from the sea livel, shows an excessive variation for Pz2 and Pz6 piezometers, data are reported into two distinct graphs, i.e. one related to Pz2 and the other one to Pz6, in Figures 6.4 and 6.5, respectively.

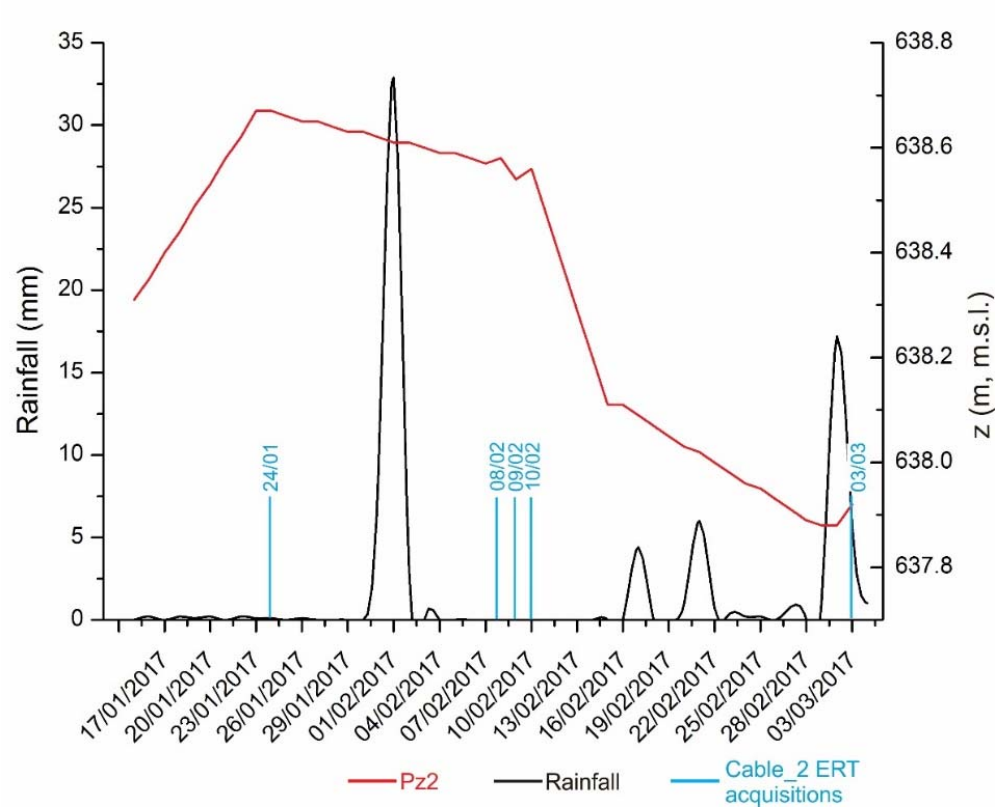

Figure 6.4. Rainfall and Pz2 piezometer monitoring data from January 2017 to March 2017. Dates represented on the ordinate, are the dates of the Cable_2 ERT acquisition.

As is shown in Figure 6.4, piezometric data recorded in Pz2, which is installed near the 3 and 4 electrodes, have a very distinct trend: piezometric levels vary with a delay of some days in response to the rainfall events.

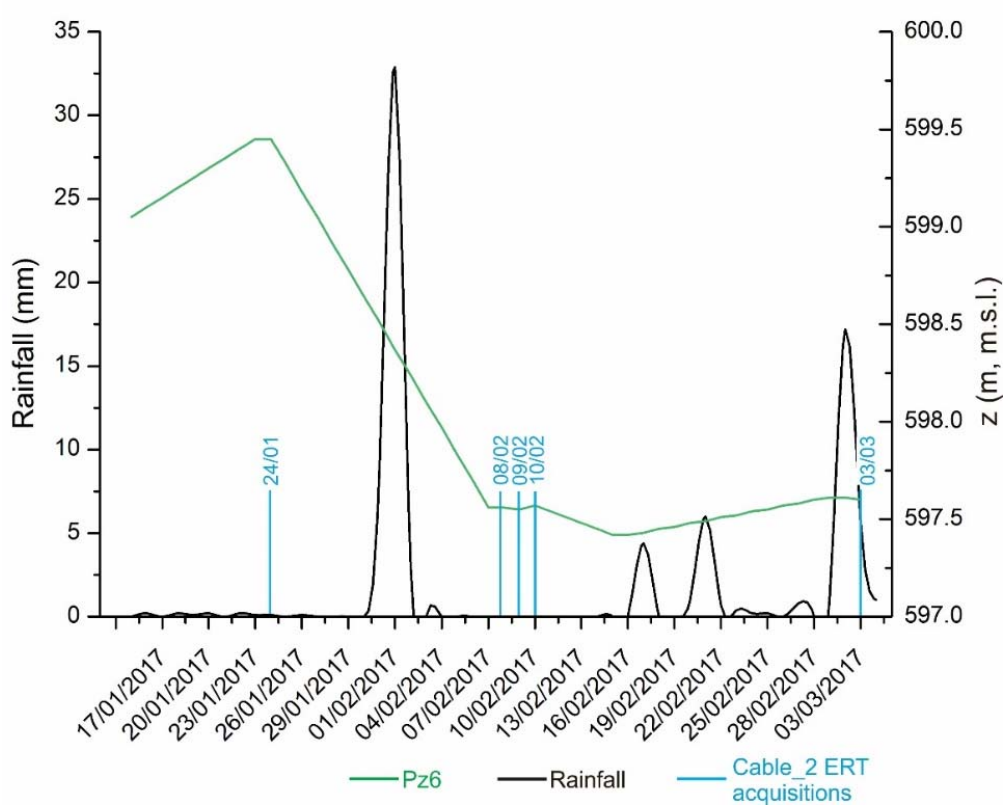

Figure 6.5. Rainfall and Pz6 piezometer monitoring data from January 2017 to March 2017. Dates represented on the ordinate, are the dates of the Cable_2 ERT acquisition.

As is shown in Figure 6.5, the groundwater level tends to decrease after the rainfall events of the first days of February 2017, despite generally groundwater levels tend to rise by over a meter after a rainy event.

From the comparison between rainfalls and piezometric data (Figure 6.6), a connection between rainfall events and recharging of the aquifers was observed. In Figure 6.6 it is possible to observe that, for each piezometer, after a rainy event, a rise in the groundwater level occurs.

Furthermore, the time period when the groundwater level is closer to the ground surface is March 2016, i.e. the period that follows the first inclinometric reading.

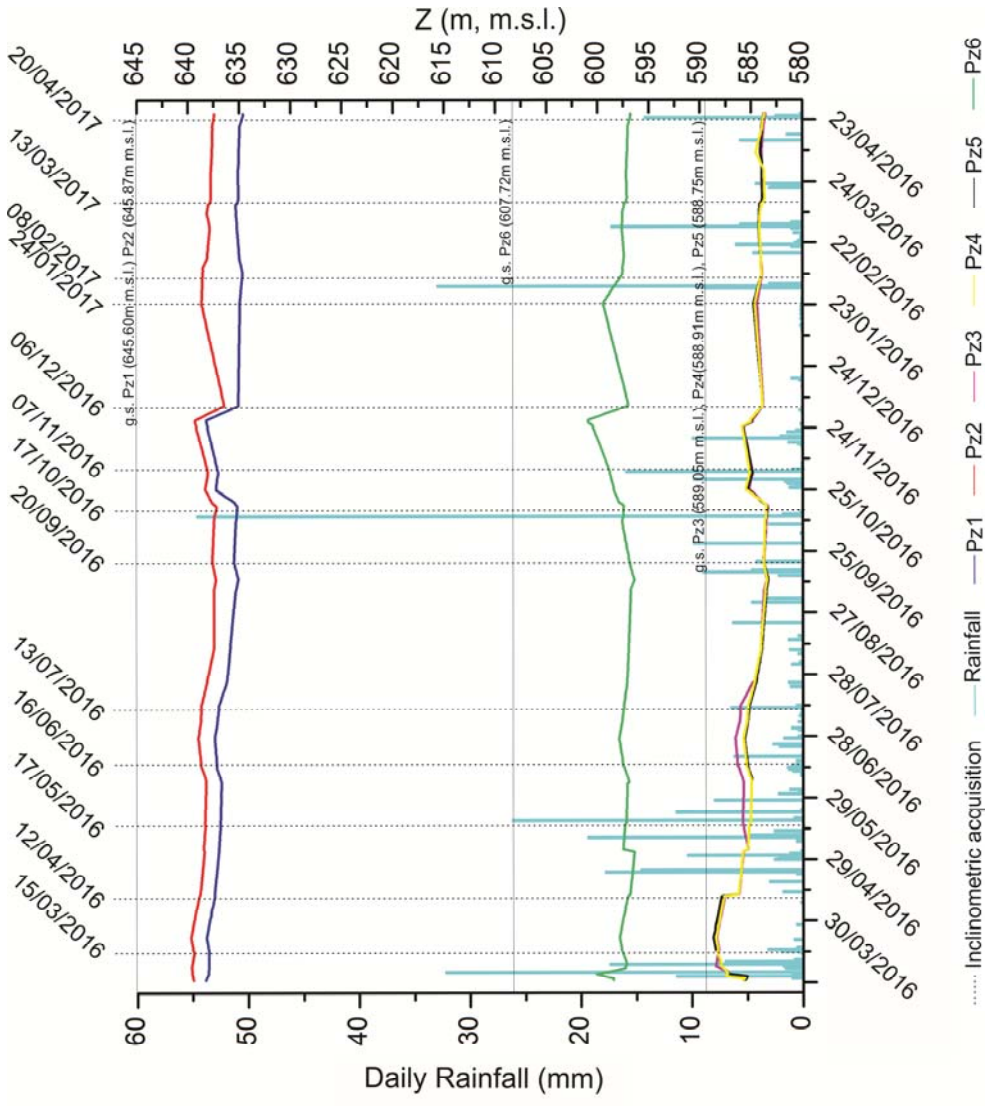

Figure 6.6. Comparison between groundwater level variations and rainfalls data, together with inclinometric data between March 2016 and May 2017. Dates of inclinometric data acquisition are also indicated.

In order to estimate the displacements of the landslide, data recorded for the Si1 and Si2 inclinometers were reported in Figures 6.7 and 6.8: the increase of the groundwater level affects the landslide with an enhanced displacement of the ground along the main and secondary sliding surfaces. In particular, for the Si1 inclinometer, the greater movements were observed in two time periods, i.e. March-April 2016 and May-July 2016, at the same depth of 23m (b.g.s.). These

two time periods occur a few weeks after the most significant rainfall events and are coincident with the peaking water levels (1-4m b.g.s).

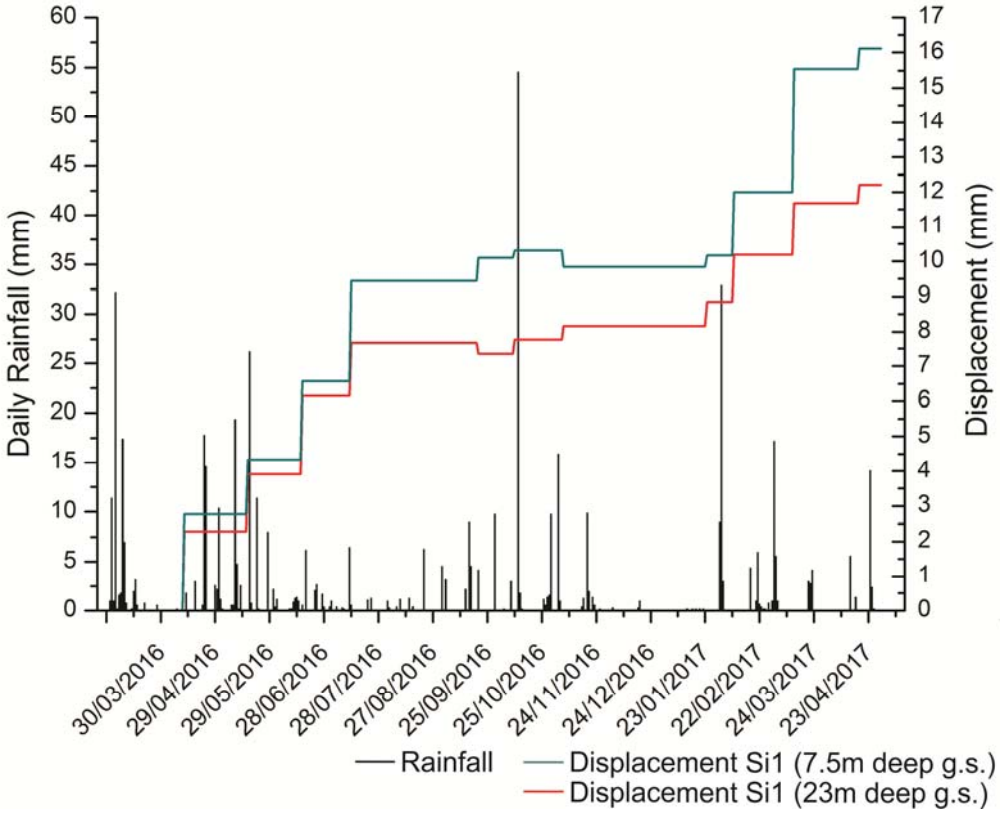

Figure 6.7. Comparison between rainfall and cumulative displacements in Si1 at depths of 23m and 7.5m from the ground surface in the period March 2016-May 2017.

In Figures 6.7 and 6.8, is shown that the larger displacement usually occur after the very intense but short rainy events belonging to the period ranging from February-March 2017. However, this can be better seen in Figure 6.7 where are reported data for Si1 inclinometer. Moreover, the short-term rainfall event affect only the more superficial portion of the ground that slips.

As shown in Figure 6.7, during the period ranging from September 2016 to January 2017, the Si1 shifts are not significant, probably due to a period of low rainfall events and a groundwater level that reaches a depht below 7-8m. On contrary, in the period ranging from March to September 2016, Si1 inclinometer

exhibits mass movements at the depth of 7.5m directly related to the rainfalls and the soil drop.

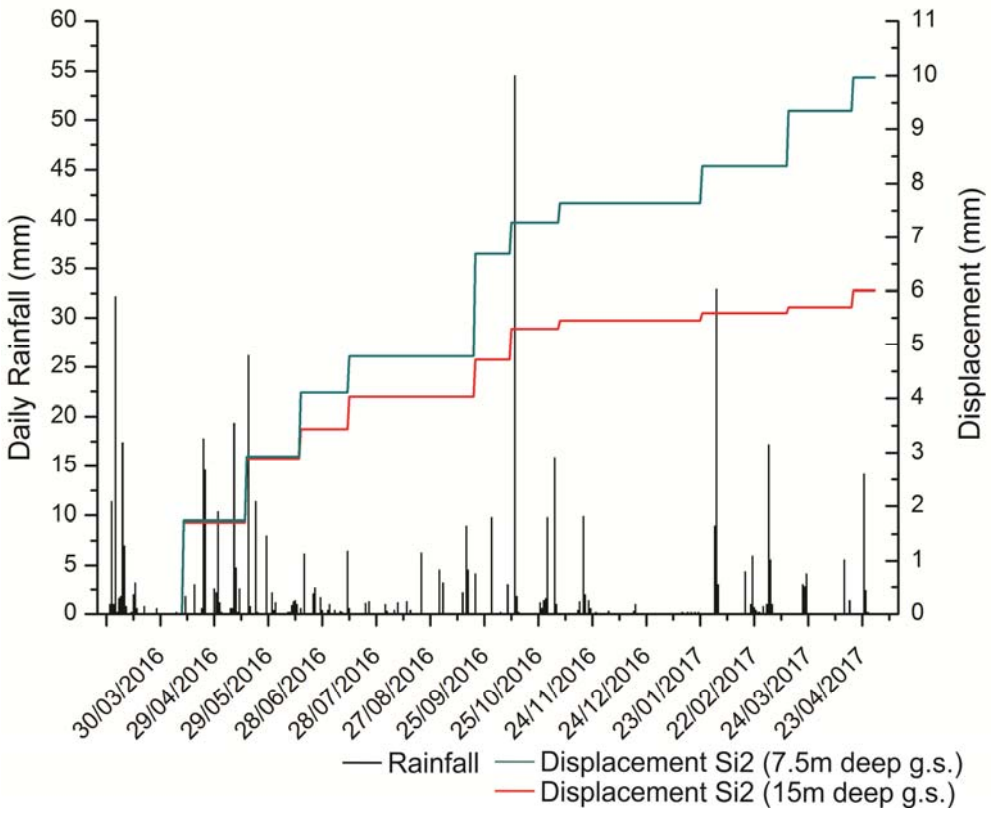

Figure 6.8. Comparison between rainfall and displacement in Si2 at depths of 15m and 7.5m from ground surface, from March 2016 to May 2017.

As shown in Figure 6.8, during the period ranging from September 2016 to May 2017, in the Si2 inclinometer, the displacements measured are not significant like those observed in the Si1 inclinometer.

Furthermore, the Si1 inclinometer shows the primary sliding surface at 23m depth (b.g.s.), while in the Si2 inclinometer (Figure 6.8), the mass movement is less deep and the primary sliding surface is located at about 15m depth (b.g.s.).

In Figures 6.9 and 6.10, is shown the average groundwater level and the displacement recorded at different depths in the Si1 and Si2 inclinometers, respectively. As is shown in these Figures, during the period ranging from March

2016 to October 2016, the average groundwater level gradually decreases, although there is a rise at the end of June 2016. In the following two months (i.e. November and December 2016) the highest peaks are recorded. Therefore, despite the groundwater level increase a lot during this period, at the end of December 2016, a steep decrease was recorded as shown by the straight and vertical line which represents groundwarer level. This can be explained because this period was without rainy events. A general rising but irregular trend is recorded in the following months that ranging from January 2017 to April 2017. Moreover, as is shown in Figures 6.9 and 6.10, the greatest inclinometric displacements were recorded during the first monitoring period, i.e. from April 2016 to July 2016, where displacement rates show a gradual increase. The same was observed between February 2017 and April 2017, while in the other monitored months, displacement rates were not recorded.

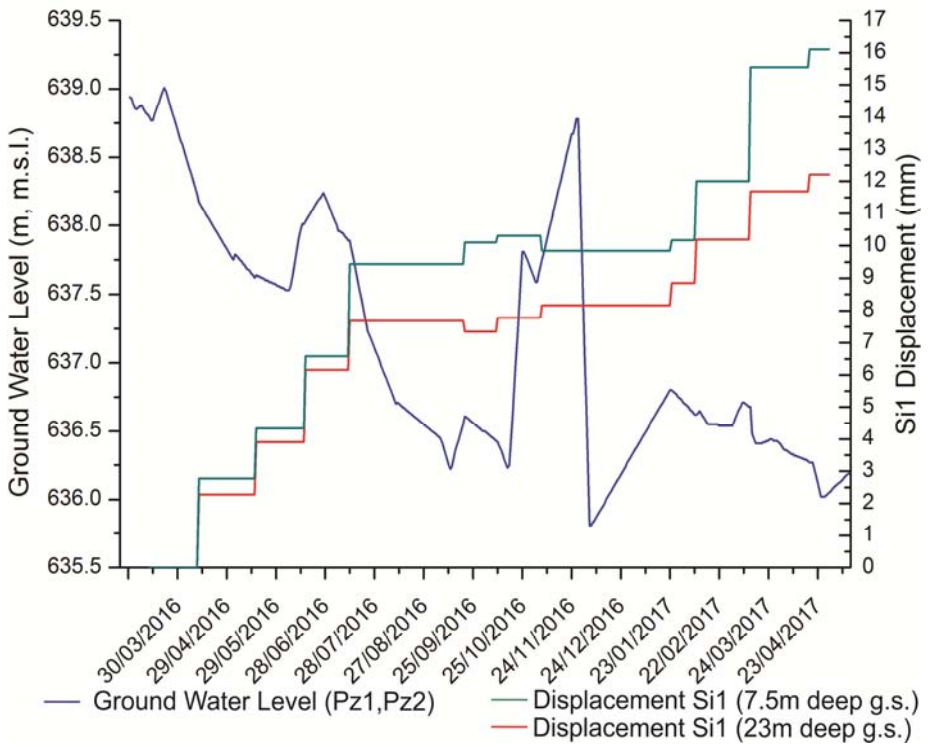

Figure 6.9. Average groundwater level calculated comparing data collected by the Pz1-Pz2 piezometers and the displacement recorded in the Si1 inclinometer at depths of 7.5m and 23m (b.g.s.), from March 2016 to May 2017.

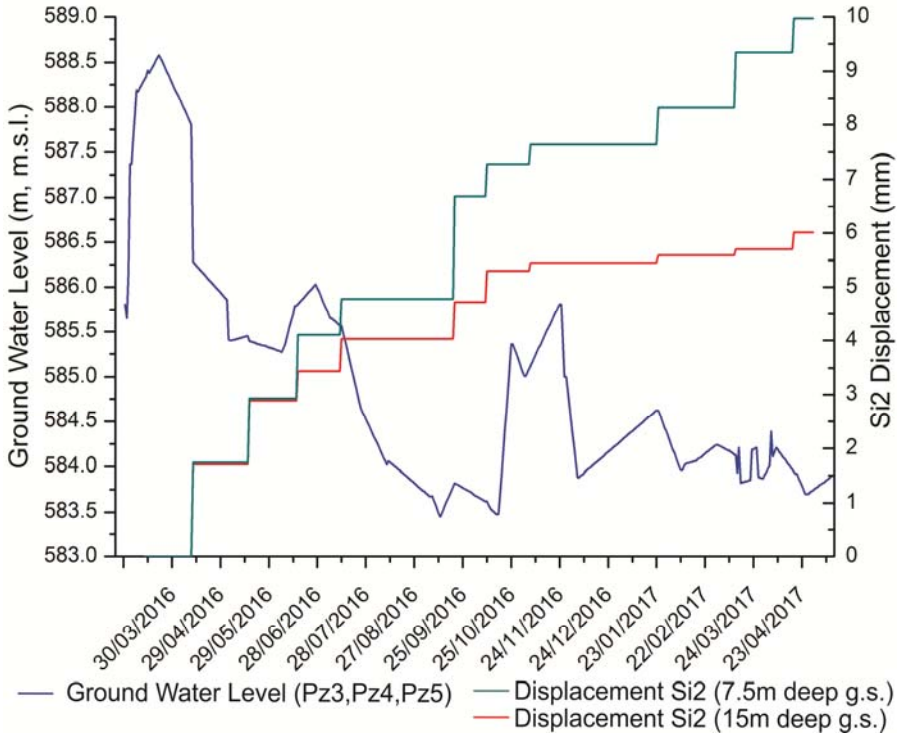

Figure 6.10. Average groundwater level calculated comparing data collected by the Pz3-Pz4-Pz5 piezometers and the displacement recorded in the Si2 inclinometer at depth of 7.5m and 15m (b.g.s.) from March 2016 to May 2017.

In conclusion and as is shown in both Figures, the most significant rates of displacement, are in correspondance of the peaks reached by the average groundwater level; this explain how the groundwater level affects the stability of the soil mass.

The magnitude of the displacement over the seven months considered, was of about 2mm/month in the Si1 inclinometer with a greater movement localized at 7m (b.g.s.), and of about 1.5mm/month in the Si2 inclinometer with a movement greater than 3m depth (b.g.s.). Therefore, in the fourteen months, that cover the whole period of study and observation, the total displacement was 18mm in Si1 and 12mm in Si2.

Furthermore, following the classification produced by Hungr (1981) and modified by Hungr et al. (2014), it is possible to classify the type of movements that characterize the landslide. Therefore the sliding movement of the Case

Pennetta landslide falls into the class 2, which indicates a very slow movement at a speed of about $5x10^{-10}$ (16mm/year).

6.3 Ground Model Discussion

Landslide movements generally depend on different factors. In this study, landslide movements are related to lithology of the Case Pennetta site and to the lithotechnical properties of the Mt. Caio Flysch and Arenarie di Scabiazza Formations. These formations have a low plastic limit, which is reached when the high water content decreases the internal cohesion, causing a ground mass movement downward.

Another factor is related to morphology: for Case Pennetta landslide which is 1.5km length there are 350 meters of difference in altitude and the slope is characterized by a steep slope angle of about 17 degree.

The model of the landslide is based on field observations, geophysical acquisitions and boreholes data. 2D ERT data were acquired in order to describe the general structure of the landslide. The model of the internal architecture of the landslide body was described also with the support of the inclinometric measurements.

Furthermore, in order to have a clearer vision of the study area and a greater control over the features of the investigated slope, the geological-geomorphological model presented in Chapter 3, was proposed, correlated and implemented with data of the multi-parametric system acquired from March 2016 to May 2017 (Figure 6.11). The model is extended from Case Ferdinando village (725m s.l.m.), that crosses the Case Pennetta village, to the downstream monitoring area (500m m.s.l.).

The model shows that, by comparing inclinometric data relatively to the Si1 borehole with those geophysical (ERT_WPD), it was possible to find a resistive anomaly. This anomalous low resistivity value is recorded where the inclinometric measurement indicates a displacement of 18mm in 14 months. Furthermore, by correlating stratigraphic data (again relatively to the Si1

borehole) with those geophysical, it was possible to observe that the transition from silty clay to rocky substrate, and it is highlighted by an increase in the resistance value. This allows to hypothesize the presence of a sliding surface within the landslide body beneath the village of Case Pennetta.

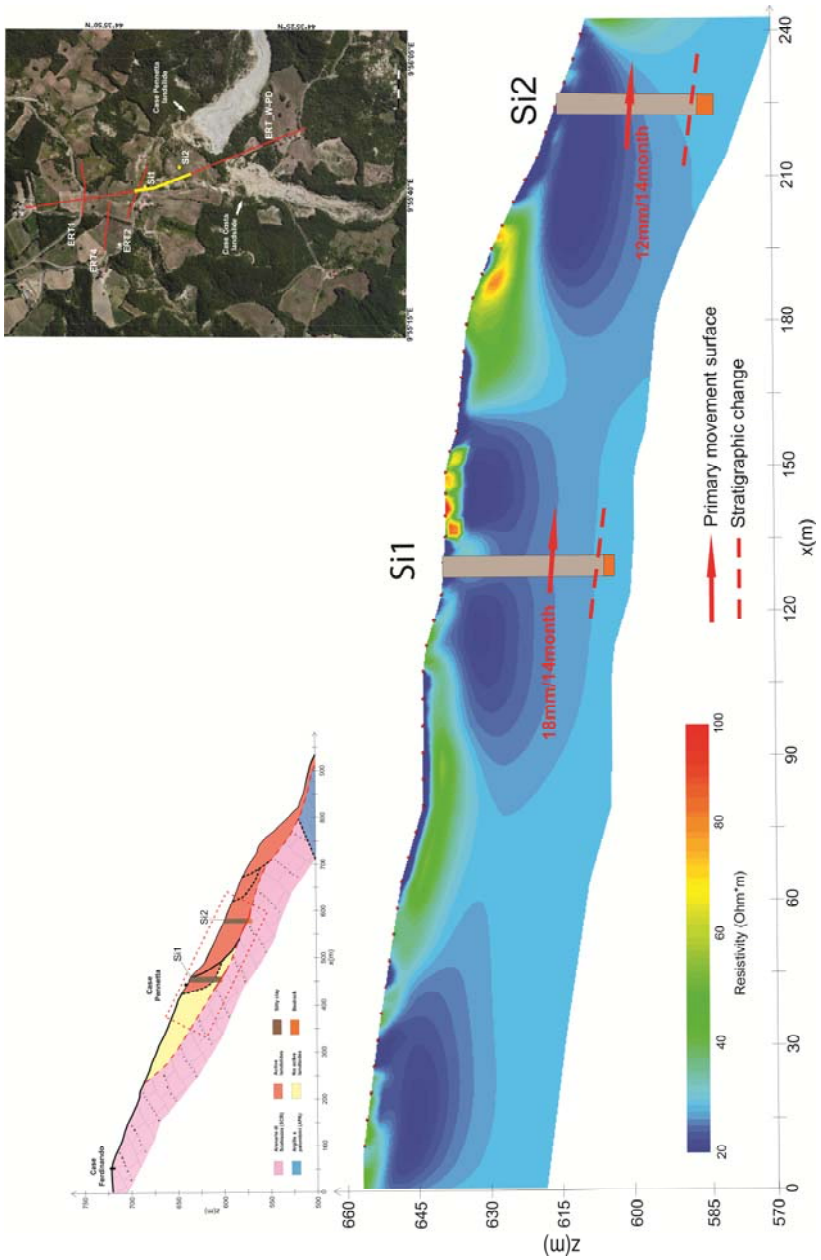

Figure 6.11. Comparison between geophysical data (ERT_W-PD yellow part) and inclinometeric-stratigraphic data (Si1 and Si2).

The good correlation with geoelectrical data is also shown by the Si2 borehole. Geophysical data exhibit a highly conductive anomaly at a depth of 15m (b.g.s.) where, in 14 months of monitoring, a shift of 12mm toward S-SW was measured, and higher resistivity values at 30m depth (b.g.s) where the transition from a silty clay to rocky substrate was observed. This may indicate a body with a smaller water content and a more competent body constituted by a lower fine component. The interpretation of the 2D architecture of the slope (Figure 3.20, Paragraph 3.4.1, Chapter 3) was developed combining the geology-geomorphological map interpretation with the results of the geotechnical, hydrogeological and geophysical analyses that have been described in the previous Chapters. Case Pennetta landslide is characterized by a roto-translative movement limited to the upper part of the slope, which is the area where the monitoring system was installed, and by an earth-flow movement towards the Taro Valley at 220m (m.s.l.) in the lower part, which includes the part of the landslide that goes downhill from the front of the earth-flow to the valley. Therefore, the Case Pennetta case study is characterized by a complex and composite movement style. The results obtained by information acquired during the monitoring time period, is shown in Figure 6.12.

The resistivity section reported in Figure 6.12, shows a lot of important results used to determinate the geometry of the landslide portion monitored by the Cable_2: in particular, it clearly reveals the subsurface geometry of the landslide. Areas with relatively high resistivity values (50-90Ωm), recorded from the surface to the shallow depths and between the electrodes 1-15 and 30-40, might be caused by the coarse material of the landslide. The thickness of this portion varies between 10 and 15m from the ground surface.

A conductive area with resistivity values of 10-25Ωm and located between the electrodes 15 and 30, is present and shown in Figure 6.12. This area might be composed of unconsolidated and water-saturated landslide material that has a higher clay and silt content, as suggested by borehole data.

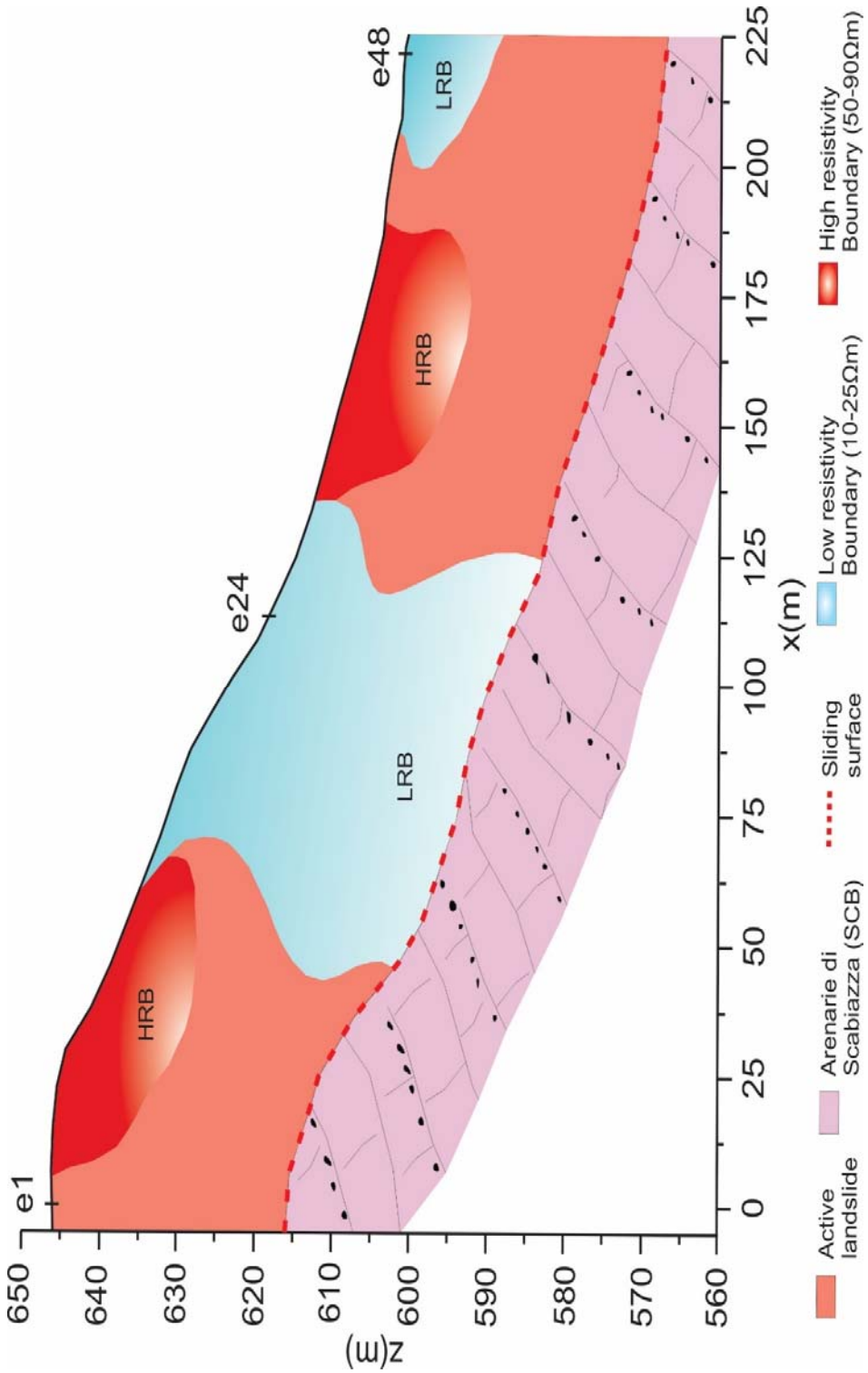

Figure 6.12. Multi-parameter model of the area monitored, below the geoelectric Cable_2. (HRB: High Resistivity Boundary, LRB: Low Resistivity Boundary).

The high water content was considered to explain the low resistivities and suggests a probable underground hydro-flow. For these reasons, the bottom of this zone can be considered the failure surface of this portion of the landslide. The low resistivity values are due to the fact that the Formations in the Northern Apennines are very rich in clayey and silty material and the high fractions of fine materials may cause similar geophysical responses.

By comparing inclinometric data with data of the multiparameter model described in Figure 6.12, it was possible to hypothesize different material properties between the shallow layer located above 7m depth (g.s), and the underlying layer, until reaching the rock substratum.

The increase in displacement recorded at 3m depth (b.g.s.), may be due to the immediate absorption of rainwater by the first meters of soil. These shallow moisture dynamics may only influence the movement surface but not the groundwater level. This has highlighted the need of a smaller electrode spacing which would allow to obtain a higher degree of resolution and, therefore, more details in the shallow layer, through which rainwater infiltration occurs. Therefore, in this work a distance of 5m between electrodes, was used.

From data obtained in the monitored time period, it was possible to provide a landslide outline picture of the area near the Case Pennetta village. Landslides movements that have two different styles of activity, were identified by the analysis of the superficial shapes observed during the detection phase. As mentioned above, the northernmost part of the landslide body, near the geophysical monitoring system, was characterized by a rotational movement that was started along a neo-formation sliding surface that, in turn, originates from the craking of the material affected by the movement. The confirmation of this type of movement was found in the counterslope features in the upstream area of the main escarpment. The activity status, according to the inclinometric measurements acquired during the monitoring time period, suggests that Case Pennetta landslide is currently considered to be active, because the causes that have triggered movements in the past are still presents and visible effects may

be observed on the ground. The movement of the landslide was classified in this way because no fresh forms indicating the recent phenomenon activity, were recorded during the geomorphological survey. All features are completely covered by vegetation and difficult to distinguish, or remodeled by other processes that followed over the years. However, direct observations are lacking due to the absence of outcrops. Proceeding down and towards the slope, the landslide is characterized by plasticized materials that assume the typical characteristics of earthflow, with deposits consisting of blocks of variable dimensions and immersed in a fine matrix.

Chapter 7

Conclusions

This study has led to obtain significant data on the evolution of a typical landslide of the Tuscan-Emilian Apennines. Geological-geomorphological and geotechnical analysis together with geophysical and hydrogeological monitoring can be used in the future to carry out a preliminary assessment of the Case Pennetta landslide. At the same time, given the presence of many landslides similar in the Northern Apennines, the results of this study could also be used as a basis for other future investigations related to other landslide events.

Taking into account this study, it is possible to affirm that in order to improve the numerical model, is necessary to consider a continuative monitoring of inclinometry, piezometry and geophysics. In our case, during the monitoring period, the landslide was not subject to long and intense rainfall events. This would have resulted in a rise of the groundwater levels over a prolonged period of time, and would have greatly affected both displacements rates and resistivity contrasts.

Despite this, it is necessary to further study the Case Pennetta landslide, its displacement and the groundwater levels, in order to confirm the validation of the model used.

However, it can be stated from the data currently available that:

- the landslide displacement is slow and consists of two kinematic types: roto-traslative movement in the upper part, and earth-flow movement in the lower part.
- displacement rates are in the order of mm/month; therefore, within a one year, the Case Pennetta landslide can move about a few centimeters or a maximum of 1 decimeter in the direction of the maximum slope;
- the groundwater level influences the movement, while its growing causes an increase in displacements;
- alarming movements have not been highlighted for the monitored period.

In conclusion, a slow and steady movement of the landslide can be assumed for the next future, with peaks only in exceptional cases, when the movement of the surface of the earthflow could grow dramatically, i.e. during very long and

intense meteoric events. The understanding of the landslide dynamics is allowed by the temporal analysis of the evolution of the fluids movement into the mass. A new approach to measure and evaluate the variation of the physical properties into the landslide by using piezometry, pluviometry and inclinometry, was proposed. Furthermore, the electrical tomography as a complementary tool to the analysis of the changes of resistivity, is used.

This integrated approach based on noninvasive electrical prospecting methods, geological investigations and geomorphological information seems to be a promising tool for investigating landslide areas (Jomard et al., 2010).

This integrated approach based on noninvasive electrical prospecting methods, geological investigations and geomorphological information seems to be a promising tool for investigating landslide areas (Jomard et al., 2010). In the future, it will be possible to study the temporal fluctuations of the subsurface resistivity values by using a monitoring strategy designed to continuously repeat an electrical surveillance. Time lapse analysis of 2D electrical images, carried out across landslide bodies, could allow to a better understanding of the time dynamics of the hydrogeological processes which are the principal causes of instability phenomena.

In particular, the advantage to use time-lapse 2D ERT method to study the landslide processes, is its sensitivity to variation in moisture content of the subsurface. ERT monitoring gives information only about how the slope responds to the rainfall infiltration and soil moisture accumulation, and not about the response of the overall landslide body.

Landslide bodies respond to changes of the ground conditions (a rise in the water table or soil moisture content) which can result in reaching of the plastic limit, which, in turn, can bring to a change in the internal physical properties of the landslide body, such as the soil strength.

This investigation confirms the suitability of ERT monitoring for observing landslide hydrogeological precursors. However, the sensitivity of the system must be harnessed correctly to represent the area of interest at a high enough

resolution and to observe the most important features. Furthermore, this investigation has shown that, electrical resistivity monitoring is a great method used to observe hydrogeological precursors to landslide activation, i.e. both soil moisture infiltration and movements at high resolution.

However, the observing capability an increase of the moisture content in time, is a powerful tool for the landslide forecasting, if it is combined with a priori additional geotechnical data. This Ph.D. represents the first brick for a more extensive and deepened study of Case Pennetta landslide. The phase of construction of the geophysical monitoring system, which I personally managed from start to finish, is the core of my three years of research and work without which any subsequent study would have not been possible. However, even though my work was planned in all its parts since the early days, it is necessary to leave some suggestions and considerations, to those who will work at this project in the future, in order to get concrete results in understanding dynamics that affecting the landslides. The logistics operations carried out during these three years involved design, construction, installation and maintenance of three geoelectric cables. Cable_1 and Cable_2, 235 m long, were installed on the surface of the landslide; each cable consists of 48 electrodes with an electrodical distance of 5m but only data obtained from Cable_2 have been shown and analyzed. Another cable was installed in the hole, up to a depth of 36m (b.g.s.) with 24 electrodes with an electrodic distance of 1.5m, but, in this case, data are not available, because the instrumentation has never been made operational during our work. An important suggestion for the future operations which could be the realization of a third geoelectric cable as the last element of the geophysical monitoring system, is the best management and organization of logistic activities, which determines the achievement of more reliable results in a short time. In conclusion, for the future, it is more appropriate that the work team consists at least of 3 people.

Moreover, for a proper correlation of geophysical data with the displacement rates and variations of the groundwater level, each geoelectrical cable must be

properly installed near piezometers and inclinometers (or vice versa), whose number and position vary according to the length of the cable. The same is true of the stratigraphic information that are needed for a correct calibration of the multi-parameter system. In addition, the number of boreholes depends on both length of the cable installed and information available on the study area.

On the contrary, the number of tomographic lines that must be realized for a full study, should be considered. The first factor to consider is the topography that strongly impacts the choice. Surely, the best choice to get a uniform data set, is a grid realization that provides the best degree of data coverage, but, as in Case Pennetta area, this is not possible. In this work the choice of geoelectrical cable installation areas was heavily affected by the territory conformation, which consequently leds to difficult logistic operations. Moreover, not knowing in advance the ground response to rainfall events, it was chosen to use a 5m electrode spacing that allows to get information which can reach a depth of 30-35m (b.g.s.), with a good degree of resolution. This choice was the best and most cautious to follow, but, as a suggestion for the future, could be more convenient the choice of reducing the electrode spacing in order to monitorate in detail the water infiltration modes, and to observe the resistivity variations in the first ground meters. Since resolution of geophysical images should be sufficient to permit the observation of the processes of interest, the suggestion is to reduce the overall coverage of the area in favor of the increase in the degree of resolution, esclusively of the most active regions of the landslide. This is because a monitoring campaign geographically focused provides data more capable of being comprehensively analyzed: in fact, bulk properties can mask the finer details of the subsurface processes and can limit their interpretatio

Bibliography

Anno, P., and Routh, P. (2007). A new 4d workflow for legacy seismic data: *77th Annual International Meeting, SEG*, Expanded Abstracts, 2888-2892.

Archie, G. E. (1942). The electrical resistivity log as an aid in determining some reservoir characteristics. *Transaction of American Institute of Mining, Metallurgical, and Petroleum Engineers*, 146, 54-62.

Argnani, A., Barbacini, G., Bernini, M., Camurri, F., Ghielmi, M., Papani, G., Rizzini, F., Rogledi, S., and Torelli, G. (2003). Gravity tectonics driven by Quaternary uplift in the Northern Apennines: insights from La Spezia-Reggio Emilia geotransect. *Quaternary International*, vol. 101-102, 13-26.

Bayliss, A., Gunzburger, M., and Turkel, E. (1982). Boundary conditions for the Numerical solution of elliptic equations in external regions. *Journal of Applied Mathematics*, vol. 42, 430-451.

Bartolini, C., Bernini, M., Carloni G.C., Costantini, A., Federici, P.R., Gasperi, G., Lazzarotto, A., Marchetti, G., Mazzanti, R., Papani, G., Pranzini, G., Rau, A., Sandrelli, F., Vercesi, P.L., Castaldini, D., and Francavilla, F. (1982). Carta neotettenica dell'Appennino settentrionale. Note illustrative, *Bollettino Della Societa Geologica Italiana*, 101, 523-549.

Banton, O., Seguin, M.K., and Cimon, M.A. (1997). Mapping field scale physical properties of soil with electrical resistivity. *Soil Science Society of America journal,* 61, 1010-1017.

Bernini, M., Vescovi, P., and Zanzucchi, G. (1997). Schema Strutturale dell'Appennino nord-occidentale. L'Ateneo Parmense. *Acta Naturalia*, 33, 43-54

Bertolini, G. (2001b). Modalità di riattivazione, interventi, caratteri geotecnica e mineralogici di una frana di argilla a struttura caotica ("Argille Scagliose" Auctt): la frana di Casoletta (Comune di Vezzano, Provincia di Reggio Emilia). *Quaderni di Geologia Applicata*, vol. 8,163-183, Bologna (Pitagora).

Bertolini, G. (2005). Monitoraggio di frane in area appenninica. In: Proceeding of the Congress "Il monitoraggio e l'assetto idrogeologico: stato dell'arte e prospettive professionali (Milano, 9-10 ottobre 2003)", *Ordine dei Geologi della Lombardia*,125-136.

Bertolini, G., and Pellegrini, M. (2001). The landslides of the Emilia Apennines (Northern Italy) with references to those which resumed activity in the 1994-1999 period and required Civil Protection interventions. *Quaderni di Geologia Applicata*, vol. 8, 27-75, Bologna (Pitagora).

Bertolini, G., and Gorgoni C. (2001). La Lavina di Roncovetro (Vedriano, Comune di canossa, Provincia di reggio Emilia). *Quaderni di Geologia Applicata,* vol. 8, 1-23, Bologna (Pitagora).

Bertolini, G., and Pizziolo M. (2008). Risk assessment strategies for the reactivation of earthflows in the Northern Apennines (Italy). *Engineering Geology*. 102, 178-192.

Bettelli, G., and De Nardo, M.T. (2001). Geological outlines of the Emilia Apennines (Italy) and introduction to the rock units cropping out in the areas of the landslides reactivated in the 1994-1999 period. *Quaderni di Geologia Applicata*, 8, 1–26, Bologna (Pitagora).

Bogoslovsky V.A., and Ogilvy A.A. (1977). Geophysical methods for the investigation of landslide. *Geophysics*, 42, 562-571.

Borie, M.P., Sirieix, C., Naudet, V., and Riss, J. (2011). Electrical resistivity monitoring with buried electrodes and cable: noise estimation with repeatability tests. *Near Surface Geophysics*, 9, 369-380.

Brabb, E.E. (1991) The World Landslide Problem. Episodes, 14, 52-61.

Brabb, E.E., and Harrod, B.L. (eds.) (1989). Landslides: Extent and economic significance. A.A. Balkema Publisher, Rotterdam, 385 pp.

Brunet, P., Clement, R., and Bouvier, C. (2010). Monitoring soil water content and deficit using Electrical Resistivity Tomography (ERT). A case study in the Cevennes area, France. *Journal of Hydrology*, 380, 146-153.

Carlini, M., Chelli, A., Vescovi, P., Artoni, A., Clemenzi, L., Tellini, C., and Torelli, L. (2016). Tectonic control on the development and distribution of large landslides in the Northern Apennines (Italy). *Geomorphology*, 253, 425-437.

Casagrande, A. (1948). Classification and identification of soils. Trans., ASCE, 113, 783-810.

Cavinato, G., Di Luzio, E., Moscatelli, M., Vallone, R., Averardi, M., Valente, A., and Papale, S. (2006). The new Col di Tenda tunnel between Italy and France: Integrated geological investigations and geophysical prospections for preliminary studies on the Italian side. *Engineering Geology*, 88, 90-109.

Cendrero, A., and Dramis, F. (1996). The contribution of landslide to landscape evolution in Europe. *Geomorphology*, 16, 191-211.

Chambers, J.E., Gunn, D.A., Wilkinson P.B., Melrum, P.I., Haslam, E., Holyoake, S., Kirkham, M., Kuras, O., Merritt, A., and Wragg, J. (2014). 4D electrical resistivity tomography monitoring of soil moisture dynamics in an operational railway embankement. *Near Surface Geophysics*, 12, 61-72.

Chambers, J.E., Wilkinson, P.B., Penn, S., Meldrum, P.I., Kuras, O., Loke, M.H., and Gunn D.A. (2013). River terrace sand and gravel deposit reserve estimation using three-dimensional electrical resistivity tomography. *Journal of Applied Geophysics*, 93, 25-32.

Chambers, J.E., Gunn, D.A., Meldrum, P.I., Wilkinson, P.B., Ogilvy, R.D., Haslam, E., Holyoake, S., and Wragg, J. (2011a). Volumetric monitoring of earth embankment internal structure and moisture movement as a tool for condition monitoring. 11th int. conf. railway engineering, London.

Chambers, J.E., Wilkinson, P.B., Kuras, O., Ford, J.R., Gunn, D.A., and Meldrum, P.I. (2011b). Three dimensional geophysical anatomy of an active landslide in Lias Group mudrocks, Cleveland Basin, UK. *Geomorphology*, 125, 472-84.

Chambers, J.E., Ogilvy, R.D., Kuras, O., Cripps, J.C., and Meldrum, P.I. (2002). 3D electrical imaging of known targets at a controlled environmental test site. *Environmental Geology,* 41, 690-704.

Chelli, A., Mandrone, G., Ruffini, A., and Truffelli, G. (2005). Dynamics and conceptual model of the Rossana castle landslide (Northern Apennines, Italy). *Natural Hazards and Earth System Sciences*, 5, 903-909.

Chelli, A., Mandrone, G., and Truffelli, G., (2006). Field investigations and monitoring as tools for modelling the Rossena castle landslide (Northern Apennines, Italy). *Landslides*, 3, 252–259.

Chelli, A., Ruffini, A., Castagnetti, S., and Tellini, C., (2015). The geomorphologic survey as tool to support risk management after landslide reactivation: the case study of Sauna di Corniglio landslide (Northern Apennines, Italy). In: Lollino, G., et al. (Eds.), *Engineering Geology for Society and Territory*, vol. 2. Springer International Publishing Switzerland, 1079-1082.

Coe, J.A., Godt, J.W., Parise, M., and Moscariello, A., (2003), Estimating debris-flow probability using debris-fan stratigraphy, historic records, and drainage-basin morphology, Interstate 70 Highway Corridor, Central Colorado: In, Rickenmann, D.and Chen, C., eds., Debris flow hazards mitigation: mechanics, prediction, and assessment, *Proceedings of the Third International Conference on Debris-Flow Hazards Mitigation*, Davos, Switzerland, September 10-12, Millpress, Rotterdam, 1085-1096.

Constable, S.C., Parker, R.L., and Constable, C.G. (1987). Occam's inversion: A pratical algorithm for generating smooth models from electromagnetic sounding data. *Geophysics*, vol. 52, 289-300.

Crozier, M.J. (1986). Landslides: causes, consequences & environment. Croom Helm Pub., London.

Crozier, M.J. (1995). Landslide hazard assessment: a review of papers presented to them G4, in Bell, D. (Ed.), Landslides. *Proceedings of Sixth International Symposium on Landslides Christchurch*, 10-14 February 1992, vol. 3, Bakema, Rotterdam, 1843-1848.

Cruden, D.M. (1991). A simple definition of a landslide. *Bulletin International Association for Engineering Geology*, 43, 27-29.

Cruden, D.M., and Varnes, D.J., (1996). Landslide types and processes. In Turner, A.K. and Schuster, R.L. (eds.), Landslides, Investigation and Mitigation. Washington D.C., National Academy Press. *Transportation Research Board Special Report*, 247, 36-75.

Day-Lewis, F.D., Harris, J.M., and Gorelick, S.M., (2002), Time-lapse inversion of crosswell radar data. *Geophysics*, 67, 1740-1752.

Day-Lewis, F. D., Lane Jr., J.W., Harris, J. M., and Gorelick, S.M. (2003). Time-lapse imaging of saline-tracer transport in fractured rock using difference-attenuation radar tomography. *Water Resources Resear*ch, 39, 1290, doi: 10.1029/2002WR001722.

Dahlin, T., Aronsson, P., and Thörnelöf, M. (2014). Soil resistivity monitoring of an irrigation experiment. *Near Surface Geophysics*, 12, 35-43.

Dahlin, T. and Loke M.H. (1998). Resolution of 2-D Wenner resistivity imaging as assessed by numerical modelling. *Journal Applied Geophysics*, 38, 237-249.

Dahlin, T., and Zhou, B. (2004). A numerical comparison of 2D resistivity imaging with 10 electrode arrays. *Geophysical Prospecting*, 52, 379-398.

Daniels F., and Alberty R.A. (1966). Physical Chemistry. John Wiley and Sons, Inc.

De Franco, R., Biella, G., Tosi, L., Teatini, P., Lozej, A., Chiozzotto, B., Giada, M., Rizzetto, F., Claude, C., Mayer, A., Bassan, V., and Gasperetto-Storiti, G. (2009). Monitoring the saltwater intrusion by time lapse electrical resitivity tomography: The Chioggia test site (Venice Lagoon, Italy). *Journal of Applied Geophysics*, 69, 117-130.

Dey, A., and Morrison, H.F., (1979). Resistivity modelling for arbitrarily shaped two-dimensional structures. *Geophysical Prospecting*, 27, 106-136.

Descloitres, M., Ruiz, L., Sekhar, M., Legchenko, A., Braun, J.J., Kumar, M.S.M., and Subramanian, S. (2007). Characterization of seasonal local recharge using electrical resistivity tomography and magnetic resonance sounding. *Hydrological Processes*, 22, 384-394.

Dikau, R., Brunsden, D., Schrott, L., and Ibsen, M.L. (eds.) (1996). Landslide recognition. Identification, movements and causes. John Wiley & Sons Ltd, Chichester, England, 251 pp.

Edwards, L.S. (1977). A modified pseudo-section for resistivity and IP. *Geophysics*, 42, 1020-1036.

Ellis, R., and Oldenburg D.W. (1994). Applied geophysical inversion. *Geophyical Journal International*, 116, 5-11.

Ewing, R.P., and Hunt, A.G. (2006). Dependence of the electrical conductivity on saturation in real porous media. *Vadose Zone Journal*, 5, 731-741.

Friedel, S., Thielen, A., and Springman, S.M., (2006). Investigation of a slope wndangered by rainfall-induced landslides using 3D resistivity tomography and geotechnical testing. *Journal of Applield Geophys*ics, 60, 100-114.

Giano, S.I., Lapenna, V., Piscitelli, S., and Schiattarella, M. (2000), Electrical imaging and self-potential surveys to study the geological setting of the Quaternary slope deposits in the Agri high valley (southern Italy). *Annali di Geofisica*, 43, 409-419.

Goryainoiv, N.N., and Martveev, N.M. (1988). Use of geophysical for landslide and mudflow investigations, Kozlovskii YA (ed). *Landslide and mudflow*. UNESCO, Moscow.

Griffiths, D.H., Turnbull, J., and Olayinka, A.I. (1990). Two-dimensional resistivity mapping with a computer- controlled array. *First Break 8*, 121-129.

Griffiths, D.H., and Barker, R.D. (1993) Two-dimensional resistivity imaging and modelling in areas of complex geology. *Journal of Applied Geophysics*, 29, 211-226.

deGroot-Hedlin, C., and Constable, S. (1990). Occam's inversion to generate smooth, two-dimensional models from magnetotelluric data. *Geophysics*, 55, 1613-1624.

Guzzetti, F., Carrara, A., Cardinali, M. and Reichenbach, P. (1999a). Landslide hazard evaluation: an aid to a sustainable development. *Geomorphology*, 31, 181-216.

Guzzetti, F., Stark, C.P., and Salvati, P. (2005c). Evaluation of flood and landslide risk to the population of Italy. *Environmental Management*, 36, 5-36.

Hack, R., (2000). Geophysics for slope stability. *Surveys in Geophysics*, 21, 423-448.

Hallof, P.G. (1957). On the interpretation of resistivity and induced polarization measurements. *Ph.D Thesis, Massachusetts*, 256 pp.

Hayashi, M. (2004), Temperature-electrical conductivity relation of water for environmental monitoring and geophysical data inversion. *Environmental Monitoring and Assessment*, 96, 119-128.

Hayley, K., Bentley, L.R., Gharibi, M., and Nightingale, M. (2007). Low temperature dependence of electrical resistivity: implication for near surface geophysical monitoring. *Geophysical Research Lett*ers, 34, L18402, doi: 10.1029/2007GL031124.

Henry, P. (1997) Relationship between porosity, electrical conductivity, and cation exchange capacity in Barbados wedge sediments, *in* T. H. Shipley, Y. Ogawa, P. Blum, and J. M. Bahr, eds., Proceedings of the Ocean Drilling Program, Scientific Results 156137–149, doi: 10.2973/ odp.proc.sr.156.020.1997.

Hesse, A., Jolivet, A., and Tabbagh, A. (1986). New prospects in shallow depth electrical surveying for archeological and pedological applications. *Geophysics*, 51, 585-594.

Hungr, O. (1981). Dynamics of rock avalanches and other types of slope movements. *Ph.D. thesis, University of Alberta, Edmonton*, 500p.

Hungr, O., Leroueil, S., and Picarelli, L. (2014). The Varnes classification of landslide types, an update. *Landslides*, 11, 167-194.

Hunt, R.E. (1984). Geotechnical engineering investigation manual. McGraw-Hill, New York.

Hutchinson, J.N. (1984) Methods of locating slip surfaces in landslides. *Bulletin of Engineering Geology and the Environment*, 20, 235-252.

Hutchinson, J.N., 1988. General report: morphological and geotechnical parameters of landslides in relation to geology and hydrology. 5th International Symposium on Landslides, Lausanne 1, 3–35.

IFFI Project. Inventory of Landslide Phenomena in Italy 2007.

Iverson, R.M., and Major, J.J. (1987). Rainfall, groundwater flow, and seasonal movement at Minor Creek landslide, northwestern California. Physical interpretation of empirical relations: *Geological Society of America Bulletin*, vol. 99, 579-594.

Iverson, R.M., (2000), Landslide triggering by rain infiltration. *Water Resources Research*, vol. 36, 1897-1910.

Iverson, R.M. (2005). Regulation of landslide motion by dilatancy and pore pressure feedback: *Journal of Geophysical Research–Earth Surface*, vol. 110, doi: 10.1029/2004JF000268

Jomard H., Lebourg T., and Tric E. (2006). Identification of the gravitational discontinuity in weathered gneiss by geophysical survey: La Clapiere landslide (France). *Journal of Applied Geophysics*, vol. 62, 47-57.

Jomard, H., Lebourg, T., Guglielmini, Y., and Tric, E. (2010). Electrical imaging of sliding geometry and fluid associated with a deep seated landslide (La Clapiere, France). *Earth Surface Processes and Landforms*, 35, 588-599.

Kearey, P., Brooks, M., and Hill, I. (2002). An introduction to geophysical exploration. *Blackwell Science*.

Keefer, D.K., and Johnson, A.M., (1983). Earth flow, Morphology, mobilization and movement. *U.S. Geological Survey Professional Paper*, 1264.

Keller, G.V., and Frischknecht, F.C. (1966). Electrical methods in geophysical prospecting. *Pergamon Press Inc., Oxford*.

Kelsey, H.M., (1978), Earth flows in Franciscan mélange, Van Duzen River basin, California. *Geology*, vol. 6, 361-364.

Koefoed, O. (1979). Geosounding Principles 1: Resistivity sounding measurements. Elsevier Science Publishing Company, Amsterdam.

Kuras, O., Pritchard, J.D., Meldrum P.I., Chambers, J.E., Wilkinson, P.B., Ogilvy R.D., and Weathall G.P. (2009). Monitoring hydraulic processes with automated time-lapse electrical resistivity tomography (ALERT). *Comptes Rendus Geosciences*, 341, 868-885.

Lane, J.W.J., Day-Lewis, F. D., and Casey, C.C. (2006). Geophysical monitoring of a field-scale biostimulation pilot project. *Ground Water*, 44, 440-443.

Larini, G., Malaguti, C., Pellegrini, M., and Tellini, C. (2001). "La Lama" di Corniglio (Appennino Parmense), riattivata negli anni 1994–1999. *Quaderni di Geologia Applicata*, vol. 8, 59-114 Bologna (Pitagora).

Lebourg, T., Binet, S., Tric, E., Jomard, H., and El Bedoui, S. (2005). Geophysical survey to estimate the 3D sliding surface and the 4D evolution of the water pressure on part of a deep seated landslide. *Terra Nova*, 17, 399-406.

Lebourg, T., Hernandez, M., Zerathe, S., El Bedoui. S., Jomard, H., and Fresia, B. (2010). Landslides triggered factors analysed by time lapse electrical survey and multidimensional statistical approach. *Engineering Geology*, 114, 238-250.

Lai, C.G., and Rix, G.J. (1998). Simultaneous inversion of Rayleigh phase velocity and attenuation for near surface site characterization. *School of Civil Environmental Engineering*. Georgia Institute of Technology.

Lebourg, T., Binet, S., Tric, E., Jomard, H., and El Bedoui, S. (2005). Geophysical survey to estimate the 3D sliding surface and the 4D evolution of the water pressure on part of a deep-seated landslide. *Terra Nova*, 17, 399-406.

LeFebvre, G. (1996). Soft sensitive clays. In Turner, A.K. and Schuster, R.L. (eds.), Landslides. Investigation and mitigation. Washington D.C: *National Academy Press, Transportation Research Board Special Report*, 247, 607-619.

Loke, M.H., (1994). The inversion of two-dimensional resistivity data. Unpubl. *PhD thesis, University of Birmingham*.

Loke, M.H. (1999). Electrical imaging surveys for environmental and engineering studies. A practical guide to 2-D and 3D surveys, http://www.abem.se/files/res/2Dnotes.pdf,accessed June 6, 2006.

Loke, M.H. (2002). RES2DINV ver. 3.50. Rapid 2-D resistivity and IP inversion using the least square method. Geotemo Software. Penang, Malaysia.

Loke, M.H., and Barker, R.D. (1995). Least-squares deconvolution of apparent resistivity pseudosections. *Geophysics,* vol. 6, 1682-1690.

Loke, M.H., and Barker, R.D. (1996a). Rapid least-squares inversion of apparent resistivity pseudosections by a quasi-Newton method. *Geophysical Prospecting*, 44, 131-152.

Loke, M.H., and Barker, R.D. (1996b). Practical techniques for 3D resistivity surveys and data inversion. *Geophysical Prospecting*, 44, 499-523.

Loke, M.H. (1997). Electrical imaging survey for environmental and engineering studies. A pratical guide to 2-D and 3-D surveys.

Loke, M.H. (2001). Tutorial: 2-D and 3-D electrical imaging surveys. Course Notes for USGS Workshop 2-D and 3-D Inversion and Modeling of Surface and Borehole Resistivity Data, Torrs, CT.

Loke, M.H., and Dahlin, T. (2002). A comparison of Gauss-Newton and quasi-Newton methods in resistivity imaging inversion. *Journal of Applied Geophysics*, 49, 149-162. DOI: 10.1016/S0926-9851(01)00106-9.

Loke, M.H., Chambers, J.E., Rucker, D.F., Kuras, O., and Wilkinson P.B. (2013). Recent developments in the direct-current geoelectrical imaging method. *Journal of Applied Geophysics*, 95, 135-156.

Loke, M.H., Dahlin, T., and Rucker D.F., (2014). Smoothness-constrained time-lapse inversion of data from 3D resistivity surveys. *Neasr Surface Geophtsics*, 12, 5-24.

Lumley, D. E. (2001), Time-lapse seismic reservoir monitoring: *Geophysics*, 66, 50-53.

Ma, R., McBratney, A., Whelan, B., Minasny, B., and Short, M. (2011). Comparing temperature correction models for soil electrical conductivity

measurement, *Precision Agriculture*, 12, 55-66, doi:10.1007/s11119-009-9156-7.

MacBeth, C., Floricich, M., and Soldo, J. (2006). Going quantitative with 4D seismic analysis: *Geophysical Prospecting*, 54, 303-317.

Mackey, B.H., and Roering, J.J., (2011). Sediment yield, spatial characteristics, and the long-term evolution of active earthflows determined from airborne LiDAR and historical aerial photographs, Eel River, California. *Geological Society of America Bulletin*. DOI.10.1130/B30306.1.1.

Marana, B. (2017). A Simplified ArcGIS Approach for Landslides Risk Assessment in the Province of Bergamo. *Journal of Geographic Information System*, 9, 699-716.

McCann, D.M., and Forster, A., (1990). Reconnaissance geophysical methods in landslide investigations. *Engineering. Geology*, 29, 59-78.

McGillivray, P., and Oldenburg, D. (1990). Methods for calculating Frechet derivates and sensitivities for the non-linear inverse problem. A comparative study. *Geophysical Prospecting*, 38, 499-524.

McGuffey, V.C., Modeer, V.A., and Turner, A.K. (1996). Subsurface exploration. In: Turner AK, Schuster RL (eds) Landslides investigation and mitigation, Spec Rep 247, Transportation Research Board, *National Research Council, Washington.*

Mohnke, O., Prokoph, K., and Yaramanci, U. (2006). Electrical resistivity tomography ERT_ as a tool for monitoring moisture dynamics in soil filled containers: Proceedings of *12th European Meeting of Environmental and Engineering Geophysics*, B026.

Molli, G. (2008). Northern Apennines-Corsica orogenic system: an updated overview. *The Geological Society of London.*

Mualem, Y., and Friedman, S.P. (1991). Theoretical prediction of electrical conductivity in saturated and unsaturated soil. *Water Resources Research*, 27, 2771-2777.

Müller, M., Mohnke, O., Schmalholz, J., and Yaramanci, U. (2003). Moisture assessment with small-scale geophysics-The Interurban Project: *Near Surface Geophysics*, 1, 171-182.

Munsell Book of Color-Matte Finish Collection (Munsell Color, Baltimore, Md., 1976).

Ogilvy, A.A. (1974). Current trends in the use of geophysical methods in the study of landslide phenomena. Moscow University. *Geology Bullettin* 29, 48-50.

Ogilvy, R.D., Meldrum, P.I., Wilkinson, P.B., Chambers, J.E., Sen, M., Pulido-Bosch, A., Gisbert, J., Jorreto, S., Frances, I., and Tsourlos, P. (2009). Automated monitoring of coastal acquifers with Electrical Resistivity Tomography. *Near Surface Geophysics*, vol. 7, 367-375.

Olayinka, A.I., and Yaramanci, U. (2000). Assessment of the reliability of 2D inversion of apparent resistivity data. *Geophysical Prospecting*, 48, 293-316.

Oldenborger, G. A., Knoll, M., Routh, P., and LaBrecque, D. (2007a). Timelapse ERT monitoring of an injection/withdrawal experiment in a shallow unconfined aquifer. *Geophysics*, 72, F177–F187.

Oldenborger, G. A., S.Routh, P., and M. D. Knoll, (2007b). Model reliability for 3D electrical resistivity tomography. Application of the volume of investigation index to a time-lapse monitoring experiment. *Geophysics*, 72, F167-F175.

Olsen, P.A., Binley, A., Henry-Poulter, S., and Tych, W. (1999). Characterizing solute transport in undisturbed soil cores using electrical and X-ray tomographic methods. *Hydrological Processes*, 13, 211-221.

Park, S.K., and Van, G.P. (1991). Inversion of pole-pole data for 3-D resistivity structures beneath arrays of electrodes. *Geophysics*, 56, 951-960.

Papadoupoulos, N.G., Tsourlos, P., Tsokas, G.N., and Sarris, A. (2006). Two-dimensional and three-dimensional resistivity imaging in archeological site investigation. *Archeological Prospecting*, vol. 13, 163-181.

Perrone, A., Lapenna, V., and Piscitelli, S. (2014). Electrical resistivity tomography technique for landslide investigation: A review. *Earth Science Reviews,* 135, 65-82.

Peruccacci, S., Brunetti, M.T., Gariano, S. L., Melillo, M., Rossi, M., and Guzzetti, F. (2017). Rainfall thresholds for possible landslide occurrence in Italy, *Geomorphology*, 290, 39-57.

Plattner, Th. (2005). Modelling public risk evaluation of natural hazards: a conceptual approach. *Natural Hazards and Earth System Science*, 5, 357-366.

Propper, C., Puissant, A., Malet, J.P., and Glade, T. (2014). Analysis of land cover changes in the past and the future as contribution to landslide risk scenarios. *Applied Geography*, 53, 11-19.

Putnam, W.C., and Sharp, R.P. (1940), Landslides and earth flows near Ventura, southern California. *Geographical Review*, vol. 30, 591-600.

Quagliarini. A., Segalini, A., Chelli, A., Francese, R., Giorgi, M., and Spaggiari, L. (2016). Joint modelling and monitoring on Case Pennetta and Case Costa active landslides system using electrical resistivity tomography and geotechnical data. *World Landslide Forum 2017.*

Ramirez, A., Daily W., LaBrecque, D. Owen, E., and Chesnut, D. (1993). Monitoring an underground steam injection process using electrical resistance tomography. *Water Resources Research*, 29, 73-87.

Ramirez, A. L., Daily, W. D., and Newmark, R. L. (1995). Electrical resistance tomography for steam injection monitoring and process control: *Journal of Environmental and Engineering Geophysics*, 0, 39-51.

Ramirez, A., Daily, W. (2001). Electrical imaging at the large block test. Yucca Mountain, Nevada. *Journal of Applied Geophysics*, 46, 85-100.

Reynolds, J.M. (1997). An Introduction to Applied and Environmental Geophysics. Wiley.

Robain, H., Albouy, Y., Dubas, M., Descoitres, M., Camerlynck, C., Mecheler P., and Tabbagh, A. (1999). The location of infinite electrodes in pole-pole electrical surveys: consequences for 2D imaging. *Journal of Applied Geophysics*, 41, 313-333.

Rossi, M., Luciani, S., Valigi, D., Kirschbaum, D., Brunetti, M.T., Peruccacci, S., and Guzzetti, F. (2017). Statistical approaches for the definition of landslide rainfall thresholds and their uncertainty using rain gauge and satellite data, *Geomorphology*, 285, 16-27.

Samouëlian, A., Cousin, I., Tabbagh, A., Bruand, A., and Richard, G. (2005). Electrical resistivity survey in soil science: a review. *Soil and Tillage Research,* 83, 173-193.

Sasaki, Y. (1989). 2-D joint inversion of magnetotelluric and dipole-dipole resistivity data. *Geophysics*, 54, 254-262.

Sasaki, Y. (1992). Resolution of resistivity tomography inferred from numerical simulation. *Geophysical Prospect Ing*. 40, 453-464.

Scollar, I., Tabbagh, A., Hesse, A., and Herzog, I. (1990). *Archaeological Prospecting and Remote Sensing*, 674 pp.

Schmutz, M., Albouy, Y. Guerin, R. Maquaire, O. Vassal, J. Schott, J.J., and Descloitres, M. (2000), Joint electrical and time domain electromagnetism (Tdem) data inversion applied to the Super Sauze earthflow (France). *Surveys in Geophysics*, 21, 371-390.

Seaton, W.J., and Burbey, T.J. (2002). Evaluation of two-dimensional resistivity methods in a fractured crystalline-rock terrane. *Journal of Applied Geophysics*, 51, 21-41.

Sharma, P.V. (1997). Environmental and engineering geophysics. Cambridge University Press, New York.

Sharpe, C.F.S., (1938). Landslides and related phenomena. A study of mass movements of soil and rock. New York, Columbia University Press.

Shevnin, V., Mousatov, A., Ryjov, A., and Delgado-Rodriquez, O. (2007). Estimation of clay content in soil based on resistivity modelling and laboratory measurements. *Geophysical Prospecting*, 55, 265-75.

Silvester, P.P., and Ferrari, R.L., (1990), Finite Elements for Electrical Engineers, second ed., *Cambridge University Press*, Cambridge.

Skempton, A.W., (1985), Residual strength of clays in landslides, folded strata and the laboratory. *Géotechnique,* vol. 35, 3-18.

Singha, K., and Gorelick, S. M. (2005). Saline tracer visualized with three-dimensional electrical resistivity tomography: Field-scale spatial moment analysis. *Water Resources Research*, 41, W05023, doi: 10.1029/ 2004WR003460.

Slater, L., Binley, A.M., Daily, W., and Johnson, R. (2000). Cross-hole electrical imaging of a controlled saline tracer injection. *J. Appl. Geophys*. 44, 85-102.

Suzuki, K., Higashi, S. (2001). Groundwater flow after heavy rain in landslide-slope area from 2D-inversion of resistivity monitoring data. *Geophysics*, 66, 733-743.

Swanson, F.J., and Swanston, D.N. (1977), Complex mass movement terrains in the western Cascade Range, Oregon. *Geological Society of America Reviews in Engineering Geology*, vol. 3, 113-124.

Tikhonov, A.N., Goncharsky A.V., Stepanov V.V., and Yagola A.G. (1995). Numerical methods for the solution of ill-posed problems. Kluwer Academic Publishers.

Torrance, J.K., (1987). Quick clays. In Anderson, M.G., and Richards, K.S. (eds.), Slope stability. *Geotechnical Engineering and Geomorphology*, John Wiley and Sons, Ltd., Chichester, United Kingdom, 447-473.

Tosatti, G., Castaldini, D., Barbier, M., D'Amato Avanzi, G., Giannecchini, R., Mandrone, G., Pellegrini, M., Perego, Susanna., Puccinelli, A., W.Romeo, R., and Tellini, C. (2008). Additional causes of seismically-related landslides in the Northern Apennines, Italy. *Revista de Geomorfologie*, 10, 5-21.

Tsourlos, P. (1995). Modelling interpretation and inversion of multielectrode resistivity survey data. *Ph.D Thesis, University of York.*

Tsourlos, P. (2004). Inversion of electrical resistivity tomography data deriving from 3D structures. *Bullettin of the Geological Society of Greece.* vol. 36.

Tsourlos, P., and Ogilvy R. (1999). An algorithm for the 3-D Inversion of Tomographic Resistivity and Induced Polarisation data: Preliminary Results. *Journal of the Balkan Geophysical Society*, 2, 30-45.

Tsourlos, P., Ogilvy, R., Meldrum, P., and Williams, G. (2003). Time-lapse monitoring in single boreholes using electrical resistivity tomography. *Journal of Environmental and Engineering Geophysics*, 8, 1-14.

Uhlemann, S., Chambers, J., Wilkinson, P., Maurer, H., Merrit, A., Meldrum, P., Kuras, O., Gunn, D., Smith, A., and Dijkstra, T. (2017). Four-dimensional imaging of moisture dynamics during landslide reactivation. *Journal of Geophysical Research: Earth Surface.* AGU Pubblications.

Van Asch, Th. W.J., Buma, J., and Van Beek, L.H. (1999). A view on some hydrological triggering systems in landslides. *Geomorphology*, 30, 25-32.

Varnes, D.J. (1978). Slope movement types and processes. In Landslides Analysis and Control, Schuster RL, Krizek RJ (eds). *National Academy of Sciences, Transportation Research Board*: Washington DC; 11-33.

Varnes, D.J. (1984). Landslide hazard zonation: a review of principles and practice. Issue 3.

Vescovi, P. (1988). Assetto strutturale del flysch di Mt. Caio nella zona del Passo della Cisa e in alta Val Baganza (Pr. Di Parma). *Rendiconti Società Geologica Italiana.*

Ward, S.H. (1990). Resistivity and induced polarization methods. Geotechnical and Environmental Geophysics. *Soc. Explor. Geophys*, Tulsa, vol. 1, 147-189.

Xu, B. (1993). Development of electrical resistivity imaging methods for geological and archaeological prospecting. *Ph.D. Thesis, University of Durham.*

Appendices

Appendix A1

Geological and Geomorphological Map

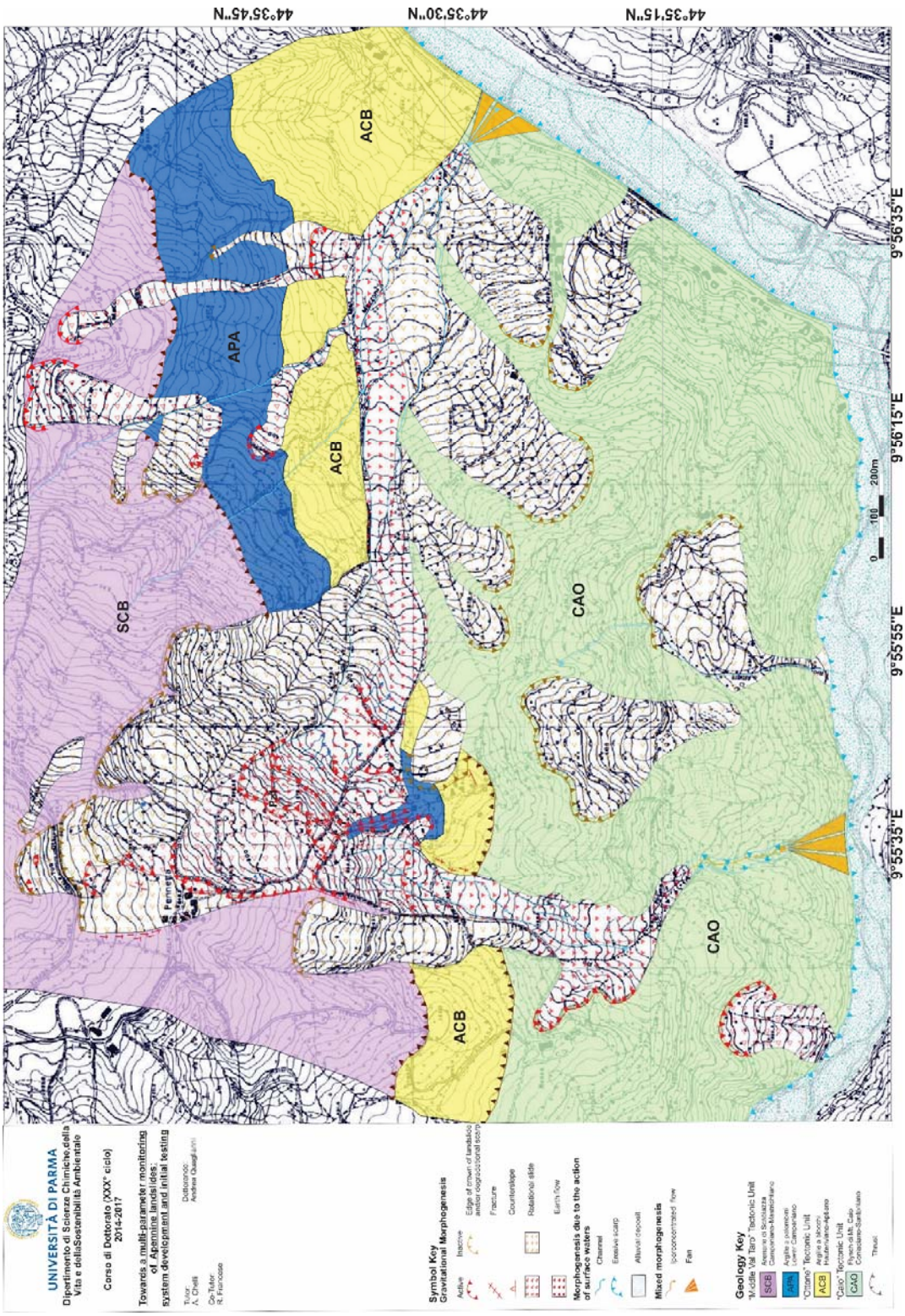
44°35'45"N
44°35'30"N
44°35'15"N
9°55'35"E
9°55'55"E
9°56'15"E
9°56'35"E
SCB
APA
ACB
CAO
0 100 200m
UNIVERSITÀ DI PARMA
Dipartimento di Scienze Chimiche,della Vita e dellaSostenibilità Ambientale
Corso di Dottorato (XXX° ciclo) 2014-2017
Towards a multi-parameter monitoring of Apennine landslides: system development and initial testing
Tutor: A. Chelli
Co-Tutor: R. Francioso
Dottorando: Andrea Quagliarini
Symbol Key
Gravitational Morphogenesis
Active
Inactive
Edge of crown of landslide and/or degradational scarp
Fracture
Counterslope
Rotational slide
Earth flow
Morphogenesis due to the action of surface waters
Channel
Erosive scarp
Alluvial deposit
Mixed morphogenesis
Concentrated flow
Fan
Geology Key
"M.delle Val Taro" Tectonic Unit
SCB
"Chiavari" Tectonic Unit
APA
"Caio" Tectonic Unit
ACB
CAO
Thrust

Appendix A2

Si1 Permeability Test

GRENTI srl
http://www.grenti.it
43040 – SOLIGNANO (PR)
Sede legale Via Marconi 6
Sede amm.va Via Marconi 1
Tel 0525 54542 (6 linee) Fax 0525 54568
e-mail: info@grenti.it
Impianto produzione calcestruzzo e inerti
43040 - GHIARE DI BERCETO (PR)
Via Molino Vecchio, 133
Tel 0525 68252 Fax 0525 620400
e-mail: cls-inerti@grenti.it
EDILIZIA IDRAULICA STRADE FORNITURE INERTI E CALCESTRUZZO

SONDAGGIO Si1 **PROVA DI PERMEABILITA' CARICO VARIABILE N°** 1

COMMITTENTE: Regione Emilia Romagna data: 04/02/2016

LOCALITA' : Solignano

CANTIERE : Case Pennetta

SONDAGGIO : Si1 Altezza rivestim. da p.c. mt 0,80

PROFONDITA' : da mt 4,50 a mt 5,50

LIVELLO FALDA : mt assente

Tempi parziali	15"	30"	1'	2'	4'	8'	16'	15'	15'	15'	15'
Tempi progressivi	15"	45"	1'45"	3'45"	7'45"	15'45"	31'45"	46'45"	61'45"	76'45"	91'45"
Livello acqua nel foro (cm)	0,4	0,7	1,3	2,7	5,9	10,1	16,9	23,4	29,1	35,6	38,1

	Sim.	U.M.		
Spessore di terreno interessato dalla prova:	L	[cm]	=	100
Diametro del foro:	D	[cm]	=	10,10
Altezza di carico idraulico iniziale:	h_1	[cm]	=	630
Altezza del carico idraulico finale:	h_2	[cm]	=	591,9
Tempo di prova:	t	[s]	=	5505
Coefficiente di forma:	CF	[n]	=	277,82

COEFFICIENTE DI PERMEABILITA' K [cm/s] = **3,267899E-06**

GRADO DI PERMEABILITA' G.P. = **MOLTO BASSO**

$$CF = \frac{3\pi l}{l_n\left[1{,}5\frac{L}{D} + \sqrt{1+\left(\frac{1{,}5L}{D}\right)^2}\right]} \qquad K = \frac{(D/2)^2\pi}{CFt}\ln\frac{h_1}{h_2} =$$

NOTE :

Tempo totale di esecuzione : 91' 45"

GRENTI srl
http://www.grenti.it
43040 – SOLIGNANO (PR)
Sede legale Via Marconi 6
Sede amm.va Via Marconi 1
Tel 0525 64542 (6 linee) Fax 0525 64568
e-mail: info@grenti.it
Impianto produzione calcestruzzo e inerti
43040 - GHIARE DI BERCETO (PR)
Via Molino Vecchio, 133
Tel 0525 69252 Fax 0525 620400
e-mail: cls-inerti@grenti.it
EDILIZIA IDRAULICA STRADE FORNITURE INERTI E CALCESTRUZZO

SONDAGGIO Si1 **PROVA DI PERMEABILITA' CARICO VARIABILE N°** 2

COMMITTENTE: Regione Emilia Romagna data: 05/02/2016

LOCALITA' : Solignano

CANTIERE : Case Pennetta

SONDAGGIO : Si1 Altezza rivestim. da p.c. mt 0,80

PROFONDITA' : da mt 12,00 a mt 16,00

LIVELLO FALDA : mt assente

Tempi parziali	15"	30"	1'	2'	4'	8'	16'	15'	15'	15'	15'
Tempi progressivi	15"	45"	1'45"	3'45"	7'45"	15'45"	31'45"	46'45"	61'45"	76'45"	91'45"
Livello acqua nel foro (cm)	1,8	3,5	6,9	11,5	20,3	38,4	53,8	69,2	82,1	92,1	101,3

	Sim.	U.M.		
Spessore di terreno interessato dalla prova:	L	[cm]	=	400
Diametro del foro:	D	[cm]	=	10,10
Altezza di carico idraulico iniziale:	h_1	[cm]	=	1680
Altezza del carico idraulico finale:	h_2	[cm]	=	1578,7
Tempo di prova:	t	[s]	=	5505
Coefficiente di forma:	CF	[n]	=	789,08
COEFFICIENTE DI PERMEABILITA'	K	[cm/s]	=	**1,147070E-06**
GRADO DI PERMEABILITA'	G.P.		=	**MOLTO BASSO**

$$CF = \frac{3\pi L}{I_N\left[1{,}5\frac{L}{D} + \sqrt{1+\left(\frac{1{,}5L}{D}\right)^2}\right]} \qquad K = \frac{(D/2)^2\pi}{CFt}\ln\frac{h_1}{h_2} =$$

NOTE :

Tempo totale di esecuzione : 91' 45"

GRENTI srl
http://www.grenti.it
43040 – SOLIGNANO (PR)
Sede legale Via Marconi 6
Sede amm.va Via Marconi 1
Tel 0525 64542 (6 linee) Fax 0525 64569
e-mail: info@grenti.it
Impianto produzione calcestruzzo e inerti
43040 - GHIARE DI BERCETO (PR)
Via Molino Vecchio, 133
Tel 0525 68252 Fax 0525 620400
e-mail: cls-inerti@grenti.it
EDILIZIA IDRAULICA STRADE FORNITURE INERTI E CALCESTRUZZO

SONDAGGIO Si1 **PROVA DI PERMEABILITA' CARICO VARIABILE N°** 3

COMMITTENTE: Regione Emilia Romagna data: 05/02/2016

LOCALITA' : Solignano

CANTIERE : Case Pennetta

SONDAGGIO : Si1 Altezza rivestim. da p.c. mt 0,80

PROFONDITA' : da mt 20,00 a mt 23,00

LIVELLO FALDA : mt assente

Tempi parziali	15"	30"	1'	2'	4'	8'	16'	15'	15'	15'	15'
Tempi progressivi	15"	45"	1'45"	3'45"	7'45"	15'45"	31'45"	46'45"	61'45"	76'45"	91'45"
Livello acqua nel foro (cm)	1,8	3,5	6,9	11,5	20,3	38,4	53,8	69,2	82,1	92,1	101,3

	Sim.	U.M.		
Spessore di terreno interessato dalla prova:	L	[cm]	=	300
Diametro del foro:	D	[cm]	=	10,10
Altezza di carico idraulico iniziale:	h_1	[cm]	=	1680
Altezza del carico idraulico finale:	h_2	[cm]	=	1578,7
Tempo di prova:	t	[s]	=	5505
Coefficiente di forma:	CF	[n]	=	629,72
COEFFICIENTE DI PERMEABILITA'	K	[cm/s]	=	**1,437351E-06**
GRADO DI PERMEABILITA'	G.P.		=	**MOLTO BASSO**

$$CF = \frac{3\pi L}{\ln\left[1{,}5\frac{L}{D} + \sqrt{1+\left(\frac{1{,}5L}{D}\right)^2}\right]} \qquad K = \frac{(D/2)^2\pi}{CFt}\ln\frac{h_1}{h_2} =$$

NOTE :

Tempo totale di esecuzione : 91' 45"

GRENTI srl
http://www.grenti.it
43040 – SOLIGNANO (PR)
Sede legale Via Marconi 6
Sede amm.va Via Marconi 1
Tel 0525 54542 (6 linee) Fax 0525 54568
e-mail: info@grenti.it
Impianto produzione calcestruzzo e inerti
43040 - GHIARE DI BERCETO (PR)
Via Molino Vecchio, 133
Tel 0525 68252 Fax 0525 620400
e-mail: cls-inerti@grenti.it
EDILIZIA IDRAULICA STRADE FORNITURE INERTI E CALCESTRUZZO

SONDAGGIO Si1 **PROVA DI PERMEABILITA' CARICO VARIABILE N°** 4

COMMITTENTE: Regione Emilia Romagna data: 06/02/2016

LOCALITA' : Solignano

CANTIERE : Case Pennetta

SONDAGGIO : Si1 Altezza rivestim. da p.c. mt 0,80

PROFONDITA' : da mt 25,00 a mt 35,00

LIVELLO FALDA : mt assente

Tempi parziali	15"	30"	1'	2'	4'	8'	16'	15'	15'	15'	15'
Tempi progressivi	15"	45"	1'45"	3'45"	7'45"	15'45"	31'45"	46'45"	61'45"	76'45"	91'45"
Livello acqua nel foro (cm)	1	1,8	3,4	6,9	12,3	21,1	36,2	49,2	61,2	71,1	77,5

	Sim.	U.M.		
Spessore di terreno interessato dalla prova:	L	[cm]	=	1000
Diametro del foro:	D	[cm]	=	10,10
Altezza di carico idraulico iniziale:	h_1	[cm]	=	3580
Altezza del carico idraulico finale:	h_2	[cm]	=	3502,5
Tempo di prova:	t	[s]	=	5505
Coefficiente di forma:	CF	[n]	=	1655,26
COEFFICIENTE DI PERMEABILITA'	K	[cm/s]	=	1,924297E-07
GRADO DI PERMEABILITA'	G.P.		=	MOLTO BASSO

$$CF = \frac{3\pi l.}{l_N\left[1{,}5\frac{L}{D} + \sqrt{1+\left(\frac{1{,}5L}{D}\right)^2}\right]} \qquad K = \frac{(D/2)^2\pi}{CFt}\ln\frac{h_1}{h_2} =$$

NOTE :

Tempo totale di esecuzione : 91' 45"

Appendix A3

Pocket Test

AIPo
Agenzia Interregionale per il fiume Po
Laboratorio di geotecnica di Boretto (RE)

DESCRIZIONE E RIPRESA FOTOGRAFICA DEL CAMPIONE

Riferimento Laboratorio geotecnico AIPO UFF.MO

Committente :	UNIPR	Data cons:	17/03/16
Località :	CASE PENNETTA	Data apertura:	18/03/16
Sond.:	Si1	Campione:	Si1A
Profondità prelievo (m) :	10,30 - 10,63 m da p.c.	Tipo del Campione:	Indisturbato

Descrizione: La lunghezza della carota prelevata è di 30 cm e all'apertura presenta una prima parte più satura (fino a 14 cm da p.c.) e una seconda meno satura. Per quanto concerne la litologia questa risulta costituita prevalentemente da limo sabbioso. La struttura del campione è omogenea con presenza di inclusi di ghiaia di forma angolare di grandi dimensioni, fino a circa 3 cm.

Colore: 2,5Y 4/1 GRIGIO SCURO

Classe campione (Q 4):

Pocket (Ka/cm ^{2}):

5 cm	10 cm	20 cm	25 cm
2,50	3,50	3,50	3,25

Torvane (Kpa):

n.d.

PROVE ESEGUITE:

Contenuto nat. acqua	X	Granulometria	X	Taglio residuo	
Peso di volume	X	Compressione sempl.		Triax UU	
Peso specifico		Espansione laterale libera		Triax CU	
Limiti consistenza	X	Taglio diretto CD (RICOSTRUITO)	X	Triax CD	

LO SPERIMENTATORE : Annalisa Alfieri

IL DIRETTORE DEL LABORATORIO : Alessandro Rosso

AIPo
Agenzia Interregionale per il fiume Po
Laboratorio di geotecnica di Boretto (RE)

DESCRIZIONE E RIPRESA FOTOGRAFICA DEL CAMPIONE

Riferimento Laboratorio geotecnico AIPO UFF.MO

Committente :	UNIPR	Data cons:	17/03/16
Località :	CASE PENNETTA	Data apertura:	18/03/16
Sond.:	Si1	Campione:	Si1B
Profondità prelievo (m) :	16,50 - 17,00 m da p.c.	Tipo del Campione:	Indisturbato

Descrizione: La lunghezza della carota prelevata è di 29 cm e all'apertura presenta una prima parte più satura (fino a 13 cm da p.c.) e una seconda meno satura. Per quanto concerne la litologia questa risulta costituita prevalentemente da ghiaia e limo sabbioso. La struttura del campione è omogenea con presenza di inclusi di ghiaia di forma angolare di grandi dimensioni, fino a circa 3 cm.

Colore: 5Y 4/2 GRIGIO OLIVASTRO

Classe campione (Q 4):

Pocket (Kg/cm ^{2}):

5 cm	10 cm	15 cm	20 cm
<0,25	1,75	2,00	3,25

Torvane (Kpa):

n.d.

PROVE ESEGUITE:

Contenuto nat. acqua	X	Granulometria	X	Taglio residuo	
Peso di volume	X	Compressione sempl.		Triax UU	
Peso specifico		Espansione laterale libera		Triax CU	
Limiti consistenza	X	Taglio diretto CD (RICOSTRUITO)	X	Triax CD	

LO SPERIMENTATORE : Annalisa Alfieri

IL DIRETTORE DEL LABORATORIO : Alessandro Rosso

AIPo
Agenzia Interregionale per il fiume Po
Laboratorio di geotecnica di Boretto (RE)

DESCRIZIONE E RIPRESA FOTOGRAFICA DEL CAMPIONE

Riferimento Laboratorio geotecnico AIPO UFF.MO

Committente :	UNIPR	Data cons:	17/03/16
Località :	CASE PENNETTA	Data apertura:	17/03/16
Sond.:	Si2	Campione:	Si2A
Profondità prelievo (m) :	6,70 - 7,30 m da p.c.	Tipo del Campione:	Indisturbato

Descrizione:La lunghezza della carota prelevata è di 40 cm.Per quanto concerne la litologia questa risulta costituita da limo prevalentemente sabbioso. La struttura del campione è omogenea con presenza di inclusi di ghiaia di forma angolare di grandi dimensioni, fino a circa 3 cm.

Colore: 5Y 4/1 GRIGIO SCURO

Classe campione (Q 4):

Pocket (Kg/cm ^{2}):

5 cm	10 cm	25 cm	30 cm	38 cm
1,75	2,5	2,25	3,25	3,75

Torvane (Kpa):

n.d.

PROVE ESEGUITE:

Contenuto nat. acqua	X	Granulometria	X	Taglio residuo	
Peso di volume	X	Compressione sempl.		Triax UU	
Peso specifico		Edometria		Triax CU	
Limiti consistenza	X	Taglio diretto CD (RICOSTRUITO)	X	Triax CD	

LO SPERIMENTATORE : Annalisa Alfieri

IL DIRETTORE DEL LABORATORIO : Alessandro Rosso

AIPo
Agenzia Interregionale per il fiume Po
Laboratorio di geotecnica di Boretto (RE)

DESCRIZIONE E RIPRESA FOTOGRAFICA DEL CAMPIONE

Riferimento Laboratorio geotecnico AIPO UFF.MO

Committente :	UNIPR	Data cons:	17/03/16
Località :	CASE PENNETTA	Data apertura:	18/03/16
Sond.:	Si2	Campione:	Si2B
Profondità prelievo (m) :	8,20 - 8,80 m da p.c.	Tipo del Campione:	Indisturbato

Descrizione: La lunghezza della carota prelevata è di 48 cm. Per quanto concerne la litologia questa risulta costituita prevalentemente da ghiaia e sabbia limosa e argillosa. La struttura del campione è omogenea con presenza di inclusi di ghiaia di forma angolare di grandi dimensioni, fino a circa 4 cm.

Colore: 5Y 4/1 GRIGIO SCURO

Classe campione (Q 4):

Pocket (Kg/cm ^{2}):

10 cm	20 cm	30 cm	40 cm
2	2,75	1,75	2,50

Torvane (Kpa):

n.d.

PROVE ESEGUITE:

Contenuto nat. acqua	X	Granulometria	X	Taglio residuo	
Peso di volume	X	Compressione sempl.		Triax UU	
Peso specifico	X	Espansione laterale libera	X	Triax CU	
Limiti consistenza	X	Taglio diretto CD (RICOSTRUITO)	X	Triax CD	

LO SPERIMENTATORE : Annalisa Alfieri

IL DIRETTORE DEL LABORATORIO : Alessandro Rosso

Appendix A4

Granulometry

AIPo
Agenzia Interregionale per il fiume Po

Laboratorio di geotecnica di Boretto (RE)

ANALISI GRANULOMETRICA

NORMA DI RIFERIMENTO: Raccomandazioni AGI 1994

Cert. N°. 110/08_14_AIPO del 10/07/2014

Committente :	UNIPR	Data Cons.	17/03/16
Località :	CASE PENNETTA	Data prova:	18/03/16
Sond.:	Si1	Campione:	Si1A
Profondità prelievo (m) :	10,30-10,63 m da p.c.	Tipo del Campione:	Indisturbato

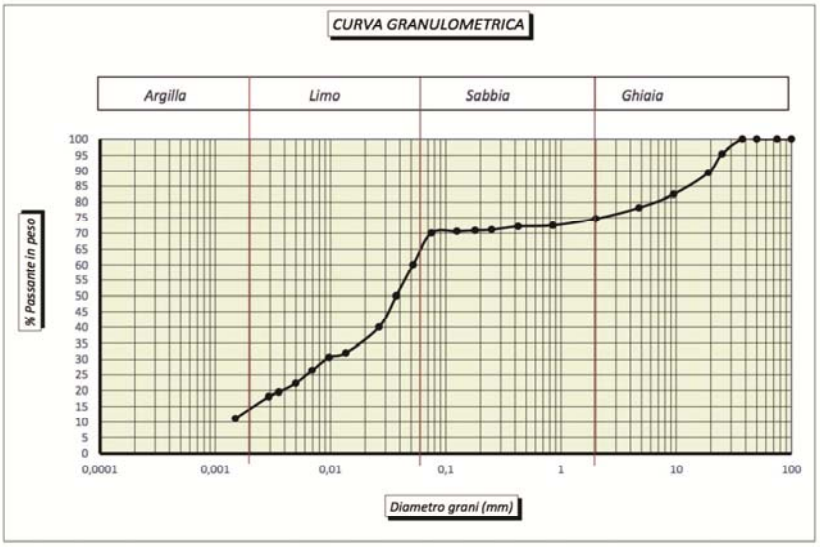

RESOCONTO GRANULOMETRICO (quantità espresse in %)

Ghiaia =	25,36	Sabbia =	9,6	Limo =	51,4	Argilla =	13,65

Classificazione AGI (1977):		Note
Dimensione [mm]	Descrizione	
> 60	Ciottoli	
2 - 60	Ghiaia	
0.06 - 2	Sabbia	
0.002 - 0.06	Limo	
< 0.002	Argilla	

Peso specifico dei grani [g/cm^3]: 2,69

LO SPERIMENTATORE Annalisa Alfieri

IL DIRETTORE DEL LABORATORIO Alessandro Rosso

AIPo
Agenzia Interregionale per il fiume Po

Laboratorio di geotecnica di Boretto (RE)

ANALISI GRANULOMETRICA

NORMA DI RIFERIMENTO: Raccomandazioni AGI 1994

Cert. N°. 110/08_14_AIPO del 10/07/2014

Committente :	UNIPR	Data Cons.	17/03/16
Località :	CASE PENNETTA	Data prova:	18/03/16
Sond.:	Si1	Campione:	Si1B
Profondità prelievo (m) :	16,50-17,00 m da p.c.	Tipo del Campione:	Indisturbato

CURVA GRANULOMETRICA

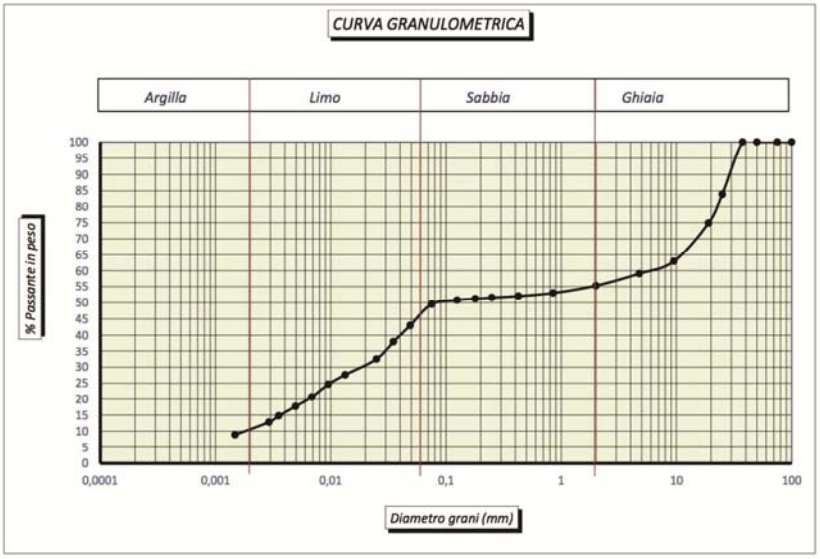

RESOCONTO GRANULOMETRICO (quantità espresse in %)

Ghiaia =	44,71	Sabbia =	9,5	Limo =	35,5	Argilla =	10,3

Classificazione AGI (1977):		Note
Dimensione [mm]	Descrizione	
> 60	Ciottoli	
2 - 60	Ghiaia	
0.06 - 2	Sabbia	
0.002 - 0.06	Limo	
< 0.002	Argilla	

Peso specifico dei grani [g/cm^3]: 2,69

LO SPERIMENTATORE Annalisa Alfieri

IL DIRETTORE DEL LABORATORIO A. Rosso

AIPo
Agenzia Interregionale per il fiume Po

Laboratorio di geotecnica di Boretto (RE)

ANALISI GRANULOMETRICA

NORMA DI RIFERIMENTO: Raccomandazioni AGI 1994

Cert. N°. 110/08_14_AIPO del 10/07/2014

Committente :	UNIPR	Data Cons.	17/03/16
Località :	CASE PENNETTA	Data prova:	17/03/16
Sond.:	Si2	Campione:	Si2A
Profondità prelievo (m) :	6.70-7.30 m da p.c.	Tipo del Campione:	Indisturbato

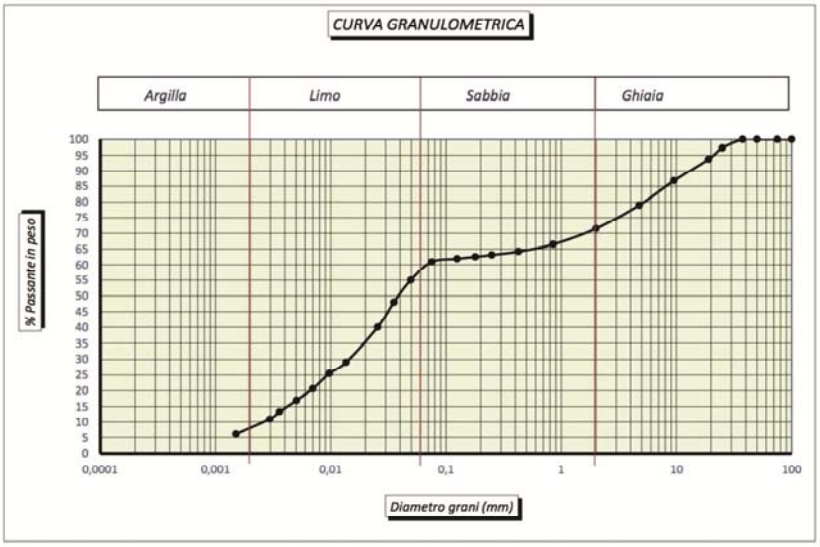

RESOCONTO GRANULOMETRICO (quantità espresse in %)

Ghiaia =	28,54	Sabbia =	13,5	Limo =	50,2	Argilla =	7,75

Classificazione AGI (1977):		Note
Dimensione [mm]	Descrizione	
> 60	Ciottoli	
2 - 60	Ghiaia	
0.06 - 2	Sabbia	
0.002 - 0.06	Limo	
< 0.002	Argilla	

Peso specifico dei grani [g/cm^3]: 2,69

LO SPERIMENTATORE Annalisa Alfieri

IL DIRETTORE DEL LABORATORIO Alessandro Rosso

AIPo
Agenzia Interregionale per il fiume Po

Laboratorio di geotecnica di Boretto (RE)

ANALISI GRANULOMETRICA

NORMA DI RIFERIMENTO: Raccomandazioni AGI 1994

Cert. N°. 110/08_14_AIPO del 10/07/2014

Committente :	UNIPR	Data Cons.	17/03/16
Località :	CASE PENNETTA	Data prova:	18/03/16
Sond.:	Si2	Campione:	Si2B
Profondità prelievo (m) :	8,20-8,80 m da p.c.	Tipo del Campione:	Indisturbato

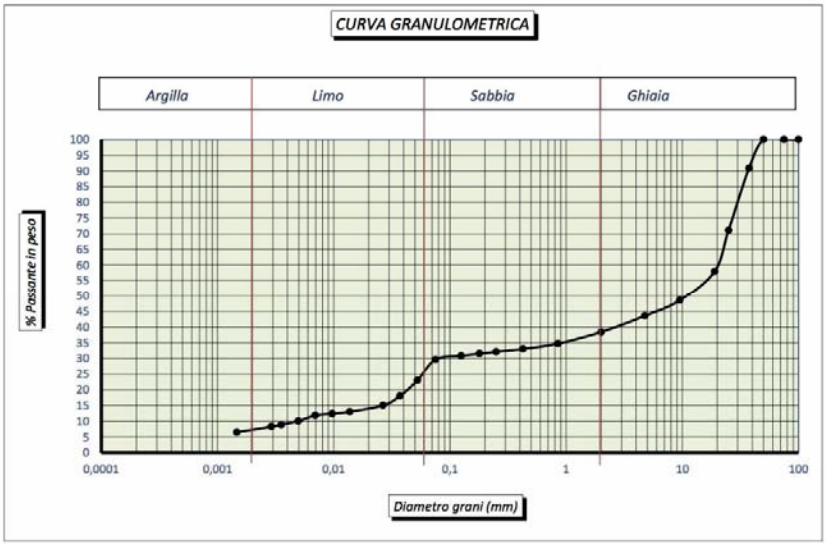

RESOCONTO GRANULOMETRICO (quantità espresse in %)

Ghiaia =	61,59	Sabbia =	13,2	Limo =	18,1	Argilla =	7,15

Classificazione AGI (1977):		Note
Dimensione [mm]	Descrizione	
> 60	Ciottoli	
2 - 60	Ghiaia	
0.06 - 2	Sabbia	
0.002 - 0.06	Limo	
< 0.002	Argilla	

Peso specifico dei grani [g/cm^3]: 2,69

LO SPERIMENTATORE Annalisa Alfieri

IL DIRETTORE DEL LABORATORIO A.Rosso

Appendix A5

Atterberg Limits

AIPo
Agenzia Interregionale per il fiume Po
Laboratorio di geotecnica di Boretto (RE)

CLASSIFICAZIONE DELLE TERRE

NORMA DI RIFERIMENTO: C.N.R. UNI 10006

Cert. N°. 055/03-12_AIPONAV_10-12

Committente :	UNIPR	Data Cons.	17/03/16
Località :	CASE PENNETTA	Data prova:	18/03/16
Sond.:	Si1	Campione:	Si1A
Profondità prelievo (m) :	10,30-10,63 m da p.c.	Tipo del Campione:	Indisturbato

ANALISI GRANULOMETRICA

Frazione passante al setaccio (%)

2 mm	74,6
0,4 mm	72,2
0,075 mm	70,0

LIMITI ED INDICI DI ATTERBERG (%)

Limite Liquido	33,43
Limite Plastico	21,27
Indice Plastico	12,16

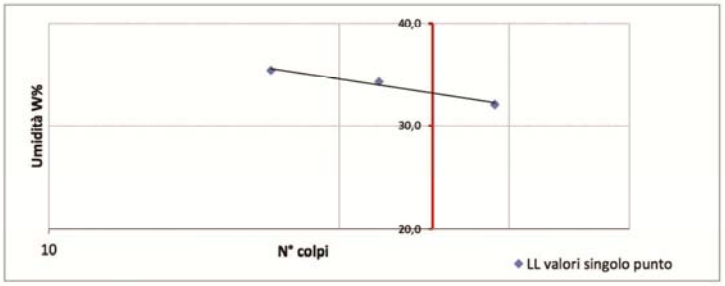

CLASSIFICAZIONE C.N.R. U.N.I. 10006

Gruppo / Sottogruppo / (Indice di gruppo)	A 6 (8)

LO SPERIMENTATORE Annalisa Alfieri

IL DIRETTORE DEL LABORATORIO Dr. A. Rosso

AIPo
Agenzia Interregionale per il fiume Po
Laboratorio di geotecnica di Boretto (RE)

CLASSIFICAZIONE DELLE TERRE
NORMA DI RIFERIMENTO: C.N.R. UNI 10006
Cert. N°. 055/03-12_AIPONAV_10-12

Committente :	UNIPR	Data Cons.	17/03/16
Località :	CASE PENNETTA	Data prova:	18/03/16
Sond.:	Si1	Campione:	Si1B
Profondità prelievo (m) :	16,50-17,00 m da p.c.	Tipo del Campione:	Indisturbato

ANALISI GRANULOMETRICA

Frazione passante al setaccio (%)

2 mm	55,3
0,4 mm	52,0
0,075 mm	49,5

LIMITI ED INDICI DI ATTERBERG (%)

Limite Liquido	32,53
Limite Plastico	20,10
Indice Plastico	12,43

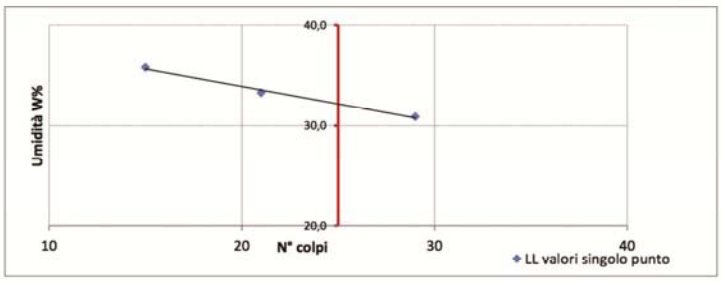

CLASSIFICAZIONE C.N.R. U.N.I. 10006

Gruppo / Sottogruppo / (Indice di gruppo)	A 6 (4)

LO SPERIMENTATORE Annalisa Alfieri

IL DIRETTORE DEL LABORATORIO Dr. A. Rosso

AIPo
Agenzia Interregionale per il fiume Po

Laboratorio di geotecnica di Boretto (RE)

CLASSIFICAZIONE DELLE TERRE

NORMA DI RIFERIMENTO: C.N.R. UNI 10006

Cert. N°. 055/03-12_AIPONAV_10-12

Committente :	UNIPR	Data Cons.	17/03/16
Località :	CASE PENNETTA	Data prova:	17/03/16
Sond.:	Si1	Campione:	Si1B
Profondità prelievo (m) :	6.70-7.30 m da p.c.	Tipo del Campione:	Indisturbato

ANALISI GRANULOMETRICA

Frazione passante al setaccio (%)

2 mm	71,5
0,4 mm	64,2
0,075 mm	60,9

LIMITI ED INDICI DI ATTERBERG (%)

Limite Liquido	30,63
Limite Plastico	17,96
Indice Plastico	12,68

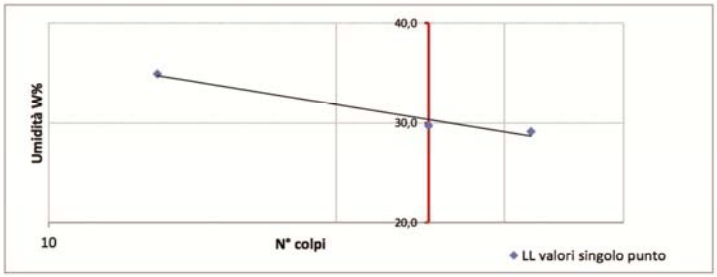

CLASSIFICAZIONE C.N.R. U.N.I. 10006

Gruppo / Sottogruppo / (Indice di gruppo)	A 6 (6)

LO SPERIMENTATORE Annalisa Alfieri

IL DIRETTORE DEL LABORATORIO Dr. A. Rosso

AIPo
Agenzia Interregionale per il fiume Po
Laboratorio di geotecnica di Boretto (RE)

CLASSIFICAZIONE DELLE TERRE

NORMA DI RIFERIMENTO: C.N.R. UNI 10006

Cert. N°. 055/03-12_AIPONAV_10-12

Committente :	UNIPR	Data Cons.	17/03/16
Località :	CASE PENNETTA	Data prova:	18/03/16
Sond.:	Si1	Campione:	Si1B
Profondità prelievo (m) :	8,20-8,80 m da p.c.	Tipo del Campione:	Indisturbato

ANALISI GRANULOMETRICA

Frazione passante al setaccio (%)

2 mm	38,4
0,4 mm	33,0
0,075 mm	29,7

LIMITI ED INDICI DI ATTERBERG (%)

Limite Liquido	28,60
Limite Plastico	15,33
Indice Plastico	13,27

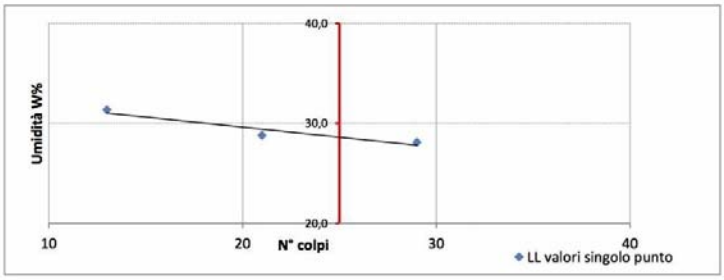

CLASSIFICAZIONE C.N.R. U.N.I. 10006

Gruppo / Sottogruppo / (Indice di gruppo)	A 2 - 6

LO SPERIMENTATORE Annalisa Alfieri

IL DIRETTORE DEL LABORATORIO Dr. A. Rosso

Appendix A6

Direct Shear

AIPo
Agenzia Interregionale per il fiume Po
Laboratorio di geotecnica di Boretto (RE)

CLASSIFICAZIONE DELLE TERRE

NORMA DI RIFERIMENTO: C.N.R. UNI 10006

Cert. N°. 055/03-12_AIPONAV_10-12

Committente :	UNIPR	Data Cons.	17/03/16
Località :	CASE PENNETTA	Data prova:	18/03/16
Sond.:	Si1	Campione:	Si1A
Profondità prelievo (m) :	10,30-10,63 m da p.c.	Tipo del Campione:	Indisturbato

ANALISI GRANULOMETRICA

Frazione passante al setaccio (%)

2 mm	74,6
0,4 mm	72,2
0,075 mm	70,0

LIMITI ED INDICI DI ATTERBERG (%)

Limite Liquido	33,43
Limite Plastico	21,27
Indice Plastico	12,16

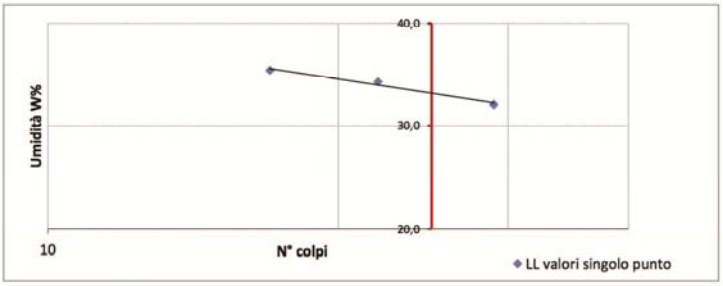

CLASSIFICAZIONE C.N.R. U.N.I. 10006

Gruppo / Sottogruppo / (Indice di gruppo)	A 6 (8)

LO SPERIMENTATORE Annalisa Alfieri

IL DIRETTORE DEL LABORATORIO Dr. A. Rosso

AIPo
Agenzia Interregionale per il fiume Po

Laboratorio di geotecnica di Boretto (RE)

PROVA DI TAGLIO DIRETTO

NORMA DI RIFERIMENTO: UNI CEN ISO/TS 17892-10:2005

Cert. N°. 055/03-12_AIPONAV_10-12

Committente :	UNIPR	Data Cons.	17/03/16
Località :	CASE PENNETTA	Data prova:	18/03/16
Sond.:	Si1	Campione:	Si1B
Profondità prelievo (m) :	16,50 - 17,00 m da p.c.	Tipo del Campione:	Indisturbato

Prova eseguita in scatola di taglio di Casagrande con anello circolare

PREPARAZIONE DEI PROVINI		Ricostruito	
CARATTERISTICHE INIZIALI	**Provino 1**	**Provino 2**	**Provino 3**
Peso specifico dei grani g/cm^3		**2,69**	
Peso di volume kN/m^3	20,82	21,11	20,95
Umidità %	16,16	16,16	16,16
Densità secca kN/m^3	17,92	18,17	18,04

CONDIZIONI A ROTTURA	**Provino 1**	**Provino 2**	**Provino 3**
Tensione di consolidazione (kPa)	203,5	353,9	504,2
Def. verticale dopo consolidazione (mm)	-1,481	-2,518	-2,065
Def. verticale a rottura (mm)	-0,284	-0,737	-0,486
Def. orizzontale a rottura (mm)	4,61	3,86	2,80
Tensione di taglio di picco (KPa)	78,163	118,1	137,2

Velocità di esecuzione della prova	0,005 mm/min
Condizioni di prova	Con saturazione

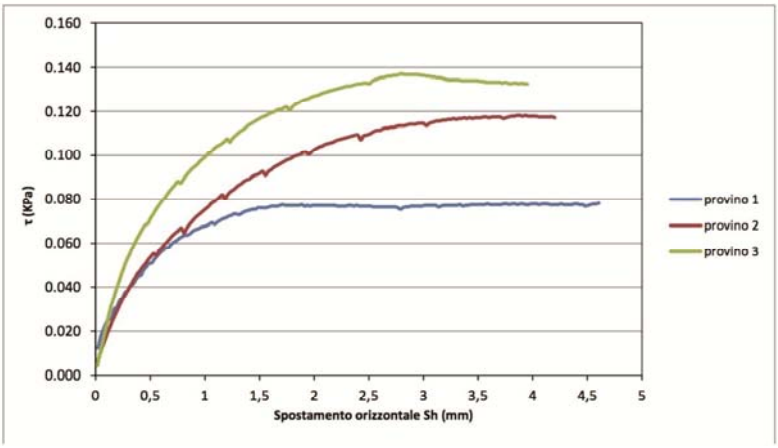

AIPo
Agenzia Interregionale per il fiume Po

Laboratorio di geotecnica di Boretto (RE)

PROVA DI TAGLIO DIRETTO

NORMA DI RIFERIMENTO: UNI CEN ISO/TS 17892-10:2005

Cert. N°. 055/03-12_AIPONAV_10-12

Committente :	UNIPR	Data Cons.	17/03/16
Località :	CASE PENNETTA	Data prova:	18/03/16
Sond.:	Si2	Campione:	Si2A
Profondità prelievo (m) :	6,70 - 7,30 m da p.c.	Tipo del Campione:	Indisturbato

Prova eseguita in scatola di taglio di Casagrande con anello circolare

PREPARAZIONE DEI PROVINI		Ricostruito	

CARATTERISTICHE INIZIALI	Provino 1	Provino 2	Provino 3
Peso specifico dei grani g/cm^3		2,69	
Peso di volume kN/m^3	21,99	22,14	22,24
Umidità %	10,90	10,90	10,90
Densità secca kN/m^3	19,83	19,96	20,06

CONDIZIONI A ROTTURA	Provino 1	Provino 2	Provino 3
Tensione di consolidazione (kPa)	106,20	203,50	300,80
Def. verticale dopo consolidazione (mm)	-1,29	-2,04	-2,40
Def. verticale a rottura (mm)	-0,47	-0,46	-0,22
Def. orizzontale a rottura (mm)	4,43	3,47	1,99
Tensione di taglio di picco (KPa)	52,70	74,98	67,20

Velocità di esecuzione della prova	0,005 mm/min
Condizioni di prova	Con saturazione

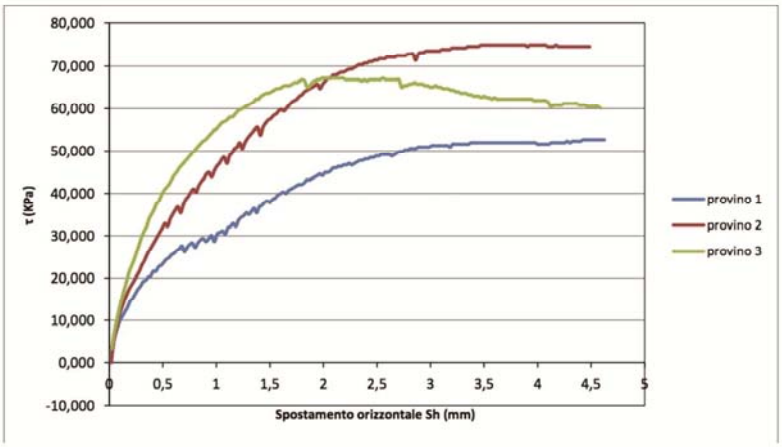

Agenzia Interregionale per il fiume Po

Laboratorio di geotecnica di Boretto (RE)

PROVA DI TAGLIO DIRETTO

NORMA DI RIFERIMENTO: UNI CEN ISO/TS 17892-10:2005

Cert. N°. 055/03-12_AIPONAV_10-12

Committente :	UNIPR	Data Cons.	17/03/16
Località :	CASE PENNETTA	Data prova:	18/03/16
Sond.:	Si2	Campione:	Si2B
Profondità prelievo (m) :	8,20 -8,80 m da p.c.	Tipo del Campione:	Indisturbato

Prova eseguita in scatola di taglio di Casagrande con anello circolare

PREPARAZIONE DEI PROVINI		Ricostruito	

CARATTERISTICHE INIZIALI	Provino 1	Provino 2	Provino 3
Peso specifico dei grani g/cm^3		2,69	
Peso di volume kN/m^3	23,54	22,15	22,24
Umidità %	8,51	8,51	8,51
Densità secca kN/m^3	21,69	20,42	20,50

CONDIZIONI A ROTTURA	Provino 1	Provino 2	Provino 3
Tensione di consolidazione (kPa)	106,2	203,5	300,8
Def. verticale dopo consolidazione (mm)	-0,873	-1,685	-0,983
Def. verticale a rottura (mm)	-0,15	-0,26	-0,33
Def. orizzontale a rottura (mm)	1,71	2,96	6,48
Tensione di taglio di picco (KPa)	28,294	67,2	94,1

Velocità di esecuzione della prova	0,005 mm/min
Condizioni di prova	Con saturazione

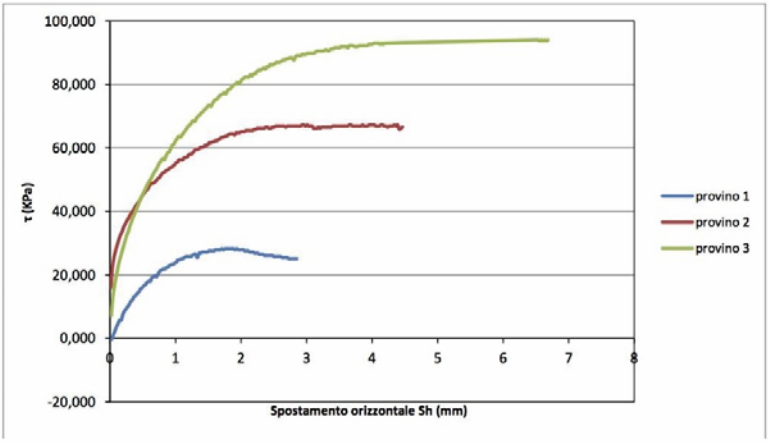

Appendix B1

ERTlab™ Sofware

ERTlab™ Software

ERTLab™ is the 3D resistivity and chargeability inversion software (developed by Geostudi Astier S.r.l. - Livorno) that has radically changed the approach to electrical resistivity tomography (ERT) surveys, allowing full flexibility in the three-dimensional arrangement of the electrodes and creating the market of resistivity surveys around buildings. Available for both 32 and **64 bits platforms (with multi-threading capabilities),** ERTLab™ is able to invert ERT measurements for any array geometry - surface, cross-hole or surface-to-hole. ERTLab™ makes use of **Finite Elements algorithm** for the accurate modeling of the terrain topography.

Features:

- Modelling the finished tetrahedral elements'
- Control and filtering data through threshold values
- Free definition and modification of topographic coordinates of measurement point.
- Hole and surface measure management with different electrode geometry.
- Free mesh definition.
- Possibility to insert any topographic model.
- Possibility to define target or resistivity model.
- Manual or automatic definition of the starting model.
- Export and manage data using ASCII files.
- Viewing data using 2-D or 3-D pseudo-maps.
- Graphic and numeric filtering of inaccurate measurements.

The ERTlab**™** software also allows to generate 2-D and 3-D sequences for superficial, bore or mixed electrodes configurations (Dipole-Dipole Linear, Dipole-Dipole Parallel, Polo-Dipole, Polo-Polo, Wenner, Wenner-Schlumberger). It features a dedicated environment for generating sequences on multiple holes and creating multiple sequences. It allows to execute different

modes of Import / Export of the sequence (Electre, ErtLab™) and Represent pseudo-maps for the analysis of the quadripular cover.

Appendix B2

Syscal R1 (IRIS Instruments)

Syscal R1 (IRIS Instrument)

The SYSCAL R1 resistivity meter, is specifically designed for medium-depth exploration. It combines a power source, transmitter up to a 200W or 600V output voltage, and a 2 channels receiver in a single unit; its compactness makes it an effective tool for intensive resistivity surveys. The different switching cards allow to work with 24 (Switch-24) up to 72 (Switch-72) electrodes. For imaging applications, Iris Instruments proposes different standard heavy-duty multi-core cables (5 traces-10m, 10 traces-5m and 10 traces-10m). Customized cables may also be assembled for special arrays or non-standard applications.

Measurement sequences can be configured through the instrument interface or via the PC software Electre Pro (provided with the Syscal). Electre Pro enables operators to develop and interrogate 2D, 3D, downhole and roll long sequences prior to heading into the field, helping to minimize potential data collection errors. The measured data can be downloaded and processed before inversion via the PC software (Prosys II, provided with the Syscal).

The measurement is fully automatic, controlled by a microprocessor: automatic self-potential correction, automatic ranging digital stacking for signal enhancement, error display in case of procedure troubles. The internal memory can store more than 800 measurements (3000 in multi-electrode mode) with full information on intensity, voltage, resistivity, IP Chargeability, geometrical parameters and station number. A serial link permits transfer of the data to a microcomputer for plotting and interpretation of the data. This versatile device is designed to work in a large number of configurations (SP measurements, sounding, profiling, 2D, roll-along, 3D and 3D monitoring surveys, etc.). The well-known reliability and accuracy of the Syscal range of resistivity meters will also mean extra value for both the contractor and the results end-user.